Aspects of beyond the Standard Model string phenomenology

João Pedro Trancoso Gomes Rosa

Oriel College

University of Oxford

A thesis submitted for the degree of

Doctor of Philosophy

Trinity 2010

This thesis is dedicated to my parents
Isabel and Jorge

and to my girlfriend
Ana Teresa

for all their love and support

Acknowledgements

I would first like to acknowledge the financial support of Fundação para a Ciência e Tecnologia (Portugal) under the grant SFRH/BD/23036/2005 during the completion of this thesis.

I am truly thankful to my supervisor, John March-Russell, for all his support and dedication to my research, for introducing me to so many different physical problems and for allowing me to explore my own ideas.

I would also like to thank all my colleagues, as well as all the administrative staff, at the Rudolf Peierls Centre for Theoretical Physics for all the great discussions about physics and beyond, especially those with whom I had the pleasure of sharing an office with - Andreas Athenodorou, Ivo Varzielas, Hélvio Vairinhos, Timothy Burns, Christopher McCabe, Maxime Gabella, Cyril Matti, Sebastian Cassel and Thomas Pickup. I am also grateful to Subir Sarkar and Graham Ross for all their support during the completion of my DPhil.

I am very grateful to Babiker Hassanain, with whom I collaborated in one of the projects presented in this thesis and with whom I had many interesting discussions and shared several painful Feynman diagrams. I also acknowledge Martin Schvellinger, Andre Lukas, Yang-Hui He, Alan Barr, Alexander Shertsnev, Stephen West and Sam Dolan for useful discussions on topics related to this thesis. I am particularly grateful to Sam Dolan for furnishing his numerical results on the Kerr superradiant instability.

I owe my deepest gratitude to Orfeu Bertolami, for teaching me how to do research in Theoretical Physics and for all his support during the completion of my DPhil.

I would also like to acknowledge Exeter College and Oriel College for providing exceptional professional and social environments and, in particular, the help and support of Pedro Ferreira, Andrew Boothroyd, Philip Stier and Frank Close.

To all my family, specially my parents, Isabel and Jorge, who taught me to love science, my sister Margarida, my grandmother Mimi and my grandparents Nelinha and Jacinto – thank you for all your love and support and for always being there for me, regardless of the distance.

To all the friends I have met in Oxford, namely my 'godsons' Inês and Pablo Paez, Raquel Oliveira, Frederico Regateiro, Luís Paixão, Filipa Simões, André Neves, Cristina Fernandes, Pedro Raposo, Vitor Marques, Susana Pires, Margarida Vareiro, Ricardo da Costa, Alonso Patron, Javier Martinez, Francisco Costela and Duarte Molha – thank you for being part of my life and for all the great things we have accomplished together. I would also like to thank my 'housemates' Abigail Balantyne, Maria Lambrakakis, Rory Cox, Wolf Richter and Kim Zinngrebe for all the great moments we have shared.

A special thank you to all my friends in Portugal, who are too many to be named individually, but without whose friendship I could not have reached this stage.

Finally, I would like to thank my girlfriend, Ana Teresa, for her endless love and dedication, for being my best friend, for listening to me and advising me, for always believing in me and, most of all, for being in my life and making it so much better.

Abstract

String theory is currently the best-known candidate for a theory of quantum gravity, having the necessary ingredients to describe all known elementary particles and interactions. It also includes several novel features, arising, for instance, from the additional six compact dimensions required for its internal consistency, making it the natural arena to construct extensions of the Standard Model. In this thesis, we analyze some of the new phenomenological aspects introduced by string theory within the framework of low energy effective theories, focusing on their applications to cosmology, astrophysics and collider experiments.

We first consider a particular realization of the brane-world scenario in branonium bound states, showing that the orbital motion of a probe antibrane about a central brane stack leads to a resonant amplification of its world-volume scalar modes. We analyze the cosmological development of this process and also its potential relevance for either dark or baryonic matter generation in the early universe.

We then focus on the spectrum of quark and lepton string excitations in warped compactifications, modeled by an effective 5-dimensional Randall-Sundrum throat. Motivated by the observed fermion mass hierarchy, we show that the spin-3/2 Regge excitation of the right-handed top quark is the lightest of such resonances in a significant region of parameter space, possibly lying below the TeV scale, and discuss its potential signatures at the Tevatron and at the LHC.

Finally, we study the emission of sub-eV scalar particles by maximally rotating Kerr black holes, motivated by the recent string axiverse proposal. We focus on the spectrum of unstable scalar bound states in the superradiant regime, leading to an exponentially large axion cloud around astrophysical black holes, and analyze two semi-analytical methods for computing the growth rate of this instability, comparing the obtained results with previous analytical and numerical analyses.

There is geometry in the humming of the strings,
there is music in the spacing of the spheres.

Pythagoras of Samos

Contents

List of Figures

Chapter 1

Introduction

1.1 Shortcomings of the Standard Model

Our understanding of elementary particles and of the interactions between them has come a long way in the past century and is now summarized in an elegant theory known as the Standard Model (SM) of particle physics [1]. The SM consists of a renormalizable quantum gauge field theory based on the group $SU(3)_c \times SU(2)_L \times U(1)_Y$ describing the three fundamental strong, weak and electromagnetic interactions. The elementary quarks and leptons arise in multiplets of the gauge symmetry group according to their colour, weak isospin and hypercharge, transforming as (anti-)fundamental or singlet representations of each unitary subgroup.

The SM incorporates a scalar weak isospin Higgs doublet, whose non-vanishing vacuum expectation value (vev), $v = 246$ GeV [2], breaks the electroweak (EW) symmetry down to the electromagnetic subgroup $U(1)_e$, generating a massless photon and three massive weak gauge bosons, $W^{\pm}$ and Z^0. This mechanism is also responsible for quark and lepton masses via Yukawa couplings between the latter and the Higgs field, leading to the observed three families of fermions with increasing masses.

The Higgs boson, corresponding to the physical excitations of the scalar field, has

yet to be observed and current searches place a lower bound $m_H > 114.4$ GeV [2] on the SM Higgs boson mass, whose value depends on its unknown self-interactions. The Large Hadron Collider (LHC), at CERN, that recently began colliding protons at unprecedented center-of-mass energies of 7 TeV and promises 14 TeV collisions, has the Higgs boson discovery as one of its main goals and will hopefully find the missing piece in the elegant electroweak symmetry breaking (EWSB) mechanism.

The SM thus provides an elegant description of almost all known properties and interactions between elementary particles, successfully describing a huge number of processes up to energies just below the EWSB scale, including scattering events and particle decays, as well as atomic and nuclear structures.

However, despite the many successes of the SM, there are several reasons to believe the new energy window that now becomes available at the LHC may reveal a much richer structure. First, the SM contains 19 unknown parameters, including 9 fermions masses, 3 quark CKM mixing angles and 1 CP-violating phase, 3 gauge couplings, 2 parameters in the Higgs sector and the QCD vacuum angle. Although the values of these parameters could simply have an anthropic explanation, one would ideally expect them to arise from a more fundamental theory.

Secondly, it is presently well-established that neutrinos undergo flavour oscillations, as demonstrated by solar and atmospheric neutrino detectors, requiring at least two massive physical eigenstates (see e.g. [3] for a recent review). This in turn almost certainly implies the existence of right-handed (rhd) neutrino components, which are necessarily singlets under the SM gauge group and hence provide the best known evidence for beyond the SM (BSM) physics. These singlet fields could then be coupled to the corresponding left-handed (lhd) components via Yukawa couplings but also have bare Majorana mass terms which, if generated at a scale much higher than the EWSB scale, may produce light neutrinos states via the so-called 'seesaw' mechanism [4].

Within the context of Grand Unified Theories (GUT) [5, 6], the SM may be embedded in a larger symmetry group, such as $SU(5)$ or $SO(10)$, which is spontaneously broken down to the observed gauge group. This is suggested by the apparent unification of the running gauge couplings at a scale $M_{GUT} \sim 10^{16}$ GeV[1]. The SO(10) GUT is particularly interesting as it naturally accommodates a rhd neutrino singlet in its **16** representation, in which case M_{GUT} sets the scale of the Majorana mass terms, producing neutrinos with sub-eV masses as required by data [2].

There are, however, other experimental and theoretical motivations to consider extensions of the SM which require more than an enhancement of the gauge symmetry, possibly pointing towards a modification of the nature and symmetries of spacetime itself and which we describe in the next subsections.

1.1.1 The hierarchy problem

As a renormalizable quantum theory, the SM produces finite results for all physical scattering amplitudes to all orders in perturbation theory, even if we take the limit of infinite momenta flowing inside loops in higher-order Feynman diagrams. However, one does not expect the SM to give accurate results up to arbitrarily high energies as, at least around the Planck scale, $M_p = 1/\sqrt{G_N} \sim 10^{19}$ GeV, quantum gravity effects should become significant. It is then natural to endow the SM with an ultraviolet (UV) momentum cut-off, Λ_{UV}.

In its simplest form, the Higgs mechanism relies on a scalar potential given by:

$$V(\phi) = -\mu^2 \phi^\dagger \phi + \frac{\lambda}{4} (\phi^\dagger \phi)^4 \,, \tag{1.1}$$

the negative sign of the quadratic piece being crucial for the existence of a clas-

[1]Some classes of non-supersymmetric GUT extensions of the SM are in fact experimentally excluded [6], this being the scale obtained for the minimal supersymmetric SM particle content, discussed in section 1.2.1.

sical minimum, with $v = \mu/\sqrt{\lambda}$. When one includes quantum corrections, self-interaction 1-loop diagrams produce positive corrections to the quadratic term of the form $\lambda\Lambda_{UV}^2\phi^\dagger\phi$. If the SM were valid all the way to the Planck scale, this would lead to a positive 1-loop correction of order $(10^{19}\ \text{GeV})^2$ (assuming $\lambda \lesssim 1$ for perturbation theory to hold). This in turn implies that the bare μ^2 value would need to compensate this enormous contribution in order to arrive at a negative value around the EWSB scale of $(100\ \text{GeV})^2$. This requires a huge fine-tuning of roughly 1 part in 10^{17} in order to make EWSB stable under quantum corrections [7].

Although there is no absolute prescription for the amount of fine-tuning which is acceptable in a theory, this suggests that $\Lambda_{UV} \gtrsim$ few TeV could ameliorate this problem, so that one expects new physics to appear at this scale.

1.1.2 Dark matter

In 1933, Zwicky [8] inferred, from measurements of the velocity dispersion of galaxies in the Coma cluster, a mass-to-light ratio of around 400 solar masses per solar luminosity, about two orders of magnitude larger than what is observed in the solar neighbourhood. This was the first hint for the existence of a non-baryonic component of matter in our universe, for which growing evidence has been accumulating.

At galactic scales, evidence for the existence of non-luminous or dark matter arises from the analysis of galactic rotation curves (see e.g. [9]). According to newtonian laws, rotational velocities should follow a profile $v(r) = \sqrt{G_N M(r)/r}$, where $M(r)$ is the mass within the radius r. The observed flattening of rotation curves beyond the edge of visible galactic disks then implies $M(r) \propto r$, thus suggesting the existence of a spherical dark matter halo surrounding the observed galaxies.

Such gravitational anomalies have also been analyzed in the context of modified gravity theories such as MOND [10], but these have generically failed to fully account for the observed discrepancies and usually require some amount of dark matter. More-

over, the case for dark matter has been considerably strengthened by studies of strong and weak gravitational lensing, velocity dispersions of dwarf spheroidal galaxies and spiral galaxy satellites and also X-ray emission [9]. One of the most convincing pieces of evidence was provided by the Bullet cluster [11], where combined X-ray and weak-lensing observations revealed a clear spatial separation between the visible and dark matter components that cannot be explained by modified gravity theories.

The total amount of dark matter in the universe can be determined from analysis of the Cosmic Microwave Background (CMB), whose temperature fluctuations of about 1 part in 10^5 measure the non-uniformities in the matter density at the time of photon decoupling and hence the size of the dark matter gravitational wells. Current fits to the WMAP seven year data give $\Omega_c h^2 = 0.1109 \pm 0.0056$ for the fraction of the critical energy density in pressureless cold dark matter (CDM) [12].

It is generically assumed that dark matter is generated thermally in the early universe following the standard 'freeze-out' mechanism, with a relic density $\Omega_c h^2 \simeq 3 \times 10^{-27}$ cm^{3}s$^{-1}/\langle \sigma v \rangle$ [9]. The WMAP results then suggest a coupling constant for dark matter annihilations close to the weak coupling for masses within an order of magnitude of the weak scale, so that dark matter candidates are generically known as Weakly Interacting Massive Particles (WIMPs). Within the framework of the SM, only neutrinos could constitute suitable candidates but current bounds on their masses preclude a significant component of dark matter in this form. Although the annihilation cross-section constrains thermal-freeze-out WIMPs to be relatively light, with masses $\lesssim 34$ TeV [9], dark matter particles with masses above 10^{10} GeV known as WIMPZILLAS can be produced non-thermally [13].

There are presently several experiments dedicated to both direct and indirect WIMP detection but, despite some recent developments [14], the fundamental nature of dark matter remains unknown, apart from the fact that it cannot be a SM particle.

1.1.3 The strong-CP problem

The QCD Lagrangian can include a topological CP-violating term of the form:

$$\mathcal{L}_\theta = \frac{\bar{\theta}}{16\pi^2} \int d^4x \mathrm{Tr}[G_{\mu\nu}\tilde{G}^{\mu\nu}] \ , \tag{1.2}$$

where $G_{\mu\nu}$ is the gluon field strength and $\tilde{G}_{\mu\nu}$ its dual. This non-perturbative term arises from the non-trivial QCD vacuum, with the QCD instanton number multiplied by the angular parameter $\bar{\theta} = \theta + \arg(\det \mathcal{M})$, which includes a bare contribution and the phase of the quark mass matrix. If one of the quarks were massless (realistically the up quark), both contributions would vanish, the bare θ term being eliminated by a chiral rotation of the quark fields. This is, however, claimed to be strongly inconsistent with hadron phenomenology and recent lattice computations [15].

Although the term in Eq. (1.2) corresponds to a total derivative and, hence, does not contribute to any perturbative phenomena, via non-perturbative effects it generates a neutron electric dipole moment, for which current experimental searches give $d_e < 2.9 \times 10^{-26}$ e cm [16]. Along with recent results for ^{199}Hg [17], this gives roughly $\bar{\theta} \lesssim 10^{-10}$. Given that, because of the observed CP-violating phase in the CKM quark-mixing matrix, no symmetry is gained as $\bar{\theta} \to 0$, such an unnaturally small value for $\bar{\theta}$ constitutes the so-called strong CP-problem.

Although other hypotheses have been discussed [18–20], the most compelling solution to this problem was proposed by Peccei and Quinn (PQ) in 1977 [21], who promoted the $\bar{\theta}$ angle to a field whose value is dynamically driven to zero. This is accomplished by introducing an additional chiral global symmetry, $U(1)_{PQ}$, spontaneously broken at a scale f_a. This generates a pseudo-Nambu-Goldstone boson, the axion, as pointed out by Weinberg and Wilczek (WW) [22,23], which acquires a small mass of order Λ^2_{QCD}/f_a from the $U(1)_{PQ}$ chiral anomaly. This is associated with QCD

instanton effects, which generate a potential in the axion field Lagrangian:

$$\mathcal{L}_a = \frac{1}{2}\partial_\mu a \partial^\mu a + \frac{a}{f_a}\frac{r}{16\pi^2}\int d^4x \mathrm{Tr}[G_{\mu\nu}\tilde{G}^{\mu\nu}] \ , \tag{1.3}$$

where r is a model-dependent constant. As the PQ symmetry acts on the axion field as a shift symmetry, we may absorb the $\bar{\theta}$ angle into the definition of a via $a \to a - f_a\bar{\theta}/r$. As the energy of the $\bar{\theta}$-vacuum is proportional to $(1 - \cos\bar{\theta})$, this is also the form of the axion potential, which is then minimized for $\langle a \rangle = 0$, as required. The corresponding axion mass is then given by [24]:

$$m_a = \frac{r f_\pi m_\pi}{2 f_a}\frac{\sqrt{m_u m_d}}{m_u + m_d} \sim 5.4 \times 10^{-6} \text{ eV}\left(\frac{1.1 \times 10^{12} \text{ GeV}}{f_a/r}\right) \ , \tag{1.4}$$

where m_π and f_π are the pion's mass and decay constant, respectively. The potential actually receives further contributions from weak CP-violating processes which give $\bar{\theta} \simeq 10^{-14}$, still consistent with experimental bounds [15].

Although the original PQWW axion, where the PQ symmetry is broken at the EW scale, was ruled out in one year [25], one can envisage an 'invisible' axion with couplings determined by a generic f_a^{-1}. In particular, a coupling to the electromagnetic field of the form in Eq. (1.3) has been the basis for experimental axion searches via photon-axion conversion and for astrophysical bounds, namely from supernova evolution, which require $f_a \gtrsim 10^9$ GeV [2].

In the early universe, for temperatures above Λ_{QCD}, instanton effects are exponentially suppressed and can be neglected, so that the axion potential is essentially flat. When these latter effects are 'turned on' at $T \sim \Lambda_{QCD}$, the axion field begins to oscillate about its minimum, producing a Bose-Einstein condensate of non-relativistic axions that behave as CDM [26]. For a initial misalignment angle not fine-tuned to be $\ll 1$, their energy density exceeds the observed dark matter density if $f_a \gtrsim 10^{12}$ GeV [2].

Hence, astrophysical and cosmological considerations set an allowed window for the axion decay constant 10^9 GeV $\lesssim f_a \lesssim 10^{12}$ GeV, which may constrain the allowed phenomenology of string theory compactifications, as we will discuss below.

1.1.4 Dark energy and the cosmological constant problem

Not only do current astrophysical and cosmological observations require a new form of matter but they also give evidence for an unknown and puzzling energy component. 'Dark energy' hypothetically permeates the whole universe and is responsible for the accelerated expansion rate inferred from Type IA supernovae at redshifts $z \lesssim 1$ [27, 28]. Moreover, the analysis of CMB anisotropies and of the large scale structure (LSS) of the universe gives a value $\Omega_\Lambda h^2 = 0.734 \pm 0.029$ [12] for the fraction of energy density in this form, as well as an equation of state close to $\rho_\Lambda = -p_\Lambda$, so that the universe seems to be presently dominated by a cosmological constant.

Such a constant may appear in Einstein's equations both as a bare geometric term and in the form of vacuum energy. This poses a major problem, as quantum field theory predicts the latter to be of order $M_p^4 \sim 10^{76}$ GeV^4 if no new physics arises below the Planck scale, about 120 orders of magnitude above the observed value, $\rho_\Lambda \sim H_0^2 M_p^2 \sim 10^{-44}$ GeV^4. Although such a large vacuum energy density may be cancelled by an equally large and opposite bare term, this corresponds to an unacceptable degree of fine-tuning. New physics at the TeV scale may alleviate this fine-tuning, but it remains nevertheless mysteriously unnatural.

An associated puzzle arises from the fact that the dark energy component only became dominant in the recent history of the universe. A possible reason for this coincidence and the smallness of ρ_Λ is based on anthropic selection [29], which would preclude the existence of observers such as ourselves in a universe with a larger value of Λ, in particular inhibiting structure formation [30]. Other scenarios, such as quintessence, consider an additional scalar degree of freedom ϕ with an equation

of state $p_\phi = w\rho_\phi$ which behaves as dark energy at late times, possibly tracking the radiation energy density until matter-radiation equality (see e.g. [31, 32]).

Whether dark energy requires the introduction of BSM ingredients is still an open problem, being, however, a crucial question to address in any BSM scenario.

1.1.5 Inflation

The observed flatness and homogeneity of the universe, as inferred from the analysis of the CMB and the LSS, cannot be accommodated within the standard 'hot Big Bang' scenario. In particular, the latter predicts that the present Hubble volume consists of about 10^5 causally disconnected regions at the time of last scattering [26], a surprising result given the uniformity of the CMB temperature across the sky.

Moreover, the observed CMB temperature fluctuations suggest a primordial spectrum which is nearly scale-invariant and slightly red-tilted, i.e. with marginally more power at large scales, with a scalar spectral index $n_s = 0.963 \pm 0.014$ [12].

All these problems can be solved by a primordial period of accelerated expansion known as inflation [33], in which the universe grows by a factor $\sim e^{60}$, also diluting unwanted relics such as magnetic monopoles. The modern mechanism [34, 35] considers an additional scalar field, the inflaton, whose potential has a nearly flat section, thus mimicking a cosmological constant that dominates the energy density at early times. The universe then expands in an accelerated manner as the field slowly rolls down its potential until it reaches its minimum and starts oscillating about it. If coupled to ordinary particles, the oscillating inflaton will damp its energy into relativistic SM degrees of freedom (d.o.f.) through decays, reheating the universe into a radiation-dominated epoch, and possibly via a resonant 'preheating' period during which the number of particles grows exponentially [36, 37]. Quantum fluctuations of the inflaton field are also amplified during inflation, producing the required nearly scale-invariant spectrum that seeds the present LSS (see e.g. [38] for a recent review).

As we will discuss below, most SM extensions include several additional pseudo-flat scalar fields, but inflaton candidates leading to a sufficiently long period of accelerated expansion are proving hard to find.

1.1.6 Baryon asymmetry

The local dominance of matter is an obvious empirical observation. Anti-matter can be produced in the laboratory and is observed in cosmic rays, but the suppression of its flux relative to that of matter, e.g. by a factor 10^4 for anti-protons, shows that no significant anti-matter abundance is present in our astrophysical neighbourhood [39].

This asymmetry is now believed to be universal, with separate domains of matter and anti-matter being disfavoured by their excessive contribution the to the diffuse γ-ray background and CMB distortion from annihilations at the boundaries between adjacent domains [40]. The baryon asymmetry can be characterized in terms of the baryon-to-photon ratio, which remains constant at late times, and is given by:

$$\eta = \frac{n_B - n_{\bar{B}}}{n_\gamma} \simeq 6 \times 10^{-10} \ , \tag{1.5}$$

where the latter value is determined from the observed primordial abundances of light elements [2] and CMB anisotropies, which give $\Omega_B h^2 = 0.02258^{+0.00057}_{-0.00056}$ [12]. Note that in a baryon symmetric universe, we would expect a small 'freeze-out' abundance $n_B = n_{\bar{B}} = 10^{-20} n_\gamma$, which is too small to account for the above observations [39].

In 1967, Sakharov pointed out that any mechanism that generates the observed asymmetry - baryogenesis - necessarily includes three fundamental ingredients: (i) baryon number (B) violation, (ii) C and CP violation and (iii) out of equilibrium processes [41]. In the SM, B is violated non-perturbatively by weak instanton configurations known as sphalerons[2] which violate B+L and are in equilibrium in the early

[2]From the greek 'ready to fall', as coined by Klinkhamer and Manton [42].

universe for temperatures below 10^{13} GeV and before the EW phase transition. We also find a small amount of CP-violation in the SM from quark CKM mixings and the QCD θ-term, but this is too small for a significant baryogenesis [39].

Several models have been proposed in the literature, including e.g. GUT baryogenesis [43], via B- and CP-violating decays of the additional heavy gauge bosons into quarks and leptons; EW baryogenesis [44], where, in an out-of-equilibrium first order phase transition, baryons naturally diffuse through bubble walls into the broken phase; and leptogenesis [45], with a lepton asymmetry generated in the decays of heavy Majorana rhd neutrinos and then converted into a baryon asymmetry by sphaleron processes (see e.g. [39] for a review of these mechanisms).

An interesting possibility known as the Affleck-Dine mechanism [46] arises in supersymmetric GUTs, where one of the many (pseudo)flat directions carrying B-charge may acquire a large value during inflation. CP-violating self-couplings then induce a non-trivial angular motion in field space, the internal angular momentum corresponding to a net baryon number. At late times, self-interactions become negligible and this baryon number is transferred to SM fermions via B-preserving decays.

1.1.7 Quantum gravity

Gravity stands alone as the only fundamental interaction outside the framework of quantum theory. Although one may question the need to reconcile general relativity and quantum physics, given their wide separation in terms of typical length scales, the historical trend for unification and the belief that quantum gravity (QG), offering a natural cut-off at the Planck scale, may cure some of the limitations of the SM make a compelling case for the quantization of gravity. Moreover, scenarios involving a non-quantized gravitational field interacting with quantum matter often lead to violations of the uncertainty principle or momentum conservation [47], as well as information loss in the process of black hole evaporation (see e.g. [48]). One also hopes that QG

effects may eliminate singularities and define initial conditions for our universe [49].

Conventional covariant quantization methods [50] are based on the observation that the Einstein-Hilbert action can be obtained from a massless spin-2 tensor field, $h_{\mu\nu}$, universally coupled to the energy-momentum tensor, in a fixed background spacetime, $\bar{g}_{\mu\nu}$. Although, in 1974, 't Hooft and Veltman obtained finite results at 1-loop order [51], the 2-loop computation showed that this theory was non-renormalizable [52].

The problem of divergences in gravitational theories can be traced to the coupling of gravity to the energy-momentum tensor, which grows with wave-number, whereas other interactions couple to mode-independent charges [53]. However, non-renormalizability is not necessarily a symptom of illness in a quantum theory, although it drastically limits its predictive power. One could speculate that QG is, in fact, finite if the perturbative series is properly summed or that the inclusion of appropriate couplings to matter fields or higher-order curvature terms may cancel undesired divergences [54]. It is also possible that metric perturbations do not constitute fundamental fields, which happens in string theory, presently the most compelling theory of QG as we will discuss below. Another approach, followed in loop quantum gravity (see e.g. [55]), argues against the validity of an expansion about smooth classical geometries and implements a background-independent quantization procedure.

1.2 Going beyond the Standard Model

The shortcomings of the SM have motivated a large number of BSM scenarios. Although an extensive review of these models is out of the scope of this thesis, it will be useful to describe two important frameworks that are the basis for most phenomenological scenarios constructed in the literature and offer the most promising experimental possibilities in the near future: supersymmetric and extra-dimensional theories.

1.2.1 Supersymmetry

The idea of supersymmetry (SUSY) as a solution of the hierarchy problem is based on the observation that bosons and fermions give opposite contributions to loop Feynman diagrams, so that additional fermionic particles may cancel the undesired quartic divergences in the Higgs potential [7].

SUSY has, however, a much deeper origin as the only possible additional spacetime symmetry of the S-matrix allowed by the Coleman-Mandula 'no-go theorem' [56]. This is due to the spinorial character of the associated conserved supercharges, which lead to a 'fermionic' extension of spacetime known as superspace.

The representations of the Poincaré group are thus extended to form supermultiplets of particles with different spins. The simplest such extension of the SM, the Minimal Supersymmetric Standard Model (MSSM) [57] includes superpartners for matter fermions (scalar squarks and sleptons), gauge bosons (spin-1/2 gauginos) and Higgs bosons (spin-1/2 Higgsinos)[3]. Each supermultiplet is described by a superfield, which can be e.g. a holomorphic chiral superfield, in the case of matter and Higgs representations, or a real vector superfield, in the case of gauge bosons (see e.g. [58]).

Extended SUSY algebras with $\mathcal{N} > 1$ supercharges can be constructed but are, however, non-chiral and, hence, cannot give realistic low-energy models. Also, renormalizable theories require $\mathcal{N} \leq 4$ and, to avoid massless particles with spin larger than two, one must have $\mathcal{N} \leq 8$.

One can also have SUSY as a local rather than a just a global symmetry, which leads to supergravity (SUGRA) theories, in the same way local Poincaré symmetry corresponds to general relativity. The gravity supermultiplet includes the spin-2 graviton and its spin-3/2 superpartner, the gravitino, with additional gravitinos as well as vector bosons, spin-1/2 states and scalars for $\mathcal{N} > 1$ (see e.g. [59, 60]).

[3]The MSSM requires two Higgs doublets in distinct EW representations coupling separately to up- and down-like superfields.

In higher-dimensional theories, which we discuss below, the larger number of fermionic generators extends the gravity supermultiplet to include additional anti-symmetric tensor fields. Despite their apparent non-renormalizability, these theories have attracted a lot of attention as they correspond to the low-energy limit of super-string theories in ten dimensions and 11-dimensional M-theory, as we discuss in the next section. Interestingly, the latter corresponds to the maximum number of dimensions consistent with a single graviton and no particles with spin greater than 2 [59], as well as to the smallest number large enough to contain the SM gauge group [61]. Recent developments also challenge the non-renormalizability of $\mathcal{N} = 8$ SUGRA and point towards a possible UV-finiteness, making it a potential candidate for QG [62].

SUSY cannot, however, be an exact symmetry at low energies, or otherwise superpartners would be degenerate with their SM counterparts and have already been observed. SUSY must, hence, be broken, ideally via a spontaneous rather than an explicit breaking mechanism, in order to preserve its appealing features. Furthermore, a dynamical SUSY breaking mechanism [63], arising from exponentially small effects, would naturally produce the necessary hierarchy to avoid a large degree of fine-tuning and introduce new physics at the TeV scale (see e.g. [64]). Also, we expect any mechanism to only produce 'soft' SUSY breaking terms in the low-energy Lagrangian, sufficient to raise the masses of superpartners above the energy scale $\sim$ 100 GeV probed in collider experiments so far, but without reintroducing unwanted quadratic divergences.

SUGRA can be spontaneously broken via the superhiggs mechanism, where a Goldstone fermion or goldstino is 'eaten' by the gravitino, which therefore gains a mass $m_{3/2} \simeq M_{\text{SUSY}}^2/M_p$, with M_{SUSY} denoting the SUSY breaking scale. However, were SUSY breaking to occur via additional Higgs scalars directly coupled to the SM particles, one would be faced with disastrous phenomenological consequences, such as scalar superpartners lighter than the top quark [57]. The current paradigm thus

considers an additional hidden/sequestered sector where SUSY is broken at a higher energy scale and communicated to the observable sector through a set of messenger fields, coupled to both sectors, at the TeV scale.

SUSY breaking in the hidden sector may occur through vevs of the auxiliary F and D-terms of hidden chiral and vector superfields, respectively. Communication to the visible sector depends on the interactions between the messenger particles and both sectors, with popular mechanisms including gravity, gauge and anomaly mediation (see e.g. [65]). It is also possible for this to produce a metastable non-supersymmetric state, which decays into the true SUSY vacuum on a time scale larger than the age of the universe, a scenario that circumvents many of the difficulties of dynamically generating a static non-SUSY vacuum [64].

SUSY theories also generically include a so-called R-symmetry or a discrete R-parity subgroup, which acts both on the superfields and the superspace variables. In the case of the MSSM, the inclusion of R-parity forbids dangerous (dimension-4) B- and L-violating terms in the superpotential leading to proton decay [7]. As all SM particles are even under this symmetry, while their superpartners are odd, the lightest supersymmetric particle (LSP) is completely stable and, if electrically neutral, constitutes an excellent dark matter candidate. In typical scenarios this corresponds to the neutralino, an admixture of the neutral higgsinos and the neutral gauginos, although other candidates such as sneutrinos and gravitinos have been considered in the literature (see e.g. [9]).

1.2.2 Extra-dimensions

Theories with additional spatial dimensions have a long history, going back to the seminal works of Kaluza and Klein [66], who considered a 5-dimensional spacetime with an extra S^1 compact dimension, y, of radius R. A 4-dimensional effective theory is then obtained if R is smaller than the smallest scale experimentally accessible.

Due to the periodic nature of the extra-dimension, the 5D momentum is necessarily quantized and corresponds to an additional rest mass for particles in the 4-dimensional effective theory, leading to an infinite set of massive states known as the Kaluza-Klein (KK) tower, with masses $m_n^2 = m_0^2 + n^2/R^2$, where $n \in \mathbb{Z}$ and m_0 denotes the 5-dimensional mass. This can be readily obtained via a KK mode-decomposition, which for a scalar field can be written as [67]:

$$\Phi(x^\mu, y) = \frac{1}{\sqrt{2\pi R}} \sum_{n=-\infty}^{+\infty} \phi_n(x^\mu) e^{\frac{iny}{R}} \ . \tag{1.6}$$

Fields in the 5-dimensional spacetime are also decomposed into 4-dimensional representations of the Poincaré group, leading to new massless and massive d.o.f.. For instance, the 5-dimensional metric, g_{MN}, leads to a 4-dimensional metric tensor, a vector field and a scalar field, associated with the KK zero-modes of $g_{\mu\nu}$, $g_{\mu 5}$ and g_{55}, respectively[4]. This suggests a possible mechanism for unifying gravity and electromagnetism, and indeed it can be shown that 5D diffeomorphism invariance gives rise to 4-dimensional $U(1)$ gauge transformations of the massless vector field. Furthermore, the purely gravitational 5D action leads to the Einstein-Hilbert and Maxwell actions in four dimensions, along with the additional massless scalar field - a flat 'modulus' effectively determining the size of the extra-dimension [67].

This procedure can be generalized to include additional d compact dimensions with more complicated topology, leading to non-abelian gauge theories and additional moduli. The 4-dimensional gauge couplings and the Planck mass are then related to the fundamental scale of the $4+d$ action, M_*, via $g_4^{-2} \sim M_*^d V_d$ and $M_p^2 \sim M_*^{d+2} V_d$, where V_d is the volume of the compact space. If all compact dimensions have a typical size R_d, this gives $R_d \sim M_p^{-1} g_4^{-\frac{d+2}{d}}$, so that effects of the extra-dimensions lie close to the Planck scale, precluding any possibility of observing them in the near future [68].

[4]Latin and greek indices denote 5- and 4-dimensional components, respectively.

More promising scenarios arise if the SM gauge bosons do not have a gravitational origin, so that 'gravi-photons' and also 'gravi-scalars' correspond to new types of particles. Particularly interesting is the case where only gravity propagates in the 'bulk' of the extra-dimensions, with SM fields confined to a (3+1)-dimensional subspace known as a 'brane'. Although such confinement can be achieved in the context of field theory [69, 70], it naturally arises from solitonic configurations in SUGRA and string theory, as we describe in the next section. This is the framework of the 'large extra-dimensions' scenario proposed by Arkani-Hamed, Dimopoulos and Dvali (ADD) [71], where the fundamental scale is $M_* \sim$ TeV, in order to address the hierarchy problem. This implies $R_d \sim 10^{30/d-17}$ cm, which for $d = 1$ implies a solar system size extra-dimension and, hence, is obviously excluded. Submillimetre extra-dimensions arise for $d \geq 2$, which slowly approach the TeV scale, e.g. $R_6 \sim (20 \text{ MeV})^{-1}$.

The radius R_d, or equivalently M_*, are experimentally constrained e.g. by deviations from Newton's law and astrophysical processes due to light KK gravitons, the latter placing the most stringent limits on $M_* > 750$ (35) TeV for $d = 2$ (3) [2]. These limits can, however, be weakened substantially by considering non-toroidal compactifications [72]. Interesting potential signatures of this scenario at the LHC include 'missing energy' events from gravitons leaking into the extra-dimensions and production of black holes, with typical lifetimes of $10^{-27} - 10^{-26}$ s, due to the stronger gravitational coupling experienced in TeV-collisions.

It is also possible for SM particles to arise from higher dimensional fields, in which case non-observation of their first KK modes requires extra-dimensions smaller than ~ 1 TeV^{-1}. Typical scenarios include 5D Z_2-orbifold compactifications, allowing for massless gauge bosons and chiral fermions in four dimensions. In the case of 'universal extra-dimensions' (UED), where all SM fields propagate in the bulk, a residual Z_2 symmetry known as KK-parity protects the lightest KK mode against decay, thus making it a potential candidate for dark matter [73], generically the first

KK excitation of the hypercharge gauge boson [74]. Limits on the size of the extra-dimension in these scenarios vary between 300 GeV and 500 GeV, depending on the Higgs boson mass [75]. Interesting applications of this framework include the gauge-Higgs unification scenario, where the Higgs boson is identified with the 5-dimensional component of a vector field associated with an extended gauge symmetry [76].

An elegant solution to the hierarchy problem can also be obtained in the context of warped geometries, of which the paramount example is the Randall-Sundrum (RS) model [77]. The latter considers an S^1/Z_2 orbifold with a fifth dimension $0 \leq y \leq L$, with $L = \pi R$. The inclusion of a bulk cosmological constant, $\Lambda < 0$, and additional vacuum terms localized at the orbifold fixed points $y = 0$ and $y = L$, or '3-branes', produce a non-factorizable geometry of the form:

$$ds^2 = e^{-2ky}\eta_{\mu\nu}dx^\mu dx^\nu + dy^2 \ . \tag{1.7}$$

The 4-dimensional sections of this geometry are, thus, flat despite the bulk cosmological constant, but are non-trivially related by the exponential 'warp' factor e^{-ky}, where $k = \sqrt{-\Lambda/24M_*^3}$ denotes the curvature of the ambient AdS_5 geometry, of which the RS model represents a finite slice. This warping is crucial to the solution of the hierarchy problem, as it exponentially suppresses all mass scales at the $y = L$ brane but not at the $y = 0$ brane, which are thus denoted as the IR and UV branes, respectively. In particular, if the SM fields, namely the Higgs boson, are localized in the IR brane, the EW scale is naturally suppressed with respect to the UV Planck scale, requiring $kR \simeq 12$ to reproduce the observed hierarchy. A stable extra-dimensional size is thus required and a stabilizing potential for the associated modulus, the radion, can be obtained via the Goldberger-Wise mechanism [78].

Another appealing feature of the warping arises if we let the SM gauge bosons and fermions, but not the Higgs boson, propagate in the bulk [79,80]. In the case of quarks

and leptons, for example, the extra-dimensional profile of the chiral zero modes can be exponentially tuned by varying their bulk mass, thus allowing for a larger or smaller overlap with the IR brane, which determines the size of the corresponding Yukawa couplings. Warped extra-dimensions thus allow for a purely geometric description of the observed fermion mass hierarchy[5], a possibility we further explore in this thesis within the natural embedding of the RS model in string theory compactifications.

As for SUSY theories, extra-dimensional models can be used to overcome many of the shortcomings of the SM, and we will describe in the next section how these two fundamental ingredients are combined in string theory, so that the latter becomes the natural arena to search for BSM physics.

1.3 String Theory

Before the development of QCD in the 1970's, early attempts to describe the strong nuclear force were based on a unified description of the plethora of known hadrons as quantum oscillations of a single fundamental object – the string. Although this still gives an accurate effective description in terms of flux tubes and remains an active area of research (see e.g. [81] and references therein), it was soon realized that string theory could be used for a much more fundamental purpose.

A string is a 1-dimensional object that, as it evolves in time, sweeps out a 2-dimensional surface in spacetime denoted as the string world-sheet. The motion of a string can then be described in terms of a dynamical mapping of the world-sheet coordinates, (σ, τ), into flat spacetime coordinates $X^\mu(\sigma, \tau)$, encoded in the string sigma-model or Polyakov action [82, 83]:

$$S_P = -\frac{T}{2} \int d\sigma d\tau \sqrt{-h} h^{\alpha\beta} \eta_{\mu\nu} \partial_\alpha X^\mu \partial_\beta X^\nu \ , \tag{1.8}$$

[5]Bulk masses are still free parameters of the model, precluding any absolute predictions, although this naturally provides exponential hierarchies.

with $T = 1/2\pi\alpha'$ denoting the string tension and $h_{\alpha\beta}$ the auxiliary world-sheet metric. The Regge slope α' is related to the string length scale, l_s, by:

$$\alpha' = \left(\frac{l_s}{2\pi}\right)^2 . \tag{1.9}$$

The classical equations of motion can equivalently be derived from the Nambu-Goto action:

$$S_{NG} = -T \int d\sigma d\tau \sqrt{-\det G_{\alpha\beta}} , \qquad G_{\alpha\beta} = \partial_\alpha X^\mu \partial_\beta X^\nu . \tag{1.10}$$

Canonical quantization of this action can then be obtained via a mode expansion of the spacetime fields, X^μ, in terms of creation and annihilation operators and by imposing appropriate boundary conditions (b.c.) for open and closed strings. In the latter case, the spectrum of excitations includes a massless spin-2 symmetric and traceless tensor, which represents an ideal candidate for the graviton, the quantum of the gravitational field [84]. Along with the massless vectors obtained in the open string spectrum, this led to the idea that string theory could actually provide a consistent QG theory and a potential candidate for the 'theory of everything' [84], with the fundamental string length lying presumably close to the Planck length, $l_p \sim 10^{-33}$ cm.

This description had, however, several problems, in particular requiring $D = 26$ dimensions to ensure the absence of negative norm states and Lorentz invariance, as well as exhibiting a tachyonic ground state for open strings. Also, having no fermionic excitations, this bosonic string cannot describe elementary quarks and leptons.

A fermionic spectrum can be obtained, however, if one introduces SUSY. This can be done in the Ramond-Neveu-Schwarz (RNS) formalism [85, 86], with world-sheet supersymmetry obtained by introducing fermionic partners $\psi^\mu(\sigma, \tau)$ to the bosonic fields, or in the Green-Schwarz (GS) perspective [87], where the world-sheet is mapped directly into superspace, with fermionic coordinates $\Theta^{Aa}(\sigma, \tau)$, with $A = 1, \ldots, \mathcal{N}$. Although the former is more easily quantized, it requires a truncation of the spec-

trum implemented via the GSO projection [88], leading to spacetime SUSY, necessary for consistency of the interacting theory and elimination of an undesired open string tachyon. On the other hand, the GS formalism automatically incorporates this projection and spacetime SUSY, requiring however a more difficult light-cone gauge quantization. Both approaches are in fact equivalent in a 10-dimensional Minkowski space, this being the critical dimension for consistency of the quantum theory [82].

These procedures give rise to five different types of superstring theories in 10D - the type I and the two heterotic theories with gauge groups $E_8 \times E_8$ and $SO(32)$, which have $\mathcal{N} = 1$ SUSY, and the two type II theories, with $\mathcal{N} = 2$. All these have been shown to be related by dualities, e.g. type IIA and type IIB theories are T-dual, with equivalent compactifications on circles of radius R and $\tilde{R} = l_s^2/R$. Another example is the S-duality of type I and $SO(32)$ heterotic theories, related by inversion of the string coupling constant, $g_s \to 1/g_s$ [82].

Along with the fact that both type IIA and the $E_8 \times E_8$ heterotic theories approach an 11-dimensional limit at strong coupling, these dualities have suggested that all superstring theories are related to a common fundamental M-theory. The elementary objects of this 11D theory cannot, however, be strings and are thought to be (2+1)-dimensional objects known as M2-branes or their (5+1)-dimensional magnetic dual M5-branes, with the former leading to fundamental strings after compactification of the eleventh dimension on a circle [82].

One of the most attractive features of string theory as a theory of QG is how it provides a solution to the problem of non-renormalizability by replacing point-like processes with non-local interactions of extended world-sheets, with string perturbation theory consisting of sums of intermediate world-sheet topologies. In fact, at each order in perturbation theory for closed oriented strings, the corresponding amplitudes have no UV divergences. The situation is more complicated for unoriented and for open strings, requiring the inclusion of non-perturbative effects such as D-branes,

which we describe below, although divergences also cancel in this case [82]. The perturbative series does not, however, converge and is not even Borel summable [89], only making sense as an expansion of some nonperturbative theory, namely M-theory.

Although a complete formulation of M-theory is still unavailable, compelling evidence for its existence comes from its low-energy limit, which gives 11-dimensional SUGRA. In fact, type II superstring theories, on which the majority of the analysis presented in this thesis is based, also yield a low-energy supergravity limit. The fields of 10-dimensional type IIA and IIB SUGRA theories arise from truncation of the closed string spectrum to the massless states, which include the graviton, two gravitinos[6], a scalar dilaton (whose vev sets the closed string coupling constant, g_s) and its spin-1/2 superpartner, the dilatino. Both cases also include a NS 2-form gauge field, $B_{\mu\nu}$, and RR p-form gauge fields $C_{\mu_1\cdots\mu_p}$, with $p = 1, 3$ in type IIA and $p = 0, 2, 4$ in type IIB[7]. In the case of type IIA SUGRA, these gauge fields can be directly obtained from dimensional reduction of the 3-form gauge field of 11D SUGRA.

String theory thus necessarily incorporates the idea of extra-dimensions, and low-energy phenomenology thus requires the extra 6-dimensional space to be compactified [90]. The requirement that at least $\mathcal{N} = 1$ SUSY remains as a low-energy symmetry, so as to implement the MSSM at the weak scale, then implies the existence of a covariantly constant Killing spinor in the compact manifold. This defines the latter to be a complex Kahler 3-fold with vanishing first Chern class and is generically denoted as a Calabi-Yau (CY) 3-fold[8] [91]. CY n-folds exhibit Ricci flatness and $SU(n)$ holonomy, canonical compact examples being T^{2n}, K^3 for $n = 2$ and the quintic in $\mathbb{C}P^4$ for $n = 3$. For $n > 2$, these manifolds may have a quite complicated topology and a complete classification is still unavailable [82].

The main problem with having an internal 6-dimensional manifold arises from the

[6] In type IIA, the two gravitinos have opposite chirality, whereas these are the same in type IIB.

[7] The nomenclature for these states arises from the type of b.c. considered in the RNS formalism for the left- and right-moving excitations of the superstring.

[8] In a vanishing NS and Yang-Mills background in the case of heterotic theories.

huge number of moduli fields determining the size and shape of the extra-dimensions and that show up as dozens or even hundreds of massless fields in the low-energy effective theory. Such scalars would source long-range gravitational forces, which we know to be pure tensor to better than 1% precision [82]. One of the major challenges and active research areas in modern string theory is, thus, to lift the degeneracy of these moduli and obtain isolated vacua with a stable internal manifold.

A successful method for moduli stabilization is the introduction of fluxes associated with the above mentioned p-form gauge fields through internal cycles of the CY manifold. This provides a stabilizing potential for the dilaton and complex structure moduli, which determine the shape of the internal manifold, but leave the Kähler moduli, e.g. the overall volume modulus, undetermined [92]. These can be stabilized, however, through the inclusion of non-perturbative effects[9]. This is the case of the KKLT scenario [93], where this procedure leads to an AdS SUSY vacuum, which can then be uplifted to a positive cosmological constant by the inclusion of $\overline{D3}$ branes.

In the BBCQ construction [94], the inclusion of both non-perturbative effects and α'^3-corrections leads to a non-SUSY AdS minimum in type IIB string theory, which can then be uplifted, making the overall volume of the CY exponentially large. The fundamental string scale $M_s^2 = 1/l_s^2 \sim M_p^2/\mathcal{V}$, where $\mathcal{V}$ denotes the volume modulus in units of the string length, could thus lie below the Planck scale. Although low-energy SUSY prefers an intermediate scale of $10^{10} - 10^{12}$ GeV, one can also obtain $M_s \sim$ TeV, thus realizing the ADD scenario discussed in the previous section[10] (see also [95] for flux compactifications in type IIA superstring theory).

Another generic effect of flux compactifications is the generation of warped geometries which can implement the RS construction described earlier. Such geometries are generically known as 'warped throats' [92, 96–100], canonical examples being

[9]These include e.g. gaugino condensation in an $\mathcal{N} = 1$ $SU(N)$ gauge theory arising in D7 branes or euclidean D3 branes in type IIB string theory.

[10]This situation leads, however, to very light moduli, which may be in conflict with fifth force experiments unless their coupling to matter is suppressed.

the Klebanov-Tseyltin/Strassler solutions (KT/KS) [101, 102] corresponding to an $AdS_5 \times T^{1,1}$ deformation of the conifold. Although the conifold is non-compact, it can be smoothly glued to a full compact CY manifold, implementing the UV brane of the RS model, while its smoothed tip in the KS geometry plays the role of the IR brane. A relevant difference with respect to the RS construction is the variation of the AdS curvature $k(y)$ along the throat, reducing in the IR [103, 104].

However, the several ways in which quantized units of flux can be introduced leads to an enormous number of possible vacua (see e.g. [105]), an often quoted number being 10^{500}, making string theory effectively lose the predictive power expected in a fundamental theory. In this 'landscape' of string vacua, one expects to find at least one realization of the (MS)SM with a small cosmological constant compatible with observations, as well as realistic inflaton candidates among the available scalar fields. Although this is still to be found, a huge effort has been made in understanding the structure of this landscape and the role of anthropic selection in this context [106].

String theory thus combines several ingredients of BSM scenarios, namely SUSY and extra-dimensions. However, it also has several novel features, leading to new interesting phenomenological applications and to which we devote the next subsections.

1.3.1 Branes

A major role in string theory compactifications is played by extended objects generically known as branes. Much like the 1-form gauge potential couples to charged point-particles in electromagnetism, the $(p+1)$-form gauge fields in the low-energy supergravity limit are naturally sourced by hypersurfaces with p spatial dimensions. These p-branes thus represent classical asymptotically flat solutions of the SUGRA equations of motion, which in type II theories in D dimensions take the form [107]:

$$ds^2 = h^{-\tilde{\gamma}} dx_p^2 + h^{\gamma} dy^2 \ , \qquad e^{\Phi} = h^{\kappa} \ , \qquad C_{01\cdots p} = \zeta(1 - h^{-1}) \ . \tag{1.11}$$

This solution represents a stack of N coincident branes with $d = p + 1$ world-volume coordinates $\{x^\mu\}$ and $D - d$ transverse coordinates $\{y^n\}$. The metric, the dilaton Φ and the gauge field C_{p+1} are given in terms of the harmonic function $h(r)$, which depends on the radial coordinate in transverse space, $r^2 = \delta_{mn} y^m y^n$, and is given by:

$$h(r) = 1 + \frac{Q_p}{r^{D-d-2}} \ . \tag{1.12}$$

The quantities that characterize the solution are given by[11]:

$$\gamma = \frac{4d}{(D-2)\Delta} \ , \qquad \tilde{\gamma} = \frac{4(D-d-2)}{(D-2)\Delta} \ , \qquad \kappa = \frac{2\alpha_n}{\Delta} \ , \qquad \zeta = \frac{2}{\sqrt{\Delta}} \ , \tag{1.13}$$

with

$$\Delta = \alpha_n^2 + \frac{2d(D-d-2)}{D-2} \tag{1.14}$$

and α_n representing the coupling of the $n = p+2$ field strength to the dilaton, which e.g. for RR forms corresponds to $\alpha_R = 2(D-2n)/(D-2)$. The total charge of the brane stack is given by

$$Q_p = c_p g_s N l_s^{D-d-2} \ , \tag{1.15}$$

with the constant $c_p = (2\sqrt{\pi})^{5-p}\Gamma\left(\frac{7-p}{2}\right)$. One can also construct anti-brane solutions with opposite charge. Both types of objects are BPS states, preserving half of the supersymmetries of the original action, although opposite supercharges are preserved for branes and anti-branes, making any composite system explicitly non-supersymmetric.

The nature of branes is, however, much deeper in the full string theory context. In particular, open strings can satisfy either Dirichlet or Neumann b.c., defining $(p+1)$-dimensional objects that correspond to the number of dimensions with b.c. of the latter type. In other words, open strings are naturally attached to Dirichlet

[11] These coefficients correspond to the Einstein frame, where the supergravity action takes the canonical Einstein-Hilbert form. Note that, in the string frame, $\gamma = \tilde{\gamma} = 1/2$ for all p-branes in $D = 10$.

branes, or D-branes for short. Polchinski then showed that different D-branes can interact via the exchange of closed string modes, in particular providing both electric and magnetic sources for the RR and NS gauge fields, so that, in fact, D-branes correspond to the same objects found in the low-energy SUGRA limit [108].

In type IIA theories, we then have electric D0 and D2 electric branes, as well as their magnetic duals, D4 and D6. We also have a D8-brane coupling to a non-dynamical F_{10} field strength. In type IIB, with a self-dual RR 5-form, we have D1, D3 and D5-branes, with the axion C_0 sourcing magnetic $D7$-branes and dual $D(-1)$-branes, which correspond to euclidean instanton solutions. We can also introduce spacetime-filling D9 branes in type IIB theory, although there are some restrictions to their occurrence [82]. Sources of the NS 2-form field correspond to fundamental strings, also known as F1, and magnetic NS5-branes. Moreover, as mentioned above, in M-theory we find membranes or M2-branes, which are electrical sources of the 3-form gauge field of 11D SUGRA, and their magnetic duals, M5-branes.

Several different configurations with multiple branes have also been studied in the literature, including parallel and intersecting sets of branes [109,110], the combination of branes with different dimensionalities [111] and also several possible embeddings in the compactified extra-dimensions [112].

In orientifold compactifications, associated with the world-sheet parity transformation $\Omega : \sigma \to -\sigma$ which reverses the orientation of a string, the loci of fixed-points under the orientifold action defines negative tension orientifold planes, or O-planes. These objects are non-dynamical but carry D-brane charge, thus contributing to the charge balance in compact spaces [82].

Branes thus have both perturbative and non-perturbative descriptions within string theory, at the same time connecting open and closed string modes and, thus, gauge and gravitational physics, respectively. A particularly interesting case is a stack of N D3-branes, which leads to a conformal $\mathcal{N} = 4$ $U(N)$ super Yang-Mills (SYM)

gauge theory, as strings attached to the different branes provide an adjoint representation of the latter group[12]. The six adjoint scalars then represent the positions of the (3+1)-dimensional branes in the CY 3-fold, constituting brane moduli.

On the other hand, the stack produces a geometry of the type in Eq. (1.11), which for a large number of branes approaches an $AdS_5 \times S^5$ geometry, in other words a throat. This has led to the conjecture by Maldacena [113, 114] that the near-horizon geometry of the stack gives an equivalent description of the world-volume conformal field theory (CFT). This AdS/CFT duality provides one of the best examples of the holographic principle, with all d.o.f. of the warped geometry encoded in its boundary, and has allowed for the study of gauge theories at strong coupling, including QCD [115], via their weakly coupled gravitational dual descriptions.

A stack of coincident branes preserves, however, too much supersymmetry, not providing chiral fermion representations that allow for a string description of the (MS)SM. These may, however, be obtained e.g. by considering branes at orbifold singularities or intersecting at angles. In the latter case, strings attached to distinct branes give rise to bi-fundamental chiral representations of the individual gauge groups, leading to the so-called quiver gauge theories that have been the basis for many SUSY and non-SUSY constructions of the SM, although generically with additional exotic vector-like matter [109,110,112]. The Higgs mechanism has also a simple geometric description in this context, as brane separations correspond to scalar fields, with finite vevs necessarily breaking the gauge symmetry of a coincident brane stack.

The construction of (MS)SM-like models and GUT extensions is an active research area, with a large effort being also made in the context of heterotic theories (see e.g. [116]) and the F-theory description of type IIB string theory with D7-branes [117]. The inclusion of D7-branes in warped throats is also a possible realization of bulk SM gauge bosons and fermions in the RS construction [118, 119].

[12] $SO(n)$ and $Sp(n)$ gauge groups can also be obtained in the presence of O-planes.

The existence of brane moduli has also motivated the search for an inflaton candidate among them, both in the context of effective field theories [71, 120] and string theory [121]. The simplest example consists of an anti-brane probing the geometry generated by a stack of D-branes of the form in Eq. (1.11), generating a potential for the separation between them. In the probe brane approximation, where its gravitational backreaction may be neglected, this potential can be determined from the p-brane action, which generalizes the Nambu-Goto action in Eq. (1.10) for a $(p+1)$-dimensional world-volume with coordinates $\{\xi^\mu\}$ [122]:

$$S_{probe} = S_{BI} + S_{WZ} = -T_p \int d^{p+1}\xi \; e^{-\Phi} \sqrt{-det(\hat{\gamma}_{\mu\nu} + 2l_s^2 \mathcal{F}_{\mu\nu})} - qT_p \int C_{p+1} \; , \quad (1.16)$$

where T_p denotes the brane tension, $q = \pm 1$ its charge in units of the latter[13], $\hat{\gamma}_{\mu\nu} = \hat{g}_{MN} \partial_\mu x^M \partial_\nu x^N$ the metric induced on the brane by the background geometry, $\hat{g}_{MN}$[14], and $\mathcal{F}_{\mu\nu}$ the world-volume $U(1)$ field strength from open string gauge modes[15]. The two contributions above are known as the Born-Infeld and Wess-Zumino actions, respectively. Notice that this procedure is valid when the probe is far away from the brane stack, $r \gg l_s$, for closed string mode exchange to dominate brane interactions, and also within the validity of the SUGRA approximation, with small curvatures and weak string coupling $g_s e^{\Phi}$ everywhere in the compact region probed by the brane.

However, the potential thus determined for a D$p-\overline{\text{D}p}$ system, which we will discuss in more detail in chapter 2 for $p = 6$, is not flat enough to allow for a sufficiently long period of inflation [124, 125]. This seems to be a generic feature of SUGRA and string theory models, where the inflaton candidates acquire an excessively large mass, although some more promising scenarios have been constructed by placing branes in highly warped throats in the context of KKLT moduli stabilization [126] and by

[13] The positive sign is defined for a brane, with a negative sign for an anti-brane.

[14] The hatted metric tensors are defined in the string frame and are related to the Einstein frame metrics, where the action takes the Einstein-Hilbert form, by $\hat{g}_{\mu\nu} = e^{\lambda\Phi} g_{\mu\nu}$, with $\lambda = 4/(D-2)$.

[15] In this thesis, we will consider the particular scenario where the classical background of these gauge fields vanishes. The role of gauge fields in brane systems was considered in [123].

considering other moduli fields (see [127] for a recent overview).

Although inflation remains an open problem in string theory, there are several other potential cosmological applications of brane systems. In particular, flux conservation in a compact space generically requires the presence of several brane stacks interacting weakly with each other, potentially only via gravitational interactions. This opens the possibility for a plethora of hidden sectors where SUSY can be broken at a high scale and where new DM candidates may be found. Another interesting potential mechanism for both dark and baryonic matter generation in the early universe is discussed in chapter 2 in the context of *branonium* bound states.

1.3.2 String excitations

One of the unique features of string theory with respect to other BSM constructions is the existence of infinite towers of higher spin states associated with the SM d.o.f., besides the KK towers arising from compactification of the 6-dimensional CY manifold, corresponding to quantized massive excitations of the fundamental strings. Due to the vectorial spacetime nature of the world-sheet fields, X^μ and ψ^μ in the RNS formulation, consecutive excitations differ by one unit of spin, with masses increasing in steps of the string scale. This leads to the well-known string Regge trajectories [128]:

$$J = J_0 + \alpha' M^2 \ , \tag{1.17}$$

with J_0 corresponding to the lowest spin in the tower. The first massive states thus correspond to spin-1 excitations of the Higgs boson, spin-2 excitations of the SM gauge bosons and spin-3/2 quark and lepton excitations. Their mass depends, of course, on the particular compactification considered and, as observation of such states at the LHC would constitute a unique smoking gun for a fundamental string theory[16], a lot

[16]Higher spin excitations of the SM fields may also arise in the context of composite models such as technicolour (see e.g. [129, 130]).

of work has been done in the context of models with $M_s \lesssim$ few TeV.

In the context of the large volume compactifications described above, with intersecting brane (MS)SM-like configurations, string excitations have been shown to be sufficiently light to induce observable effects in current TeV-scale experiments [128, 131–134], both through virtual and real effects. For instance, $2 \to 2$ scattering amplitudes with exchange of virtual string modes have the Veneziano form, which after neglecting kinematical factors is given by [128]:

$$\mathcal{A}(k_1, k_2, k_3, k_4; \alpha') \sim -\frac{\Gamma(-\alpha' s)\Gamma(1-\alpha' u)}{\Gamma(-\alpha' s - \alpha' u)} = \sum_{n=0}^{+\infty} \frac{\gamma(n)}{s - M_n^2} \ , \tag{1.18}$$

where k_i, $i = 1, \cdots, 4$, denote the external momenta, while s, t and u are the usual Mandelstam invariants. The integer n labels the string excitations exchanged in the interaction, with masses $M_n^2 = M_s^2 n$, which appear as s-channel poles in the amplitude with a coefficient $\gamma(n) \sim (-\alpha' u)^n$. Hence, the α' expansion gives rise to contributions from SM particles ($n = 0$) and higher spin excitations ($n > 0$) and these amplitudes have been analyzed in the context of both SM processes and processes which are absent at tree-level in the SM, such as $gg \to g\gamma$ and also $gg \to \gamma\gamma$.

Other interesting possibilities for TeV-scale string excitations arise in the context of warped geometries, which as discussed above are quite generic in the context of flux/D-brane compactifications. In the type IIB $\mathrm{AdS}_5 \times S^5$ solution, dual to a $SU(N)$ SYM gauge theory, the string scale is parametrically heavier than the KK scale k arising from the S^5 by a factor $M_s/k \sim (g_s N)^{1/4}$, and thus decouples from the theory in the formal N and $g_s N \to \infty$ limits in which supergravity is a good description of the gravitational side of the duality [114]. However, in string realizations of RS throats, the curvature length $1/k$ of the AdS_5 space is not much longer than the 5D Planck length, $M_5/k \sim N^{2/3} \sim$ few being typical. Since we expect (or require) $g_s < 1$, we deduce that the string oscillators may be only slightly heavier than the bulk KK modes

in this case. Also, as mentioned above, the effective curvature length changes along the throat, reducing in the IR tip. Presently, we do not have a good understanding of this variation, so that $M_5/k(y_{IR})$ is taken as a free parameter, and in fact $\mathcal{O}(1)$ values have significant potential phenomenological advantages in ameliorating the problems of the EW phase transition in RS scenarios [104,135], with N-enhanced contributions to precision EW observables possibly reduced to acceptable levels (see also [136–138] for other phenomenological consequences). Furthermore, compactification of the full 10-dimensional space into a 5-dimensional RS description may also reduce the bulk masses of string excitations with respect to M_s.

We thus expect that, in realizations of the warped RS scenario, the masses of low-lying string excitations are not necessarily much heavier than the KK modes at the tip of the throat, which has recently been confirmed in the analysis of particular compactifications done in [139]. Given the present experimental constraints on the KK mass scale, M_{KK}, we therefore do not expect the LHC to explore the kinematic regime $\sqrt{s} \gg M_s$ where soft Veneziano-like behaviour applies, but a regime where at most one or two Regge excitations might be directly produced, a possibility we further explore in chapter 3 by directly including the lightest spin-3/2 resonances of bulk SM fermions in the RS model.

1.3.3 Axions in string theory

As described in 1.1.3, the QCD axion is presently the best known solution to the strong CP-problem, so that one should expect any realistic BSM theory to incorporate it. In fact, axion-like particles arise in string theory as KK zero modes of the antisymmetric NS and RR gauge p-forms after dimensional reduction to four dimensions. For example, in type II theories, the RR p-form field C_p is described by the

low-energy supergravity action [24]:

$$S_{RR} = -\frac{2\pi}{l_s^{8-2p}} \int \frac{1}{2} F_{p+1} \wedge \star F_{p+1} + 2\pi \int C_p \ , \tag{1.19}$$

where the field is normalized so that the corresponding field strength F_{p+1} has integer periods and the second term represents the Wess-Zumino coupling of the field to D$(p-1)$-branes. We may then consider a basis $\{Q_i\}$ of cycles for the homology group $H_p(X, \mathbb{Z})$ of the compactification manifold X and a dual cohomology basis $\{\omega_j\}$ normalized such that

$$\int_{Q_i} \omega_j = \delta_{ij} \ . \tag{1.20}$$

In this basis, RR-axions arise from the decomposition:

$$C_p = \frac{1}{2\pi} \sum_i a_i \, \omega_i \ , \qquad i = 1, \cdots, b_p(X) \ . \tag{1.21}$$

If we replace this *ansatz* in Eq. (1.19), we obtain the axions kinetic terms:

$$S_{kin} = -\frac{1}{2} \sum_{i,j} \int d^4x \, \gamma_{ij} \partial_\mu a_i \partial^\mu a_j \ , \qquad \gamma_{ij} = \frac{1}{2\pi l_s^{8-2p}} \int_X \omega_i \wedge \star \omega_j \sim \frac{R^{6-2p}}{2\pi l_s^{8-2p}} \ , \tag{1.22}$$

where $V_X = R^6$ and we omitted $\mathcal{O}(1)$ factors. Axionic couplings to gauge bosons then arise from the Chern-Simons term for branes wrapping each cycle $\{Q_i\}$:

$$S_{CS} = 2\pi \int_{\mathbb{R}^{3,1} \times Q_i} C_p \wedge \frac{1}{8\pi^2} \mathbf{tr} F \wedge F \qquad \Rightarrow \qquad S_{gauge} = \sum_i r_i \int d^4x \, a_i \frac{\mathbf{tr} F \wedge F}{8\pi^2} \ , \tag{1.23}$$

where $r_i = \int_{Q_i} \omega_i$ are integers. These couplings then break the axion shift symmetry, inherited from the 10-dimensional gauge symmetry of the RR fields, producing the axion potential required to solve the strong CP-problem. Canonically normalizing

the fields and comparing with Eq. (1.3), one obtains an axion decay constant

$$f_a \sim \left(\frac{R^{6-2p}}{2\pi l_s^{8-2p}}\right)^{1/2} \sim M_p \left(\frac{l_s}{R}\right)^p \sqrt{\frac{g_s^2}{64\pi^3}} \ , \qquad M_p^2 = \frac{1}{2g_s^2}\frac{V_X}{l_s^6} M_s^2 \ . \tag{1.24}$$

The string coupling determines the gauge coupling of the theory living in the D-branes' world-volume via $g_s = \alpha(R_Q/l_s)^p$, so that validity of perturbation theory requires a 'vanishing' cycle with size $R_Q \ll R$ and $R \gg l_s$ in order for f_a to satisfy the cosmological bound discussed earlier, which may be obtained in the context of the large volume scenarios.

However, typical compactifications give $f_a \sim 10^{16}$ GeV, which largely exceeds the phenomenological bounds [15, 24]. Some proposals have been made to relax this bound, namely through anthropic arguments [140] (e.g. in the context of the string landscape), which select a small value for the initial misalignment angle in order to avoid overclosure of the universe by axionic dark matter, usually predicting a significant amount of the latter. Other possibilities include e.g. a strongly coupled QCD in the early universe [141], a late entropy production due to particle decays [142] and an extremely low reheating temperature [143, 144]. An asymmetric CY manifold or a compactification with large warping can also be used to achieve this [24, 145].

Given their extra-dimensional origin, string theory axions may also receive contributions to their potential from other non-perturbative sources besides QCD, such as gravitational instantons [146], world-sheet instantons [147] and euclidean branes [148], as well as gauge instantons from other factors of the gauge group. Contributions from both instantons and anti-instantons give a generic potential of the form:

$$V(a) = -2\mu^4 e^{-S} \cos(a + \psi) \ , \tag{1.25}$$

where S is the instanton action (roughly the volume of the corresponding cycle), ψ is an arbitrary phase and the UV scale $\mu^4 = M_p^2 M_{SUSY}^2$ if the axion potential

arises from the superpotential generated by string instantons. In order to satisfy the experimental bounds on $\bar{\theta}$, these contributions must be suppressed with respect to the QCD potential at the minimum, so that [24]:

$$e^{-S} < 10^{-10} r \frac{f_\pi^2 m_\pi^2}{\mu^4} \qquad \Rightarrow \qquad S \gtrsim 200 \ . \tag{1.26}$$

Furthermore, one generically obtains $f_a \lesssim M_p/(\sqrt{8\pi}S)$, leading to the generic GUT-scale decay constants mentioned above. For instance, for the C_0 axion in type IIB string theory, associated with D3-branes 'wrapping' a point, one finds:

$$f_a = \frac{g_s}{2\pi} \frac{M_p}{\sqrt{16\pi}} \ , \tag{1.27}$$

while its shift symmetry is broken by D(-1)-brane instantons on the D3-branes world-volume, with an action $S = 2\pi/g_s$.

The above constraint applies, of course, only to the QCD axion, which one expects to find amongst the plethora of available axion-like fields arising from the large number of homologically non-equivalent cycles present in typical compactifications. Some of these fields may, however, be completed removed from the low-energy spectrum in the presence of fluxes, branes and O-planes, which lead to large tree-level masses for axions in the corresponding cycles [105, 149]. However, the requirement of a QCD axion implies that at least one of these fields is present in the light particle spectrum, disfavouring SUSY-preserving moduli stabilization scenarios such as KKLT, where both the axion and its superpartners acquire large SUSY-preserving masses.

As argued in [150], however, it would be surprising if only the QCD axion survived in the low-energy spectrum, and one expects a plethora of other light axions in generic compactifications. Their masses will only be determined by string instanton effects, $m \sim M_{SUSY} S e^{-S/2}$, being exponentially sensitive to the size of the corresponding cycles. This leads to the expectation that, in realistic string compactifications solving

the strong CP-problem, there should be a landscape of ultra-light axions uniformly populating all mass scales, possibly down to the present Hubble scale, $H_0 \sim 10^{-33}$ eV. The authors of [150] denoted this as the 'string axiverse', an exciting proposal which suggests string theory may lead to observable signatures in the sub-eV range (see [151] for a concrete construction). They also suggested several phenomenological applications of this proposal, including rotation of the CMB polarization, steps in the matter power spectrum and superradiant emission from rotating black holes. In chapter 4, we focus on the quantitative aspects of the latter mechanism, while a detailed phenomenological analysis can be found in [152].

1.4 Outline

In this thesis, we explore some of the phenomenological aspects of string theory described above. In the absence of a complete realization of the (MS)SM, we consider particular low-energy models which illustrate the inclusion of string theory ingredients in BSM scenarios. This bottom-up approach isolates particular mechanisms and features which allow one to make generic predictions for potential BSM signatures of string theory. The phenomenologically allowed parameter space will then have to be constrained by embedding these scenarios in realistic compactifications.

As discussed earlier, one expects string theory to introduce a plethora of new physical effects, arising from different levels of compactification of the internal 6-dimensional manifold and spanning a wide range of energy scales, potentially from the deep sub-eV limit all the way up to the Planck scale. This suggests one should look for signatures of string theory not only in collider experiments such as the LHC, but also in astrophysical systems and early universe physics.

In the next chapter, based on the original work done in [153], we analyze the cosmological significance of brane-world scenarios, focusing on the *branonium* system,

a brane/anti-brane bound state. Although too simple for a realistic realization of the (MS)SM, this system provides the natural framework to study the interplay between bulk gravitational interactions and the world-volume particle dynamics. In particular, we show that the elliptical orbits of the D6-$\overline{\text{D6}}$ system lead to a resonant production of particles, which may be responsible for dark or baryonic matter generation in the early universe. This constitutes an intrinsically 'stringy' realization of the well-known preheating mechanisms, although it is not necessarily connected with inflation. We study several aspects of this system, in particular how Hubble expansion and the compact nature of the transverse space affect the particle production mechanism.

Chapter 3 is dedicated to the study of collider signatures of spin-3/2 excitations of SM fermions arising in warped compactifications, based on the original work done in [154]. As discussed above, the 5-dimensional RS construction provides an effective description of these throats, so that we analyze the spectrum of string excitations in this framework, guided by the observed fermion mass hierarchy and other phenomenological constraints. Since the rhd top quark excitation is the lightest of these resonances in a large region of the allowed parameter space, we then focus on its potential observability at both the Tevatron and the LHC.

On the opposite end of the string theory spectrum, we analyze in chapter 4 the production of (pseudo-)scalar particles via the superradiant instability of Kerr black holes, motivated by the recent string axiverse proposal. The growth rate of this instability is a crucial issue for phenomenological signatures of string theory axions and earlier works suggest that it is maximal for extremal black holes and scalar masses in the range where the associated Compton wavelength is comparable to the horizon radius. Recent attempts to address this regime exhibit, however, largely discrepant results, so that we present a novel procedure for computing the spectrum of superradiant bound states that eliminates some of the deficiencies of previously employed methods, based on the original work done in [155].

We conclude in chapter 5 with a summary and critical appreciation of our results.

Unless otherwise stated, we will use natural units $\hbar = c = 1$. Other conventions and notation are specific to each chapter and clearly indicated where appropriate. All Feynman diagrams were created using JaxoDraw [156].

Chapter 2

Branonium

The name *branonium* was introduced in [122] to denote a bound state of branes with opposite charges, in the same way an e^+e^- bound state is known as *positronium*, despite the different interactions involved. As discussed in chapter 1, branes interact via the exchange of closed string modes, which allows one to study them as massive point-like charged objects moving along the dimensions transverse to their world-volumes.

The analysis of [122] considered a probe anti-brane moving in the background geometry created by a fixed central stack of N branes with the same dimensionality, given by Eq. (1.11), neglecting the gravitational backreaction of the probe. In this work, several properties of this system were analyzed, including the classical orbits, the associated quantum dynamics and possible compactification schemes. In the particular case of $D6$-branes, the probe's trajectory follows closed elliptical orbits similar to those found in planetary systems. It was also suggested that the probe's motion would lead to radiation of particles into both the bulk space and the probe's world-volume, making otherwise stable orbits decay. The stability of this system was further studied in [157], where it was shown that orbital decay necessarily occurs when geometric moduli of the background spacetime are allowed to vary.

In this chapter, we explore some properties of such branonium systems, focusing on the mechanism leading to particle production in the world-volume of the probe brane, showing how in the case of $D6$-branes it leads to a parametric resonance regime similar to the one behind the phenomenon of preheating after inflation[1].

This mechanism is highly dependent on the orbital parameters of the system, so that we analyze several effects that may potentially modify the orbital motion, namely the Hubble expansion of the three extended dimensions parallel to the probe's world-volume and the compact nature of the transverse space where it moves. Other sources of orbital instability such as radiation into bulk modes are also discussed.

The cosmological significance of this system and the associated particle production mechanism is also dependent on the final configurations of the system, so that we study the consequences of both stable states and brane–anti-brane annihilation.

2.1 Orbital motion in an expanding universe

Before analyzing the motion of the probe brane, we need to consider possible compactifications of the 10-dimensional spacetime that yield our 4-dimensional world at low energies. Compactification of dimensions parallel and transverse to the world-volume of the p-branes involve different procedures. In the case of dimensions parallel to the branes, it suffices to consider the KK *ansatz*. If we start with the D-dimensional spacetime Eq. (1.11) and compactify along a periodic coordinate $z \simeq z + 2\pi R$ with radius R, so that the branes are wrapped around this dimension, we obtain a $D' = (D-1)$-dimensional spacetime with metric given by [107]:

$$ds_D^2 = e^{2\hat{a}\varphi} ds_{D'}^2 + e^{2\hat{b}\varphi}(dz + \mathcal{B}_\mu dx^\mu)^2 \ , \quad ds_{D'}^2 = h^{-\tilde{\gamma}'} dx_{p'}^2 + h^{\gamma'} dy^2 \ , \quad e^{\varphi} = h^{\rho} \ , \tag{2.1}$$

[1]Discussions of preheating in brane systems other than branonium can be found in [158].

where

$$\begin{aligned} \hat{a} &= \frac{1}{2(D'-1)(D'-2)} \ , \qquad \hat{b} = -(D'-2)\hat{a} \ , \qquad \rho = \frac{\tilde{\gamma}}{2(d'-2)\hat{a}} \ , \\ \gamma' &= \gamma - 2\hat{a}\rho \ , \qquad \tilde{\gamma}' = \tilde{\gamma} + 2\hat{a}\rho \ . \end{aligned} \tag{2.2}$$

The dilaton field Φ is not altered by this compactification, while the $(p+1)$-form RR field can be decomposed as follows:

$$C_{p+1} = B_{p+1} + B_p \wedge dz \tag{2.3}$$

and we take the following truncation of these fields:

$$B_{p+1} = 0 \ , \qquad (B_p)_{01\cdots p-1} = \zeta(1 - h^{-1}) \ . \tag{2.4}$$

This truncation leads to a $(p-1)$-brane supergravity solution in $D-1$ dimensions, characterized by the same harmonic function $h(r)$. Applying this *toroidal compactification* procedure j times we obtain $(p-j)$-brane solutions in a $(D-j)$-dimensional spacetime, with the same number of transverse dimensions.

Compactification of the dimensions transverse to the branes is not as straightforward due to the lack of translational invariance which results from the presence of the branes. In particular, to make a given transverse coordinate z' periodic one needs to include the appropriate 'image branes' of the source branes, which ensure the invariance of the configuration under $z' \to z' + 2\pi R'$, R' being the radius of the compact dimension. For example, if a source brane is located at $z' = 0$, an image brane has to be considered at $z' = 2\pi R'$. This implies a generalization of the harmonic function in Eq. (1.12) to include branes located at different points in the transverse space [107]:

$$h(\mathbf{y}) = 1 + \sum_i \frac{Q_p}{|\mathbf{y} - \mathbf{y_i}|^{D-d-2}} \ , \tag{2.5}$$

where $\mathbf{y_i}$ denote the brane positions and $|\mathbf{y} - \mathbf{y_i}|^2 = \delta_{mn}(y^m - y_i^m)(y^n - y_i^n)$.

These two compactification schemes allow us to reduce a 10-dimensional solution of the supergravity field equations to a 4-dimensional spacetime which resembles our world. As mentioned above, we are interested in studying the particular case of D6-branes. As was shown in [122], when the probe carries an anti-brane charge, the system yields closed elliptical orbits which can be solved analytically, while for other values of $p < 7$ the orbits fail to close.

Compactifying three of the dimensions parallel to the branes, we obtain effective D3-branes moving in a 3-dimensional transverse space, the shape of the orbits not being affected by this toroidal compactification scheme as mentioned before. If the transverse dimensions are finite but their typical size is much larger than that of the compact parallel dimensions and the interbrane distance, we may consider them to be infinite and neglect the brane images described before. Although this would correspond to a 7-dimensional spacetime, from the point of view of world-volume fields it is effectively 4-dimensional. The dynamics in the transverse space will, nevertheless, affect the 4-dimensional dynamics of the fields, as we will discuss later in this chapter.

In order to make the system more similar to the observable universe, we consider a modification of the solution Eq. (1.11) so that, after compactification of three of the parallel dimensions, the 4-dimensional world-volume of the branes has a flat Friedmann-Robertson-Walker (FRW) geometry. This is a particular case of the system studied in [157], where the moduli governing the size of both parallel and transverse dimensions were allowed to vary. Here, we will assume that some dynamical mechanism, such as those discussed in chapter 1, fixes all moduli except the scale factor of the three non-compact dimensions parallel to the branes. Hence, in the Einstein frame, the complete 7-dimensional line element is given by:

$$ds_7^2 = h^{-\tilde{\gamma}_4}[-dt^2 + a^2(t)\delta_{ij}dx^i dx^j] + h^{\gamma_4}\delta_{mn}dy^m dy^n \ , \tag{2.6}$$

where $i, j = 1, 2, 3$, $m, n = 1, 2, 3$ and $h(r) = 1 + Q_6/r$. The exponents γ_4 and $\tilde{\gamma}_4$ can be obtained using Eq. (1.13) and applying Eq. (2.2) for the compactification on a 3-torus, but their precise values are not relevant for subsequent calculations.

The motion of the probe brane is described by the action Eq. (1.16), so that, for $p = 6$ and after compactification into four dimensions, one obtains an effective action:

$$S_4 = -T_6 V_3 \int d^4x \; a^3(t) \left[\frac{1}{h} \sqrt{1 - h v^2} + q \left(1 - \frac{1}{h} \right) \right] , \tag{2.7}$$

where V_3 gives the volume of the compact 3-torus around which the D6-branes are wrapped. We have assumed that the transverse space coordinates are exclusively time-dependent, $y^m = y^m(t)$ and defined the velocity of the probe as $v^2 = \delta_{mn} \dot{y}^m \dot{y}^n$, with dots denoting time derivatives. As mentioned before, the bound orbits of the probe brane can be exactly solved for the case where the scale factor is constant and it was shown in [122] that they correspond to closed ellipses. We now wish to analyze the effects of the varying scale factor on these orbits. In this case, a full analytical solution is hard to obtain and it is simpler to consider the evolution of the system when the probe brane moves at larges distances from the stack with small velocities. These two conditions can be expressed as $h v^2 \ll 1$. One must recall that we considered initially that the transverse dimensions can be considered infinite in extent. Hence, our analysis will hold as long as the radial coordinate is large compared to the typical length scale of the harmonic function, given by Q_6 (assumed larger than the string scale and the compactification scale), but still much smaller than the typical size of the transverse dimensions (assumed much larger than Q_6). With this hierarchy in mind, we may expand the probe brane's action to obtain, to lowest order,

$$S_4 \approx -T_6 V_3 \int d^4x \; a^3(t) \left[\frac{1}{h} \left(1 - \frac{1}{2} h v^2 - q \right) + q \right] . \tag{2.8}$$

Our subsequent analysis will not be affected by the constant term so that we may

drop it. For a probe anti-brane,

$$S_4 \approx T_6 V_3 \int d^4x \; a^3(t) \left[\frac{1}{2} \sum_i \dot{y}_i^2 - \frac{2}{h} \right] . \tag{2.9}$$

The rotational symmetry of the problem implies that the probe's trajectory will be confined to a plane, which we may choose to be $y^3 = 0$. Then, we may define the canonically normalized complex scalar field

$$\phi \equiv \sqrt{\frac{T_6 V_3}{2}} (y^1 + i y^2) \; , \tag{2.10}$$

so that its action is, in the non-relativistic and large distance limit,

$$S_\phi = \int d^4x \; a^3(t) \big(- g^{\mu\nu} \partial_\mu \phi \partial_\nu \phi^* - V(\phi) \big) \; , \tag{2.11}$$

where $g_{\mu\nu}$ is the 4-dimensional flat FRW metric of the spacetime where the field is defined and the potential is given by:

$$V(\phi) = 2 T_6 V_3 h^{-1} \approx 2 T_6 V_3 \left(1 - \sqrt{\frac{T_6 V_3}{2}} \frac{Q_6}{|\phi|} \right) \; , \tag{2.12}$$

so that it only depends on $\rho = |\phi|$. Note that in writing the action in this form one must take into account that the spatial derivatives of the field, $\partial_i \phi$, $i = 1, 2, 3$, are assumed to vanish, i.e. the probe brane should remain parallel to the source branes during its motion. The analysis of the classical motion of the probe brane is in this way reexpressed as a classical field theory problem of a complex scalar field in the background of a flat FRW spacetime. Before deriving the equations of motion for the field ϕ, it is useful to consider some of the symmetries of the action. First, the rotational symmetry of the problem in the plane transverse to the branes is associated with a conserved angular momentum. In terms of the field theory approach, this

corresponds to the global $U(1)$ invariance of the action under $\phi \to e^{i\alpha}\phi$, where α is a constant. The associated Noether current induces a conserved charge which gives, in the quantum theory, the particle number operator associated with the field. Writing the field as $\phi = \rho e^{i\theta}$ and defining the comoving angular momentum as $l \equiv \rho^2\dot{\theta}$, the comoving particle number density is given by:

$$n = i(\dot{\phi}^*\phi - \dot{\phi}\phi^*) = 2\rho^2\dot{\theta} = 2l \ , \tag{2.13}$$

while the total particle number, which corresponds to the conserved Noether charge, is given by $N = a^3 n$. The energy density and pressure of the field can be obtained from its energy-momentum tensor, yielding:

$$\epsilon \equiv T_{00} = |\dot{\phi}|^2 + V(\phi) = \dot{\rho}^2 + \frac{l^2}{\rho^2} + V(\rho) \ , \qquad p \equiv \frac{T_{ii}}{a^2} = |\dot{\phi}|^2 - V(\phi) = \dot{\rho}^2 + \frac{l^2}{\rho^2} - V(\rho) \ . \tag{2.14}$$

The covariant conservation of the energy-momentum tensor, $T^{\mu\nu}{}_{;\nu} = 0$, can then be expressed in the form of the First Law of Thermodynamics, $dE = -pdV$, where the energy of the field is defined as $E \equiv a^3\epsilon$ and $V = a^3$ is the volume of the expanding FRW spacetime. Defining the Hubble parameter $H \equiv \dot{a}/a$, we can write this as:

$$\frac{d\epsilon}{dt} = -3H(\epsilon + p) \ . \tag{2.15}$$

From Eqs. (2.14) and (2.15) we conclude that $\frac{d\epsilon}{dt} \leq 0$, the equality holding only for $H = 0$. Thus, in an expanding universe ($H > 0$), the system evolves with a strictly decreasing energy density. The angular momentum evolves according to:

$$\frac{dl}{dt} + 3Hl = 0 \ , \tag{2.16}$$

so that the total particle number N is conserved. Hence, in an expanding universe,

the absolute value of the angular momentum decreases, vanishing asymptotically.

We, thus, conclude from this simple analysis of conservation laws that the expansion of the universe will make the system reduce both its energy density and its angular momentum. To analyze the details of this evolution, we need to determine the equations of motion for the field ϕ. Varying the action Eq. (2.11) with respect to ϕ^*, and taking this variation to vanish, we obtain:

$$\ddot{\phi} + 3H\dot{\phi} + \frac{\partial V(|\phi|)}{\partial \phi^*} = 0 \ . \tag{2.17}$$

In terms of the transverse space coordinates y^m, $m = 1, 2, 3$, and the radial distance r this can be written as:

$$\ddot{y}^m + 3H\dot{y}^m + 2Q_6 \frac{y^m}{r^3} = 0 \ . \tag{2.18}$$

This implies that the polar variables ρ and θ satisfy:

$$\ddot{\rho} + 3H\dot{\rho} - \frac{l^2}{\rho^3} + \frac{1}{2}\frac{\sigma}{\rho^2} = 0 \ , \qquad \ddot{\theta} + 2\frac{\dot{\rho}}{\rho}\dot{\theta} + 3H\dot{\theta} = 0 \ , \tag{2.19}$$

where we have defined the constant

$$\sigma \equiv 4Q_6 \left(\frac{T_6 V_3}{2} \right)^{3/2} \ , \tag{2.20}$$

so that, apart from constant factors, the large distances potential is $V(\rho) = -\frac{\sigma}{\rho}$. It is easy to check that the equation for θ simply gives the evolution of the angular momentum that we obtained previously in Eq. (2.16).

The evolution of the radial field ρ is determined by the Hubble parameter, given by the energy density content of the universe via the Friedmann equation in the usual way. This may include not only the energy density of the field ϕ but also all other

matter, radiation or vacuum energy components. The possibility that this scalar field may drive (slow-roll) inflation if, in the early universe, it dominates the energy density has been analyzed in [124], for the case where the probe brane moves in a linear trajectory, i.e. $l = 0$. However, as mentioned in chapter 1, the interbrane potential in type II supergravity/string theories is not sufficiently flat to produce the required number of e-foldings, which is intrinsically related to the assumption that r is much smaller than the size of the transverse dimensions.

An inflationary period driven by the angular field variable θ was proposed in [122], where it is argued that, despite having a flat potential, this field may provide the constant energy density necessary for inflation if the probe brane moves in a circular orbit with $\dot{\rho} = 0$. However, we need to take into account the fact that, during inflation, the angular momentum decays exponentially as $l \propto e^{-3Ht}$, from Eq. (2.16). The system will hence quickly tend to the $l = 0$ case, where sufficient inflation is difficult to obtain. Furthermore, the decay of the angular momentum will necessarily alter the evolution of ρ and the value of H, so that a slow-roll inflationary mechanism with the probe brane moving in a circular orbit would be hard to construct[2].

Although we do not wish to completely discard such inflationary mechanisms, we will from now on assume that some other field is responsible for inflation and analyze how the compactified $D6 - \overline{D6}$ system evolves in the post-inflationary eras.

Before analyzing in detail the effects of the expansion on the trajectory of the probe, let us recall the general bound orbits of the system in a non-expanding universe. In this case, the system reduces to the well-known problem of a particle in a central $1/\rho$ attractive potential, admitting closed orbit solutions of the form:

$$\rho(\theta) = \frac{R(1-e^2)}{1 + e\cos\theta} \ . \tag{2.21}$$

[2]Some work has been done recently in the context of D-branes moving in warped throats [159]. The role of angular variables in providing accelerated periods of expansion was discussed in [160].

These are closed ellipses with eccentricity and semi-major axis given by:

$$e = \left(1 + \frac{4\epsilon l^2}{\sigma^2}\right)^{\frac{1}{2}} , \qquad R = -\frac{\sigma}{2\epsilon} . \tag{2.22}$$

The properties of such orbits may be obtained by studying the effective potential $V_{eff}(\rho) = l^2/\rho^2 + V(\rho)$. This potential has a minimum at $-(\sigma/2l)^2$, tends to $+\infty$ at the origin and to zero at large distances. The condition $\dot{\rho} \geq 0$ then implies that orbits with $-(\sigma/2l)^2 < \epsilon < 0$ will be bounded, with $0 < e < 1$. In this case, ρ will oscillate between its minimum and maximum values, $\rho_{min} = R(1-e)$ and $\rho_{max} = R(1+e)$, which can be obtained from Eq. (2.21) by setting $\theta = 0$ and $\theta = \pi$, respectively. At the minimum of $V_{eff}(\rho)$, the orbits will be circular with $\rho = \rho_c = 2l^2/\sigma$, and $e = 0$. For $\epsilon \geq 0$, the orbits will only be bounded from below with e.g. $\rho \geq l^2/\sigma$ for $\epsilon = 0$, which corresponds to an $e = 1$ parabolic orbit. The linear trajectory, with $l = 0$, is a particular case of the latter with no bounds on the value of ρ except for the trivial $\rho \geq 0$. For $\epsilon > 0$, the orbits are hyperbolic.

Consider now the expanding case with the scale factor evolving as $a(t) \propto t^\alpha$. This power law behaviour is typical of the post-inflationary stages of the universe's evolution, where one may consider a single fluid to give the dominant contribution to the total energy density. For example, in the radiation era we have $\alpha = 1/2$ and in the matter era $\alpha = 2/3$. We can also take $\alpha = 2/3$ at the end of inflation, when the oscillations of the inflaton about the minimum of its potential, with an equation of state corresponding to that of non-relativistic matter, dominate the energy density. This model only holds away from the transitions between these periods as in these cases at least two of the components give similar contributions to the energy density.

We will consider the evolution of the branonium system for arbitrary α, starting at some instant t_0 when the scale factor has a value $a_0 \equiv a(t_0)$. The Hubble parameter is then of the form $H = \frac{\alpha}{t}$, which implies from Eq. (2.16) that the angular momentum

evolves according to:

$$l = l_0 \left(\frac{t}{t_0}\right)^{-3\alpha} , \tag{2.23}$$

with l_0 being the initial value of the angular momentum. The equation for the radial field ρ can now be written as:

$$\ddot{\rho} + \frac{3\alpha}{t}\dot{\rho} - \frac{l_0^2}{\rho^3}\left(\frac{t}{t_0}\right)^{-6\alpha} + \frac{1}{2}\frac{\sigma}{\rho^2} = 0 \ . \tag{2.24}$$

Let us start by analyzing how the system evolves when placed initially in a would-be circular orbit, so that

$$\rho(t_0) = \frac{2l_0^2}{\sigma} \equiv \rho_{c0} \ , \tag{2.25}$$

as $\ddot{\rho}(t_0) = \dot{\rho}(t_0) = 0$. It is easy to see that ρ cannot remain constant for $t > t_0$ due to the decay of the angular momentum. We may, however, look for solutions where the condition for circular orbits is maintained during the motion of the probe brane, i.e.

$$\rho(t) = \frac{2l^2(t)}{\sigma} = \rho_{c0}\left(\frac{t}{t_0}\right)^{-6\alpha} \equiv \rho_c(t) \ . \tag{2.26}$$

Substituting into Eq. (2.24) we obtain

$$\frac{\rho_{c0}}{t_0^2}\left(\frac{t}{t_0}\right)^{-6\alpha-2} 6\alpha(3\alpha+1) = 0 \ , \tag{2.27}$$

which is satisfied only in the non-expanding case, $\alpha = 0$, and for $\alpha = -1/3$. As we are interested in cases where $\alpha > 0$, we conclude that $\rho_c(t)$ is not an exact solution of the equations of motion. It is, however, an approximate solution at late times and, as we will check later, gives the global evolution of the system, so that it is useful to consider some of its properties. In particular, the angular frequency evolves as:

$$\dot{\theta}_c = \frac{l}{\rho_c^2} \propto \left(\frac{t}{t_0}\right)^{9\alpha} , \tag{2.28}$$

so that the orbital period decreases as $T_c(t) \propto (t/t_0)^{-9\alpha}$. Such a solution eventually fails to satisfy the non-relativistic and large distance approximation as the radius of the orbit decreases and its angular velocity grows. In particular, the parameter hv^2 which controls this approximation grows, for $t \gg t_0$, as

$$hv^2 \to \frac{1}{2}(T_6 V_3)^4 \left(\frac{Q_6}{l_0}\right)^4 \left(\frac{t}{t_0}\right)^{12\alpha} . \tag{2.29}$$

Hence, given the values of T_6 and V_3, it is the ratio Q_6/l_0 that controls how long the approximations remain valid.

Consider now trajectories with a non-vanishing initial eccentricity. In an expanding universe, the effective potential becomes time-dependent, although its asymptotic properties at the origin and at infinity remain the same. As the angular momentum redshifts away, the minimum of the effective potential decreases, the same happening with the value of ρ at this minimum, according to the circular solution defined in Eq. (2.26). As discussed earlier, the energy density of the field always decreases during the motion of the probe brane. Hence, if the system is initially in one of the closed orbits with $\epsilon < 0$, the latter condition will be satisfied for all $t > t_0$ and the probe brane is always in one of the closed elliptical orbits defined earlier. From Eq. (2.22), we also conclude that the semi-major axis decreases as the energy density evolves to more negative values. The eccentricity of the orbits may, however, not remain constant, as it depends on the variation of both the energy density and the angular momentum. In fact, using Eqs. (2.15) and (2.16), one can show that

$$\frac{de^2}{dt} = -12H\frac{l^2}{\sigma^2}(3\epsilon + p) = -24H\frac{l^2}{\sigma^2}(2T + V) , \tag{2.30}$$

where $T = \dot{\rho}^2 + \frac{l^2}{\rho^2}$, so that $\epsilon = T + V$ and $p = T - V$.

Thus, in an expanding universe, for finite l_0, one expects the eccentricity of the orbit to vary unless $T = -V/2$. This last condition is satisfied on average in the non-

expanding case, corresponding to the virial theorem. It does not necessarily hold, however, in an expanding universe, with the semi-major axis of the orbits decaying as discussed above. It is nevertheless clear that, at late times, as H and l decrease, the variation of the eccentricity of the orbits should be smaller. The sign of $2T+V$ is also not definite, so that the eccentricity may either increase or decrease during the motion of the probe brane. From Eqs. (2.22) and (2.26), we obtain:

$$R(t) = \frac{\rho_c(t)}{1-e^2(t)} \ . \tag{2.31}$$

Hence, the variation of the semi-major axis follows the decrease of the circular solution obtained earlier, being also affected by the variation of the eccentricity.

In order to have a better understanding of the evolution of the probe brane's motion in an expanding universe, we have solved the equations of motion numerically. Measuring all quantities in terms of the string length, i.e. setting $l_s = 1$, we choose, as an example, the values $V_3 = (T_6)^{-1}$ and $Q_6 = 100$[3]. We set the initial conditions at $t = t_0$ to be those of a non-expanding elliptical orbit with angular momentum l_0 and eccentricity e_0, which we take to be the only free orbital parameters. The field is initially at its maximum value $\rho_0 = \frac{\rho_{c0}}{1-e_0}$, with $\dot{\rho}_0 = 0$ and $\theta = \pi$. After determining the numerical solution for $\rho(t)$, we computed the corresponding energy density and eccentricity evolution, according to Eqs. (2.14) and (2.22), respectively. We used the numerical solution for the eccentricity to compute $R(t)$, according to Eq. (2.31), and also the maximum and minimum values of $\rho(t)$ at each orbit, given by:

$$\rho_{min}(t) = R(t)(1-e(t)) \ , \qquad \rho_{max}(t) = R(t)(1+e(t)) \ . \tag{2.32}$$

We have also determined the evolution of the angular frequency using $\dot{\theta}(t) = l(t)/\rho(t)^2$.

[3]For the value of Q_6 we follow the example analyzed in [157].

In Figure 2.1 we have plotted the results obtained for the values $l_0 = 2000$[4] and $e = 0.2$ in a matter-dominated universe, $\alpha = 2/3$, with $t_0 = 10^8$. Notice that the latter is measured in units of the string time $t_s \sim 10^{-43}$ s if $M_s \sim M_p$.

Observing the plots shown in this figure, we conclude that, as expected, the probe brane evolves continually through elliptical orbits of decreasing semi-major axis, so that they fail to close. The radial field then oscillates between minimum and maximum values which decrease in time. The global decrease follows that of the circular solution, Eq. (2.26), but exhibits an oscillating behaviour associated with the variation of the energy density. Although the latter strictly decreases, as expected, it also oscillates with decreasing period and amplitude, so that at later stages its evolution tends to be smooth. Consequently, one observes oscillations in the evolution of the eccentricity of the orbit. In the example shown in Figure 2.1, these oscillations have a small amplitude. However, at earlier times, when the effects of Hubble expansion are more significant, numerical simulations show that this amplitude can be quite large. All simulations show that $e(t)$ starts increasing and, as both the period and the amplitude of the oscillations decay, it tends to a constant value.

This behaviour can be interpreted following our previous discussion. The quantity $2T + V$ changes sign periodically as the probe brane moves from the maxima to the minima of the orbits with decaying radius, making $\frac{de^2}{dt}$ oscillate. This in turn produces oscillations of the eccentricity and the energy density of the field. At later stages, the decrease in the Hubble constant and in the angular momentum suppresses the variation of the eccentricity, according to Eq. (2.30), tending to stabilize its value. It is clear that the larger the initial value of the Hubble constant the larger the initial variations of the eccentricity will be, as observed numerically, and the probe may quickly evolve towards linear trajectories with $e = 1$ at early times. The decreasing period of the eccentricity oscillations is related to the decay of the orbital period.

[4]The non-relativistic and large distance approximation holds for this value of l_0.

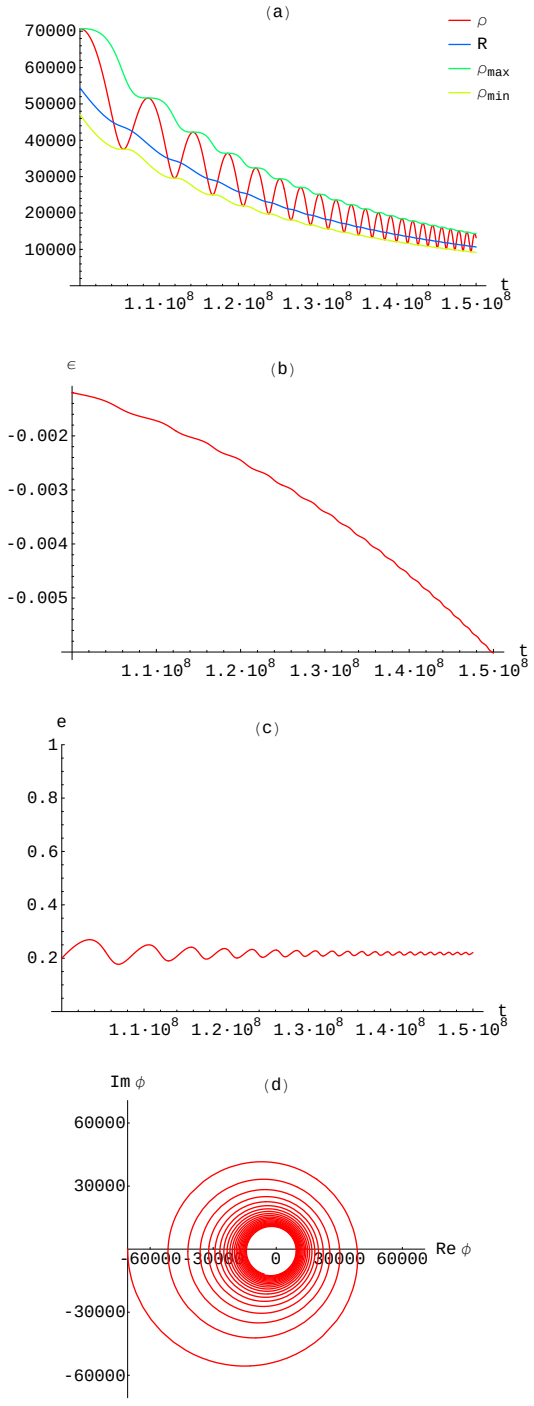

Figure 2.1: Numerical results obtained for $l_0 = 2000$ and $e = 0.2$ in a matter-dominated universe, $\alpha = 2/3$, with $t_0 = 10^8$. The plots show (a) the radial field and associated quantities, (b) the energy density, (c) the eccentricity and (d) the motion of the probe brane in the complex plane of the field ϕ.

This makes $2T + V$ vary more quickly, so that, on average, this quantity vanishes.

The numerical simulations thus suggest that, at late times, the eccentricity is approximately constant, so that, on average, the energy density should vary as

$$\langle \epsilon(t) \rangle \propto l^{-2}(t) \propto \left(\frac{t}{t_0} \right)^{6\alpha} , \tag{2.33}$$

tending to more negative values as observed in Figure 2.1. Then, from Eq. (2.15),

$$\left\langle \frac{d\epsilon}{dt} \right\rangle = -3H \langle \epsilon + p \rangle = 6H \langle \epsilon \rangle , \tag{2.34}$$

so that $\langle 3\epsilon + p \rangle = 0$ or, equivalently, $\langle 2T + V \rangle = 0$. Thus, although at early times Hubble expansion makes the eccentricity vary significantly, the system *virializes* at late times, evolving smoothly between decaying orbits of constant eccentricity.

Another consequence of Hubble expansion is a rotation of the axis of the elliptical orbits with time, although this is a small effect in the example shown in Figure 2.1. This is simply a result of the growing eccentricity of the orbits which deviates the maximum and minimum values of ρ from $\theta = \pi$ and $\theta = 0$, respectively. The orbital axis will, however, stabilize at late times, as $e(t)$ tends to a constant value.

Numerically one also observes a decrease in the oscillation amplitude of $\rho(t)$:

$$\Delta\rho(t) \equiv \rho_{max}(t) - \rho_{min}(t) = R(t)e(t) , \tag{2.35}$$

which is thus mainly due to the decrease in $R(t)$.

The asymptotic value of the eccentricity depends not only on t_0 but also on the initial values of the orbital angular momentum and eccentricity. Numerical simulations show that larger values of l_0 lead to a more pronounced growth of the eccentricity, in agreement with Eq. (2.30). The dependence on e_0 is less trivial and numerically one finds a larger eccentricity variation for e_0 close to 0 and to 0.9. This is, however, very

small for e_0 close to 1, which is expected, as the energy density of the field cannot increase to produce hyperbolic orbits with $e > 1$ if initially $\epsilon < 0$. The eccentricity always grows if initially $\dot{\rho} = 0$, so that $2T + V < 0$ and $\frac{de}{dt} > 0$, as most of the eccentricity variation occurs initially when Hubble expansion is more significant. The opposite behaviour should be observed if initially $2T + V > 0$.

Although we have focused so far on a matter-dominated universe, $\alpha = 2/3$, these results hold for all $\alpha > 0$, in particular for an $\alpha = 1/2$ radiation-dominated universe.

To summarize the results of this section, we conclude that, in an expanding universe, the probe brane follows elliptical orbits with decreasing radius and increasing frequency and whose eccentricity exhibits an oscillating behaviour and asymptotically tends to a constant value larger than the initial one. If the motion of the probe brane begins at late times with a small angular momentum, the latter effect is negligible.

The probe brane will asymptotically collide with the central branes, as $\rho \to 0$, but our approximations will break down before this happens, so that we expect the motion of the probe brane to deviate significantly from our previous results as its angular velocity grows and it spirals towards the central stack. The collision will, however, occur if nothing prevents the probe from losing energy and angular momentum as the universe expands, which may lead to the annihilation of the probe anti-brane with one of the source branes, an issue we will return to later in this chapter.

2.2 Particle Production

In the original discussion of the branonium system [122], it was argued that the fields confined to the probe brane, such as the gauge fields mentioned earlier, become time-dependent due to the motion of the probe through the background spacetime created by the central stack. Consequently, an observer bound to the probe interprets this variation as corresponding to the production of particles associated with these fields.

Such radiation of energy into brane particle-modes arises only if the distance between the probe and the stack varies in time, thus creating a time-dependent background from the point of view of brane-bound observers. Although the power radiated into these modes was estimated in [122], many aspects of this particle production mechanism remain unclear. In this section, we will analyze this mechanism in more detail, revealing some new properties of particle production in branonium, and discuss how the expansion of the universe modifies this process.

The fields confined to the brane arise from open strings whose endpoints are attached to the brane, as discussed in chapter 1. For a stack of branes, these include bosonic fields such as gauge bosons and scalar fields, as well as their fermionic superpartners. Here, we will study the simplest case of a real scalar field η confined to the probe brane and follow an effective field theory approach. For the $D6-\overline{D6}$ system, the effective action for this scalar field is given by:

$$S_\eta = -T_6 \int d^7\xi \; e^{-\Phi}\sqrt{-\hat{\gamma}}\Big(-\frac{1}{2}\hat{\gamma}^{\mu\nu}\partial_\mu\eta\partial_\nu\eta - \frac{1}{2}m^2\eta^2\Big) \,, \tag{2.36}$$

where m denotes the mass of the scalar field, which includes its bare mass as well as quantum corrections. When compactifying three of the dimensions parallel to the brane as before, the scalar field will be decomposed in its KK modes. We will then focus on the evolution of the zero mode, with mass m. To simplify the notation, we will denote this mode as η, although one must bear in mind that it is not the original 7-dimensional field. Also, the global factor of T_6 will not affect our discussion and we may absorb it into the definition of the field.

Let us first consider the case $m = 0$. Then, the classical equations of motion arising from the action Eq. (2.36) are given by:

$$\partial_\mu(e^{-\Phi}\sqrt{\hat{\gamma}}\hat{\gamma}^{\mu\nu}\partial_\nu\eta) = 0 \,. \tag{2.37}$$

Defining $f(t) \equiv [h(1-hv^2)]^{\frac{1}{2}}$, we can write this as

$$\ddot{\eta} + (3H - F)\dot{\eta} - \frac{1}{a^2}(1-hv^2)\nabla^2\eta = 0 \ , \tag{2.38}$$

where $F = \dot{f}/f$ and ∇^2 is the flat 3-dimensional Laplacian.

To construct the associated quantum description, we follow the semi-classical approach to the quantization of scalar fields in curved space [161]. In a curved background spacetime with a time-varying geometry, as is the case of the world-volume of the probe brane, the induced time-variation of the fields modifies the usual canonical quantization procedure, as quantum operators are themselves time-dependent. In particular, the creation and annihilation operators associated with the field evolve in time as the background changes, the same happening with the associated multi-particle states. This is the main reason behind the production of particles in a dynamical background. Let us start by expanding the field in Fourier modes of the form:

$$\eta(\mathbf{x},t) = \int \frac{d^3k}{(2\pi)^{\frac{3}{2}}}\left(a_{\mathbf{k}}\chi_{\mathbf{k}}(t)e^{i\mathbf{k}\cdot\mathbf{x}} + a^{\dagger}_{\mathbf{k}}\chi^{*}_{\mathbf{k}}(t)e^{-i\mathbf{k}\cdot\mathbf{x}}\right) \ . \tag{2.39}$$

In the quantum theory, $a_{\mathbf{k}}$ and $a^{\dagger}_{\mathbf{k}}$ become the annihilation and creation operators associated with the Fourier mode $\mathbf{k}$ of the field. Expanding the field in this way, we include all the time dependence of the field in the functions $\chi_{\mathbf{k}}(t)$ and $\chi^{*}_{\mathbf{k}}(t)$, while the operators remain time-independent. The conjugate momentum to the field η, obtained by computing $\delta S_{\eta}/\delta\dot{\eta}$, can then be written as

$$\pi(\mathbf{x},t) = \frac{a^3}{f}\int \frac{d^3k}{(2\pi)^{\frac{3}{2}}}\left(a_{\mathbf{k}}\dot{\chi}_{\mathbf{k}}e^{i\mathbf{k}\cdot\mathbf{x}} + a^{\dagger}_{\mathbf{k}}\dot{\chi}^{*}_{\mathbf{k}}e^{-i\mathbf{k}\cdot\mathbf{x}}\right). \tag{2.40}$$

If the creation and annihilation operators satisfy the canonical commutation relations

$$[a_{\mathbf{k}}, a_{\mathbf{k}'}] = [a^{\dagger}_{\mathbf{k}}, a^{\dagger}_{\mathbf{k}'}] = 0 \ , \qquad [a_{\mathbf{k}}, a^{\dagger}_{\mathbf{k}'}] = \delta^3(\mathbf{k}-\mathbf{k}') \ , \tag{2.41}$$

then the canonical commutator $[\eta(\mathbf{x},t),\pi(\mathbf{y},t)] = i\delta^3(\mathbf{x}-\mathbf{y})$ can only be obtained if the mode functions satisfy the following Wronskian normalization condition:

$$\chi_{\mathbf{k}}\dot{\chi}^*_{\mathbf{k}} - \chi^*_{\mathbf{k}}\dot{\chi}_{\mathbf{k}} = i\frac{f}{a^3} \ . \tag{2.42}$$

This condition is essential for consistency of the quantization procedure. We now follow a semi-classical approach and consider the evolution of the field modes given by the classical equations of motion, assuming that any quantum corrections to their propagation can be neglected. Substituting Eq. (2.39) into Eq. (2.38), we see that each of the Fourier modes evolves independently according to

$$\ddot{\chi}_{\mathbf{k}} + (3H - F)\dot{\chi}_{\mathbf{k}} + \frac{k^2}{a^2}(1 - hv^2)\chi_{\mathbf{k}} = 0 \ , \tag{2.43}$$

and similarly for the complex conjugate modes $\chi^*_{\mathbf{k}}$. Notice that this equation depends only on $k^2 \equiv |\mathbf{k}|^2$ but not the direction of the momenta $\hat{k} \equiv \frac{\mathbf{k}}{k}$. This is a consequence of the isotropy of our metric *ansatz*, and we may write without loss of generality $\chi_{\mathbf{k}}(t) = \chi_k(t)$. It is also clear, from Eq. (2.43), that the physical momentum of the modes is related to their comoving momentum k via

$$k_{phys} = \frac{k}{a}\sqrt{1 - hv^2} \ . \tag{2.44}$$

This expression includes both the expected redshift of the modes in an expanding universe and the effect of the probe's motion through the dynamical background. Let us now rescale the field modes by defining $X_k(t) \equiv a^{\frac{3}{2}}(t)f^{-\frac{1}{2}}(t)\chi_k(t)$, which satisfy

$$\ddot{X}_k + \omega_k^2 X_k = 0 \ , \tag{2.45}$$

which corresponds to a harmonic oscillator with a variable frequency given by:

$$\omega_k^2 = \frac{k^2}{a^2}(1 - hv^2) - \frac{1}{4}(3H - F)^2 - \frac{1}{2}(3\dot{H} - \dot{F}) = k_{phys}^2 + \Delta^2 \ , \tag{2.46}$$

where we have defined

$$\Delta^2(t) \equiv -\frac{1}{4}(3H - F)^2 - \frac{1}{2}(3\dot{H} - \dot{F}) \ . \tag{2.47}$$

As each mode behaves as a harmonic oscillator with $E_k = \omega_k(n_k + 1/2)$, we can define the associated particle number via

$$n_k = \frac{\omega_k}{2}\left(\frac{|\dot{X}_k|^2}{\omega_k^2} + |X_k|^2\right) - \frac{1}{2} \ . \tag{2.48}$$

It is well known that this quantity is an adiabatic invariant for a harmonic oscillator with variable frequency, as happens, for example, in an oscillating pendulum whose length is decreased infinitely slowly [161]. Thus, the number of *quanta* in a given Fourier mode k can only change if its frequency varies in a non-adiabatic way, which can be expressed by the following condition [37]:

$$\left|\frac{d\omega_k}{dt}\right| \gtrsim \omega_k^2 \ . \tag{2.49}$$

For our particular case, this gives, in the limit $hv^2 \ll 1$,

$$|Hk_{phys}^2 - \Delta\dot{\Delta}| \gtrsim (k_{phys}^2 + \Delta^2)^{\frac{3}{2}} \ . \tag{2.50}$$

This condition will then constrain the number of particles produced in each physical momentum mode by the motion of the probe brane.

To quantify this number of particles, we need to look for solutions of the mode equation, Eq. (2.45). These solutions are usually obtained via an adiabatic *ansatz*,

where one separates the positive and negative frequency parts of each mode $X_k(t)$ and introduces time-dependent coefficients for each part, known as the Bogolubov coefficients [37, 161]. These coefficients mix the time-independent creation and annihilation operators in Eq. (2.39) to give the corresponding physical time-dependent operators. This reflects the fact that, in a curved dynamical spacetime, both the quantum operators and states vary in time. The evolution of each mode can then be obtained by solving the first-order differential equations for these coefficients. It can also be shown that, in an initial vacuum state with zero particle number, only positive frequency modes are present.

Although the Bogolubov coefficients give a good insight into the quantum theory behind the particle production mechanism and allow us to set the appropriate initial conditions, we will follow a different approach and look directly for solutions of Eq. (2.45). We will start by discussing what happens in a non-expanding universe and then we will analyze the effects of Hubble expansion.

2.2.1 Non-expanding universe

Consider the motion of the probe brane in a non-expanding universe, $H = 0$, and assume that the non-relativistic and large distance approximations discussed earlier are valid. As we have seen in section 2.1, the probe follows closed elliptical trajectories if its energy density is negative. If $hv^2 \ll 1$, we have to leading order:

$$1 - hv^2 \simeq 1 \ , \qquad k_{phys} \simeq k \ , \qquad f \simeq h^{1/2} \ . \tag{2.51}$$

Then, we may take the following approximations:

$$F = \frac{\dot{f}}{f} \simeq \frac{1}{2}\frac{\dot{h}}{h} \ , \qquad \dot{F} \simeq \frac{1}{2}\left[\frac{\ddot{h}}{h} - \left(\frac{\dot{h}}{h}\right)^2\right] \ , \tag{2.52}$$

so that we can write:

$$\Delta^2 = -\frac{1}{4}F^2 + \frac{1}{2}\dot{F} \simeq -\frac{5}{16}\left(\frac{\dot{h}}{h}\right)^2 + \frac{1}{4}\frac{\ddot{h}}{h} \ . \tag{2.53}$$

An exact analytical expression for the time variation of the radial field $\rho(t)$ can be obtained in a non-expanding universe, being given implicitly by

$$\rho(t) = R\big[1 - e\cos\big(\psi(t)\big)\big] \ . \tag{2.54}$$

The angular variable $\psi(t)$ satisfies

$$t - t_0 = \Omega^{-1}\big[\psi - \psi_0 + e(\sin\psi - \sin\psi_0)\big] \ , \tag{2.55}$$

where $\psi_0 \equiv \psi(t_0)$ and $\Omega = \sqrt{\frac{\sigma}{2}}R^{-\frac{3}{2}}$ is the angular frequency of the orbit. The angular variables ψ and θ are related by:

$$\tan\left(\frac{\theta}{2}\right) = \sqrt{\frac{1+e}{1-e}}\tan\left(\frac{\psi}{2}\right) \ . \tag{2.56}$$

For small eccentricity orbits, $e \ll 1$, Eq. (2.55) gives, to leading order in e:

$$\psi \simeq \psi_0 + \Omega(t - t_0) \ . \tag{2.57}$$

Choosing $\psi_0 = \pi$ we have, in this approximation,

$$\rho(t) \simeq R\big[1 + e\cos\big(\Omega(t - t_0)\big)\big] \ . \tag{2.58}$$

This allows us to determine the non-relativistic and large distance expression for Δ^2,

in the case of small eccentricity orbits. To lowest order, we then obtain:

$$\Delta^2 \simeq \frac{1}{4}\sqrt{\frac{T_6 V_3}{2}}\frac{Q_6}{R} e\Omega^2 \cos\big(\Omega(t-t_0)\big) \ . \tag{2.59}$$

Defining the quantity

$$\delta^2 \equiv \frac{1}{4}\sqrt{\frac{T_6 V_3}{2}}\frac{Q_6}{R} e\Omega^2 \ , \tag{2.60}$$

the variable frequency of the mode with comoving momentum k can, hence, be approximated by:

$$\omega_k^2(t) \simeq k^2 + \delta^2 \cos\big(\Omega(t-t_0)\big) \ . \tag{2.61}$$

Rewriting Eq. (2.45) in terms of the dimensionless variable $z \equiv \frac{\Omega}{2}(t-t_0)$, we have:

$$X_k'' + \big(A_k - 2q\cos(2z)\big)X_k = 0 \ , \tag{2.62}$$

where

$$A_k \equiv \frac{4k^2}{\Omega^2} \ , \qquad q \equiv -2\frac{\delta^2}{\Omega^2} \ . \tag{2.63}$$

Eq. (2.62) has the form of the well-known Mathieu equation [162] with parameters A_k and q determined by the orbital parameters of the probe brane and by the value of the comoving momentum k of each mode. In the parameter space (A_k, q), the Mathieu equation exhibits both stable and unstable solutions, the latter being closely associated with the phenomenon of parametric resonance [163]. As we are working under the assumption that the probe brane's orbit has a large radius and a small eccentricity, it is easy to check that $|q| \ll 1$[5]. In this region of parameter space, the Mathieu equation exhibits instabilities in a series of narrow resonance bands near $A_k \sim n$, n being a positive integer, with a width in comoving momentum space given by $\Delta k^n \sim |q|^n$. In these resonance bands, the solution evolves as $X_k \propto e^{\mu_k^{(n)} z}$, with a real exponent $\mu_k^{(n)}$, according to Floquet's Theorem.

[5]The analysis is independent of the sign of q.

The most important of these is the first resonance band, which occurs when

$$1 - |q| - \frac{1}{8}q^2 \lesssim A_k \lesssim 1 + |q| - \frac{1}{8}q^2 \ . \tag{2.64}$$

The exponent $\mu_k \equiv \mu_k^{(1)}$ can then be approximately written as

$$\mu_k \simeq \frac{1}{2}\sqrt{q^2 - (A_k - 1)^2} \ . \tag{2.65}$$

This is, as claimed, real for $1 - |q| \lesssim A_k \lesssim 1 + |q|$, having a maximum value of $|q|/2$ for $A_k \simeq 1$. This implies that modes lying inside this resonance band will be exponentially amplified, leading to a resonant production of particles.

From Eq. (2.63), the centre of the resonance band occurs for comoving momentum $k_c \simeq \Omega/2$, while its lower and upper bounds are given by

$$k_\pm \simeq \sqrt{\left(\frac{\Omega}{2}\right)^2 \pm \frac{\delta^2}{2}} \simeq k_c\left[1 \pm \left(\frac{\delta}{\Omega}\right)^2\right] \ , \tag{2.66}$$

so that the resonance band has a width in comoving momentum space of $\Delta k_{res} \equiv k_+ - k_- \simeq \delta^2/\Omega$. This is quite small compared to the value of the centre of the resonance, as $\Delta k_{res}/k_c \simeq |q| \ll 1$, which means that particle production occurs in a regime of narrow parametric resonance. The particles produced by this mechanism have typical energies of order $\omega_k \simeq \Omega/2$, i.e. with half the typical energy of the field ϕ. This agrees with the discussion in [122], where it is stated that particles are produced in pairs with opposite momenta, as if resulting directly from the decay of the interbrane distance field, which can be seen as a classical condensate of zero momentum particles. We have found in this analysis, however, that these particles are produced resonantly, the associated field modes being exponentially amplified.

After the modes inside the resonance band have been sufficiently amplified, we

may write, from Eq. (2.48),

$$n_k \propto e^{2\mu_k z} = e^{\mu_k \Omega (t-t_0)} \ , \tag{2.67}$$

where we used that $\mu_k \lesssim |q|/2 \ll 1$, so that the term involving $|\dot{X}_k|^2$ in Eq. (2.48) can be neglected. This also implies that, although the particle number in each mode grows exponentially, the resonance takes a long time to develop. In particular, the typical resonance time, $\Delta t_{res} = (\mu_k \Omega)^{-1}$, is much larger than the orbital period of the probe brane, which is of order $2\pi\Omega^{-1}$. This is characteristic of the narrow resonance regime and, hence, a significant particle number is only produced after the probe brane has completed a large number of orbits, given by $(2\pi\mu_k)^{-1}$.

To have an idea of the order of magnitude of these quantities, consider the scenario studied in section 2.1, where $V_3 = T_6^{-1}$ with $Q_6 = 100$. Then, for an orbit with eccentricity $e = 0.01 \ll 1$ and an angular momentum $l = 500$, we have $\sqrt{T_6 V_3/2}\frac{Q_6}{R} \simeq 0.03$, which satisfies the large distances approximation, and $|q| \simeq 10^{-4} \ll 1$. This implies that the probe brane will have to complete approximately 3×10^3 orbits for the particle number to be amplified by one e-folding.

To illustrate the results obtained earlier, we have solved Eq. (2.45) for the example described above. An initial vacuum state with zero particle number corresponds to the following initial conditions:

$$X_k(t_0) = \frac{1}{\sqrt{2\omega_k(t_0)}} \ , \qquad \dot{X}_k(t_0) = -i\sqrt{\frac{\omega_k(t_0)}{2}} \ . \tag{2.68}$$

In Figure 2.2 we have plotted the numerical results obtained for the comoving momentum at the centre of the resonance band, k_c. The linear evolution observed for the logarithm of the particle number shows that, as expected, this quantity is being amplified exponentially with time, but that a significant number of particles is produced only after the probe brane has completed a few thousands of orbits.

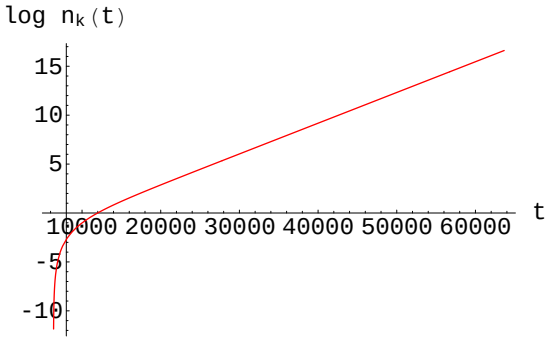

Figure 2.2: Numerical results obtained for the mode in the centre of the resonance band, for an orbit with $e = 0.01$ and $l = 500$, giving $q \simeq 10^{-4}$. The time coordinate t is given in units of the orbital period $T = 2\pi\Omega^{-1} \simeq 1.57 \times 10^5$.

We note that, although this solution was obtained numerically, a formal analytical solution of the Mathieu equation can be written in terms of the Mathieu sine and cosine functions. In Figure 2.3 we also show the evolution of the particle number for a mode outside the limits of the resonance band. In this case, μ_k takes imaginary values and n_k exhibits an oscillating behaviour with a small amplitude, confirming that only for comoving momenta $k_- \leq k \leq k_+$ a significant particle number is produced by the elliptical motion of the probe brane. It is also worth mentioning that, in the limit of circular orbits, $e \to 0$, the parameter q vanishes and there is no amplification of any of the particle momentum modes. This confirms our earlier assumption that the interbrane brane distance needs to vary for particle production to occur.

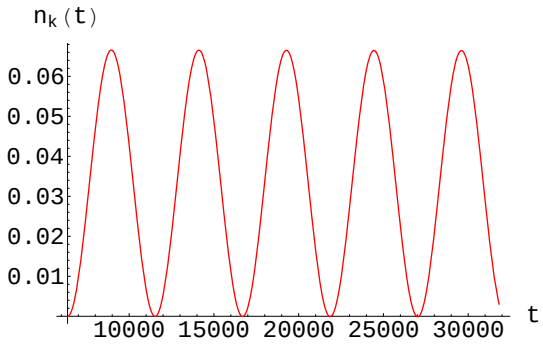

Figure 2.3: Numerical results obtained for a mode outside the resonance band for an orbit with $e = 0.01$ and $l = 500$, giving $q \simeq 10^{-4}$. The comoving momentum of the mode is $k = k_c\left(1 + 4\frac{\delta^2}{\Omega^2}\right) > k_+$. The time coordinate t is given in units of the orbital period $T = 2\pi\Omega^{-1} \simeq 1.57 \times 10^5$.

Consider now the case where the field has a non-vanishing mass, $m \neq 0$. In this case, the classical equations of motion Eq. (2.37) can be generalized to

$$\partial_\mu(e^{-\Phi}\sqrt{\hat{\gamma}}\hat{\gamma}^{\mu\nu}\partial_\nu\eta) - e^{-\Phi}\sqrt{-\hat{\gamma}}m^2\eta = 0 \ , \tag{2.69}$$

or, explicitly,

$$\ddot{\eta} + (3H - F)\dot{\eta} - \frac{1}{a^2}(1 - hv^2)\nabla^2\eta + \frac{(1 - hv^2)}{h^{\frac{1}{2}}}m^2\eta = 0 \ . \tag{2.70}$$

Each of the Fourier modes then evolves independently according to

$$\ddot{\chi}_k + (3H - F)\dot{\chi}_k + \left[(1 - hv^2)\frac{k^2}{a^2} + \frac{(1 - hv^2)}{h^{\frac{1}{2}}}m^2\right] . \tag{2.71}$$

This implies that all modes have, in this case, an effective physical mass which differs from the mass parameter m due to the motion of the probe brane:

$$m^2_{eff} = \frac{(1 - hv^2)}{h^{\frac{1}{2}}}m^2 \ . \tag{2.72}$$

Notice that the mass is not modified by Hubble expansion. The rescaled mode functions $X_k(t)$ again satisfy the equation for a harmonic oscillator with a varying frequency, which is now given by:

$$\omega^2_k = k^2_{phys} + m^2_{eff} + \Delta^2 \ , \tag{2.73}$$

where all the quantities are time-dependent in the general case. Let us now set $H = 0$ and compare these results with the ones obtained for the particle production mechanism in the massless case. First, notice that, in the non-relativistic and large distance approximation, we have $m^2_{eff} \simeq m^2$. Thus, the leading order modification introduced by the mass of the field can be obtained by simply replacing $k^2 \to k^2 + m^2$.

Following the same procedure as before, one can reduce the particle-mode equation to the Mathieu equation, with the parameter A_k being now given by:

$$A_k = \frac{4(k^2 + m^2)}{\Omega^2} \ , \tag{2.74}$$

while the parameter q, which quantifies the strength and width of the resonance phenomenon, is not modified, so that we expect the particle production mechanism to occur as before. In this case, however, the centre of the resonance band is shifted to a lower momentum, $k_c = \sqrt{(\Omega/2)^2 - m^2}$, which gives $A_k = 1$. The upper and lower limits of the resonance band are also modified, being now given by:

$$k_\pm = \sqrt{(\Omega/2)^2 - m^2 \pm \frac{1}{2}\delta^2} \ , \tag{2.75}$$

which in turn alters the width of the resonance band in the obvious way. If, as in the massless case, we have $\delta^2/2 \ll k_c^2$, we may write $\Delta k_{res} \simeq \delta^2/2k_c$, which is larger than the corresponding value in the massless case, nevertheless satisfying the narrow resonance condition. Notice that this implies an upper bound for the mass of the particles which can be produced by this mechanism,

$$m \leq \sqrt{\left(\frac{\Omega}{2}\right)^2 - \frac{1}{2}\delta^2} \simeq \frac{\Omega}{2} \ . \tag{2.76}$$

In the particle description discussed earlier, this simply means that each 'particle' in the interbrane distance field ϕ must have enough energy to decay into two η-particles at rest. Recalling the definition of ϕ in terms of the physical interbrane distance, Eq. (2.10), we may write the upper bound of Eq. (2.76) in terms of the physical semi-major axis of the orbit, $R_{phys} = \sqrt{2/T_6 V_3}R$. Inserting back the missing l_s factors, we obtain:

$$m_{max} = \sqrt{\frac{Q_6}{2R_{phys}}}\frac{l_s}{R_{phys}}M_s \ . \tag{2.77}$$

Since the probe brane and supergravity approximations require $r \gg Q_6 \gg l_s$, it is clear from this expression that $m_{max} \ll M_s$, which allows nevertheless for the production of very massive particles. For the example studied earlier in this section, with orbital frequency $\Omega \simeq 4 \times 10^{-5} M_s$, particles up to masses of order 10^{13} GeV can be resonantly created if the string scale is close to the Planck scale.

In general, particles living in the world-volume of the probe brane will be massive, so that we need to use the results obtained above to describe the parametric resonance. For masses which are small compared to the typical orbital energies, the simpler treatment of the $m = 0$ case will be sufficient.

2.2.2 Expanding universe

Let us now consider the case of an expanding universe, with $H = \frac{\alpha}{t} > 0$. The inclusion of the scale factor will modify our previous analysis of particle production in several ways. First, it will change the frequency of each harmonic oscillator particle-mode, namely modifying the factor $\Delta^2(t)$, given in Eq. (2.47). Also, the physical momenta of the particle-modes will be redshifted as the universe expands, so that, in the non-relativistic and large distance approximation, we have $k_{phys} \simeq k/a \propto (t/t_0)^{-\alpha}$. Finally, the motion of the probe brane will be altered, as we have seen in section 2.1, so that the semi-major axis of elliptical orbits will decrease as $R(t) \propto (t/t_0)^{-6\alpha}$, making the angular frequency increase as $\Omega(t) \propto (t/t_0)^{9\alpha}$. Furthermore, if the Hubble parameter is sufficiently large, the eccentricity may exhibit a significant growth.

All these modifications make a complete analytical study of particle production in the probe brane rather complex. In order to determine the leading consequences of Hubble expansion, we will consider the motion of the probe brane at sufficiently late times, so that some of its effects can be discarded. As we have concluded in section 2.1, the variation of the eccentricity is negligible in this regime. The explicit effects of the expansion in modifying the factor Δ^2 may also be discarded in this limit, provided

that $|F| \gg 3H$ and $|\dot{F}| \gg |3\dot{H}|$, or explicitly

$$t \gg \frac{6\alpha}{e\Omega}\left(\frac{R_{phys}}{Q_6}\right) , \qquad t^2 \gg \frac{6\alpha}{e\Omega^2}\left(\frac{R_{phys}}{Q_6}\right) . \tag{2.78}$$

The first of these conditions will, *a priori*, be more constraining. For the example we have been following in this section, the first condition gives $t \gg 5 \times 10^8$, while the second only implies the constraint $t \gg 3.5 \times 10^6$.

With these constraints in mind, we now have to analyze how Hubble expansion modifies the factors F and $\dot{F}$ in the variable harmonic oscillator frequency. The radial field ρ can now be written, in the low eccentricity approximation, as:

$$\rho(t) \simeq R(t)\big[1 + e\cos\big(\Omega(t)(t - t_0)\big)\big] , \tag{2.79}$$

with

$$R(t) = R_0\left(\frac{t}{t_0}\right)^{-6\alpha} , \qquad \Omega(t) = \Omega_0\left(\frac{t}{t_0}\right)^{9\alpha} . \tag{2.80}$$

Computing the corresponding time derivatives, we find that these involve terms arising from Hubble expansion which are suppressed by at least one power of t, being negligible at late times. Also, terms involving $(t-t_0)/t_0$ can be discarded if the typical resonance time scale is smaller than the age of the universe. After some algebra, the leading order modification to Δ^2 is then given by

$$\Delta^2(t) \simeq \delta^2(t)\cos\big(\Omega(t)(t - t_0)\big) . \tag{2.81}$$

The quantity δ^2 is now time-dependent and can be obtained by including the time variation of the orbital parameters in Eq. (2.60), yielding

$$\delta^2(t) = \delta_0^2\left(\frac{t}{t_0}\right)^{24\alpha} , \qquad \delta_0^2 \equiv \frac{1}{4}\sqrt{\frac{T_6 V_3}{2}}\frac{Q_6}{R_0}e\Omega_0^2 . \tag{2.82}$$

Taking into account the momentum redshift, the mode equation becomes, to lowest order,

$$\ddot{X}_k + \left[k^2\left(\frac{t}{t_0}\right)^{-2\alpha} + \delta_0^2\left(\frac{t}{t_0}\right)^{24\alpha}\cos\left(\Omega(t)(t-t_0)\right)\right]X_k = 0 \ . \tag{2.83}$$

Following the same reasoning as in the non-expanding case, we rescale the time coordinate by defining the variable $z \equiv \frac{\Omega(t)}{2}(t-t_0)$. As the angular frequency of the orbit is now time-dependent, this change of variables will introduce new terms in the equation. These will, however, be suppressed by powers of t and involve first and second derivatives of the mode function X_k. In the non-expanding case, these were quite small compared to X_k, and one expects them to be negligible in this case as well. Using that, to lowest order, $z \simeq \frac{\Omega_0}{2}\Delta t$, we may write the leading order equation for the mode function in terms of the variable z as

$$X_k'' + [A_k(z) - 2q(z)\cos(2z)]X_k = 0 \ , \tag{2.84}$$

with

$$A_k(z) \equiv A_{k0}(1-\gamma z) \ , \qquad q(z) \equiv q_0(1+\xi z) \ , \tag{2.85}$$

where $A_{k0} \equiv 4k^2/\Omega_0^2$ and $q_0 \equiv -2\delta_o^2/\Omega_0^2$ correspond to the initial values of the parameters of the Mathieu equation, given by their non-expanding case expressions, and the Hubble expansion coefficients γ and ξ are given by

$$\gamma \equiv \frac{40\alpha}{\Omega_0 t_0} \ , \qquad \xi \equiv \frac{12\alpha}{\Omega_0 t_0} = \frac{3}{10}\gamma \ . \tag{2.86}$$

We, hence, conclude that the leading order effect of an expanding universe is to make the coefficients of the Mathieu equation vary in time. In particular, their variation is, to a first approximation, linear in the variable z and controlled by the single parameter γ, which is small at late times. One must take into account, however, that Eq. (2.84) is not the Mathieu equation and, namely, does not satisfy the conditions of

Floquet's Theorem. Nevertheless, we can use the properties of the Mathieu equation as a guide to describe the evolution of the modes when $H > 0$.

First, notice that, as A_k decreases with z, the position of the centre of the resonance band, at $A_k = 1$, will be shifted towards higher momentum modes:

$$k_c(z) = \frac{k_{c0}}{1 - \gamma z} , \qquad k_{c0} \equiv \frac{\Omega_0}{2} . \tag{2.87}$$

Thus, we expect modes with comoving momentum larger than k_{c0} to be excited as the probe's orbit decays. To better understand the evolution of each mode, let us analyze the evolution of the exponent $\mu_k(z)$, which is given by:

$$\mu_k(z) \simeq \frac{1}{2}\sqrt{q_0^2(1+\xi z)^2 - (A_{k0}(1-\gamma z) - 1)^2} . \tag{2.88}$$

The zeros of $\mu_k(z)$ then occur for

$$z_1 = \frac{-|q_0| + A_{k0} - 1}{\gamma A_{k0} + \xi |q_0|} , \qquad z_2 = \frac{|q_0| + A_{k0} - 1}{\gamma A_{k0} - \xi |q_0|} , \tag{2.89}$$

with $z_2 > z_1$. This means that $\mu_k(z)$ will be real for $z_1 \leq z \leq z_2$ and pure imaginary for $z < z_1$ and $z > z_2$. Figure 2.4 illustrates the typical evolution of $\mu_k(z)$ for a generic Fourier mode.

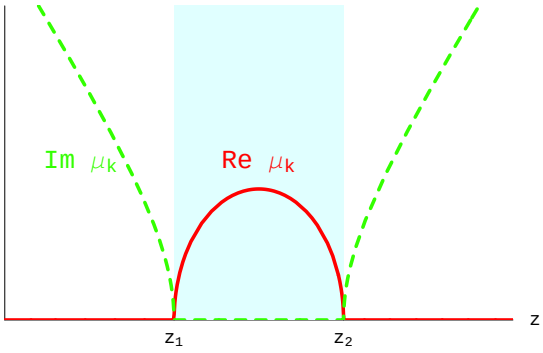

Figure 2.4: Evolution of the real and imaginary parts of the exponent $\mu_k(z)$ for a generic mode. The shaded area represents the period the mode spends inside the resonance band.

Thus, each mode may only experience the resonant regime during a finite amount of time, when $\mu_k(z)$ is real and the mode is inside the resonance band. During the periods where $\mu_k(z)$ is pure imaginary, we expect the particle number to exhibit an oscillating behaviour. The frequency and amplitude of these oscillations are controlled by Im μ_k, so that we expect these quantities to vary in an expanding universe. Similarly, as Re μ_k is not constant when the mode is inside the resonance band, the strength of the resonance is also expected to vary.

Particle modes will then have different behaviours according to their position relative to the initial resonance band, which can be parametrized by:

$$A_{k0} \equiv 1 + \beta|q_0| \ . \tag{2.90}$$

Recalling that the centre of the initial resonance band ($z = 0$) corresponds to $\beta = 0$, we need to distinguish three different types of modes:

(i) $\beta < -1$: as both z_1 and z_2 are negative in this case, these modes will always be outside the resonance band, with an imaginary exponent $\mu_k(z)$ for all $z \geq 0$.

(ii) $-1 \leq \beta \leq 1$: this case corresponds to modes inside the resonance band in a non-expanding universe, with $z_1 \leq 0$ but $z_2 \geq 0$. Hence, they will start inside the resonance band but stop experiencing the resonant regime for $z > z_2$.

(iii) $\beta > 1$: although these modes are outside the initial resonance band, they will experience the resonant behaviour at some later stage, as $z_2 > z_1 > 0$.

For both type (ii) and type (iii) modes, the maximum value of Re $\mu_k(z)$ occurs for $z_{max} = (z_1 + z_2)/2$, giving, for $|q_0| \ll 1$,

$$\mu_k(z_{max}) \simeq \frac{|q_0|}{2}\left(1 + \frac{3}{10}\beta|q_0|\right) \ , \tag{2.91}$$

which gives the same result as in the non-expanding limit for $\beta = 0$. The total time each type (ii) or (iii) mode spends inside the resonance band is given by:

$$\Delta z_{band} \equiv z_2 - z_1 \simeq \frac{2|q_0|}{\gamma}\left(1 - \frac{7}{10}\beta|q_0|\right) . \tag{2.92}$$

This quantity decreases with γ, so that the smaller the Hubble parameter the longer each mode is excited. For $\gamma \to 0$, $\Delta z_{band} \to +\infty$, but in this limit only type (ii) modes are inside the resonance band. Also, higher momentum modes spend less time inside the resonance band, which suggests these will be less excited.

The analysis of the properties of the exponent $\mu_k(z)$ thus provides a very clear insight into the qualitative evolution of all momentum modes. We would like, however, to be able to quantify the particle number produced by the resonance in each mode. In the non-expanding case, $X_k(z) \propto e^{\mu_k z}$, which implied $n_k(z) \propto e^{2\mu_k z}$ in the limit of large particle number. Despite the variation of μ_k in the $H > 0$ case, we may take this exponent to be approximately constant during an infinitesimal interval between z and $z + dz$. Then, during this interval, X_k will be amplified by a factor $\exp(\mu_k(z)dz)$ if the mode is inside the resonance band. Integrating this result, we thus expect that, after a significant number of particles has been resonantly produced,

$$n_k(z) \propto \exp\left(2\int_{z_i}^{z} \mu_k(z')dz'\right) . \tag{2.93}$$

The initial time z_i refers to the time the mode enters the resonance band, i.e. $z_i = 0$ and $z_i = z_1$ for type (ii) and type (iii) modes, respectively. One can use Eq. (2.93) to estimate the total particle number resonantly produced in each mode. The details of this calculation are given in Appendix A, yielding at $z = z_2$:

$$\log n_k^{(ii)} = \frac{q_0^2}{2\gamma}\frac{1}{1+\beta|q_0|}\left(\beta\sqrt{1-\beta^2} + \frac{\pi}{2} + \arcsin\beta\right) , \qquad \log n_k^{(iii)} = \frac{q_0^2}{2\gamma}\frac{\pi}{1+\beta|q_0|} . \tag{2.94}$$

Eq. (2.94) constitutes the main result of this section, giving the leading order expressions for the particle number density produced by the resonance in an expanding universe. From these approximate expressions, we see that the q_0^2/γ controls the strength of the resonance, a significant number of particles being produced only if $\gamma \lesssim q_0^2$. Recall that, in the non-expanding case, the typical resonance time was given by $\Delta t_{res} = (\mu_k \Omega)^{-1} \sim (|q_0|\Omega_0/2)^{-1}$. The typical time a mode spends inside the resonance band in the expanding case is, from Eq. (2.92), $\Delta t_{band} \sim \frac{4q_0}{\gamma}\Omega_0^{-1}$. Hence, apart from numerical factors, the condition for a significant particle production is simply stating that the time a given mode spends inside the resonance band should be greater than the typical time the resonance takes to develop, $\Delta t_{band} \gtrsim \Delta t_{res}$.

From the results in Eq. (2.94), we can also conclude that the total particle number produced increases with β for $-1 \leq \beta \leq 1$. On the other hand, for $\beta > 1$, it exhibits a slow decrease with β, showing that the production of higher momentum modes is suppressed, in agreement with our expectations.

To check the results obtained so far for an expanding universe, we have solved Eq. (2.84) numerically. To simplify the computation, we have rescaled the mode functions via $\tilde{X}_k \equiv \sqrt{2\omega_k(t_0)}X_k$, so that initially we have approximately

$$\tilde{X}_k(0) \simeq 1 \ , \qquad \tilde{X}_k'(0) \simeq -i \ . \tag{2.95}$$

We then computed the function

$$\tilde{n}_k(z) = |\tilde{X}_k(z)|^2 + |\tilde{X}_k'(z)|^2 \ , \tag{2.96}$$

which is related to the physical particle number density of each mode, given by Eq. (2.48), approximately by $n_k \simeq \frac{\tilde{n}_k}{4a(t)}$, taking the limit of large particle number. Note that $\tilde{n}_k = 2$ initially, as we neglected the $1/2$ factor in Eq. (2.48), which has to be taken into account before a significant number of particles is produced.

In Figure 2.5, we illustrate the results obtained for the three types of modes, along with the analytical predictions from Eq. (2.93)[6].

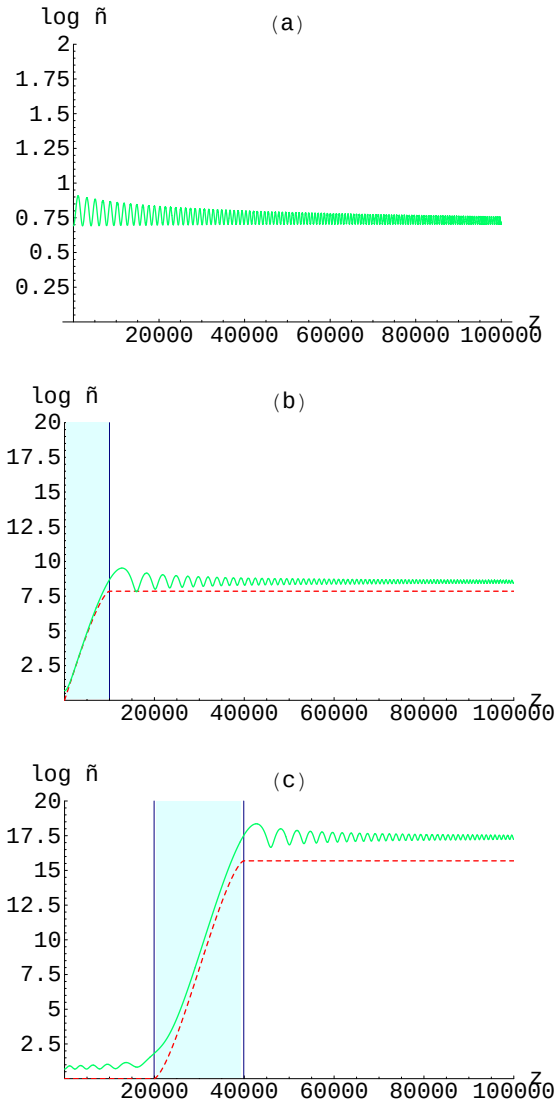

Figure 2.5: Numerical results obtained for the particle number with $|q_0| = 10^{-3}$ and $\gamma = 10^{-7}$. The plots (a), (b) and (c) correspond to modes with $\beta = -3,\ 0$ and 3, respectively. The solid (dashed) line represents the numerical (analytical) solution, with the shaded area denoting the period each mode is in the resonance band.

The plots in this figure show that all three modes follow the expected behaviour. The type (i) mode exhibits an oscillating particle number, with oscillations of de-

[6]The parameters of these simulations ensure the validity of our approximations and that a significant particle number is produced for the types (ii) and (iii) modes.

creasing amplitude and period, with no net particle number produced[7]. Both type (ii) and (iii) modes are exponentially amplified during a finite period, after which their particle number oscillates with decreasing amplitude and period, tending to an adiabatically constant value. Also, as expected, the type (iii) mode exhibits an oscillating behaviour before entering the resonance band.

We also conclude from Figure 2.5 that the particle number follows the predicted evolution inside the resonance band, the main differences between the numerical and the analytical solutions occurring near the limits of the resonance band, where the transitions between resonant and oscillating regimes take place. The discrepancies for low particle number are also due to the normalization of $\tilde{n}_k$, as discussed earlier. It is nevertheless clear that Eq. (2.93) gives a good description of the resonant regime in an expanding universe, although it underestimates the particle number density, and that the contributions of the non-resonant periods are subdominant, as expected.

The total particle number produced by the end of the resonant regime, $\tilde{n}_k(z_2)$, was computed for several values of β, keeping $|q_0|$ and γ fixed at the values chosen above. The results we have obtained are shown in Figure 2.6.

One observes that $\tilde{n}_k(z_2)$ increases with β for type (ii) modes and slowly decreases with β for type (iii) modes, in agreement with Eq. (2.94). The main discrepancies between the numerical results and the analytical prediction are again due to the smooth transition between the resonant and non-resonant regimes at z_2, with the latter regime giving a subdominant contribution to the total particle number, which is more significant for type (iii) modes.

The different number of oscillations the modes undergo before entering the resonance band give the oscillations that can be observed in Figure 2.6. These are suppressed for large β as the pre-resonance oscillations of the particle number give a negligible contribution for high momentum modes.

[7]The positive value of $log\ \tilde{n}_k$ reflects the normalization chosen in Eq. (2.96) and does not correspond to a physical particle number.

Numerical simulations also show that, as expected, the particle number in all modes decreases with γ, so that Hubble expansion may inhibit the resonant amplification of particle modes at early times.

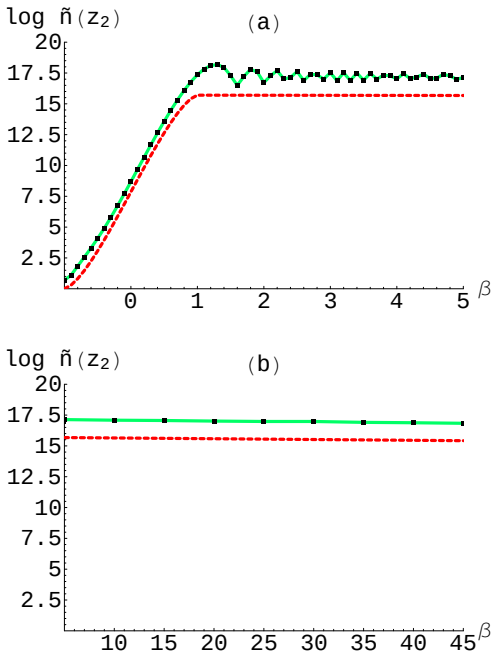

Figure 2.6: Numerical results for the total particle number produced by the resonance as a function of β. Plot (a) shows the results for small values of β, including type (ii) and (iii) modes, and plot (b) shows the results for large values of β, where only type (iii) modes are present. The solid (dashed) line corresponds to the numerical (analytical) results, for $|q_0| = 10^{-3}$ and $\gamma = 10^{-7}$.

Thus, our analysis of the resonance regime gives a good description of branonium particle production in an expanding universe, with subdominant contributions from non-resonant regimes. Extrapolation of this discussion to high momentum modes is, however, difficult, as these will only be excited at late times, where our approximations may no longer hold. The production of high momentum particles is nevertheless suppressed, as we have concluded earlier. Furthermore, at each given time $z > 0$, only the modes with $z_1 < z$ have entered the resonance band, which means that only those modes for which

$$A_{k0} < \frac{1 + |q_0|(1 + \xi z)}{1 - \gamma z} \tag{2.97}$$

have started being excited. This gives the following momentum cut-off for modes which have already been amplified at $t > t_0$:

$$k_+(t) = \frac{1}{2}\left[2\delta_0^2\left(1 + 6\alpha\frac{\Delta t}{t_0} + \Omega_0^2\right)\right]^{\frac{1}{2}}\left(1 - 20\alpha\frac{\Delta t}{t_0}\right)^{-\frac{1}{2}} . \tag{2.98}$$

This leads to the expected cut-off in the limit $\alpha \to 0$, given by k_+ in Eq. (2.66).

The generalization of these results for massive particles follows the same reasoning used in the non-expanding case, with the substitution $k_{phys}^2 \to k_{phys}^2 + m^2$ within our approximations. Note that, in the expanding case, the physical momentum of the particles is redshifted while their mass remains the same as the universe expands. This modification will then produce a more complex evolution of the parameter $A_k(z)$ in the modified Mathieu equation, Eq. (2.84), given to lowest order by:

$$A_k(z) = A_{k0}(1 - \gamma z) + \frac{4m^2}{\Omega_0^2}(1 - \frac{9}{10}\gamma z) . \tag{2.99}$$

This has, however, no significant effects on the qualitative features of the resonant mechanism, so that we will not analyze this case in more detail.

We, thus, conclude that, to lowest order, the parametric resonance survives in an expanding universe, although modes are excited only during a finite period. These results hold only at late times but we note once again that all quantities are measured in string units. We need, however, to bear in mind that Eq. (2.84) is not the Mathieu equation and that several other terms in Eq. (2.43) may become important at early times. These may alter the excitation time and the amplification of each mode, or even prevent any particle production. It is nevertheless clear that the effects of Hubble expansion are suppressed at the typical energies involved in the probe's motion, so that one still expects a significant number of particles to be produced.

2.2.3 Energy radiated into brane modes

As the resonance develops, the probe brane loses energy to excited η-particle modes and one may wonder whether the energy radiated by this mechanism is sufficient to affect the probe brane's motion.

Let us start by computing the energy density of massless particles produced by the resonance in a non-expanding universe. We have seen that each rescaled mode function X_k has an associated harmonic oscillator energy function $E_k = \omega_k(n_k + 1/2)$. For the mode functions $\chi_k = \sqrt{f}X_k$, the associated energy function is approximately the same in the non-relativistic and large distance limit, where $f \simeq 1$. Hence, the total energy density radiated into brane particle-modes is given by:

$$\epsilon_p = \int \frac{d^3k}{(2\pi)^3} E_k = \frac{1}{2\pi^2} \int_0^{+\infty} dk\ k^2 \omega_k \left(n_k + \frac{1}{2} \right) , \tag{2.100}$$

where we have used the momentum space isotropy discussed earlier. After a significant number of particles has been produced, we may take $n_k \gg 1/2$ and neglect the $1/2$ factor in Eq. (2.100). Also, we know that particles are produced in a narrow resonance band centered at $k_c = \Omega/2$ with a band width $\Delta k_{res} \simeq \delta^2/\Omega = |q|\Omega/2$. The particle number distribution in momentum space can then be well approximated by a Gaussian distribution of the form:

$$n_k(t) = n_{k_c}(t) \exp\left(-\frac{1}{2} \frac{(k - k_c)^2}{\Delta k(t)^2} \right) . \tag{2.101}$$

The gaussian distribution width Δk should correspond to a fraction of the resonance band width, so that we may write $\Delta k(t) = \lambda(t)\Delta k_{res}$. The coefficient λ is expected to be time-dependent as the central mode k_c is more amplified than all the other modes in the resonance band, so that the distribution should become more sharply peaked about this value with time. The advantage of writing the particle number

distribution in this form is that it allows us to further approximate the result by a δ-function distribution, taking into account that $\Delta k/k_c \ll 1$, as discussed earlier. Introducing the correct normalization, we may then write:

$$n_k(t) \simeq n_{k_c}(t)\sqrt{2\pi}\Delta k(t)\delta(k-k_c) \ . \tag{2.102}$$

Using $\omega_{k_c} \simeq k_c = \Omega/2$, we obtain:

$$\epsilon_p \simeq \frac{\lambda}{\pi\sqrt{2\pi}}\left(\frac{\Omega}{2}\right)^3 \Delta k_{res} n_{k_c} \simeq \frac{\lambda}{\pi\sqrt{2\pi}}|q|\left(\frac{\Omega}{2}\right)^4 n_{k_c} \ , \tag{2.103}$$

where the time dependence of n_{k_c}, λ and consequently ϵ_p is implicit. Notice that, when $q \to 0$, we have $\epsilon_p \to 0$, as the resonance vanishes in this limit. To have an estimate of the order of magnitude of this quantity, take the example we have considered before in the discussion of particle production in a non-expanding universe, for which $|q| = 10^{-4}$ and $\Omega = 4 \times 10^{-5}$, in units of the string length. By solving the equations of motion numerically and fitting the obtained particle number distribution to the gaussian distribution given in Eq. (2.101), we may determine the values of λ and n_{k_c}. For an initial time $t_0 = 10^9$, we obtained the following results:

$$\begin{aligned} n_{k_c}(5t_0) &\simeq 7.5 \times 10^2 \ , \qquad \lambda(5t_0) \simeq 0.20 \ , \\ n_{k_c}(10t_0) &\simeq 1.6 \times 10^7 \ , \qquad \lambda(10t_0) \simeq 0.12 \ . \end{aligned} \tag{2.104}$$

These two examples confirm that, indeed, the gaussian distribution width decreases in time. From Eq. (2.103), we obtain for these two cases $\epsilon_p(5t_0) \simeq 3 \times 10^{-22}$ and $\epsilon(10t_0) \simeq 4 \times 10^{-18}$, in units of the string energy scale.

The energy density radiated into brane particle-modes should then be compared with the energy density of the interbrane distance field ϕ, given by $\epsilon = -(\sigma\Omega/2)^{\frac{2}{3}}$. For the example considered above, $\epsilon \simeq -2 \times 10^{-2}$, so that the value obtained for

the energy density radiated into particles up to $t = 10t_0 = 10^{10}$ is negligible when compared to the probe brane's energy density. In general, we obtain:

$$\frac{\epsilon_p}{|\epsilon|} \simeq \frac{\lambda}{\pi\sqrt{2\pi}} \frac{|q|}{\sigma^{\frac{2}{3}}} \left(\frac{\Omega}{2}\right)^{\frac{10}{3}} n_{k_c} \ , \tag{2.105}$$

which gives the main result of this subsection. This means that, in the previous example, if we take $\lambda \sim 0.01 - 0.1$, up to a η-particle number density of $10^{23} - 10^{24}$ can be produced without affecting significantly the motion of the probe brane.

These results can be easily generalized for the massive case, by taking into account the changes in k_c and Δk_{res} discussed earlier. For $\delta^2/2 \ll k_c^2$, we obtain:

$$\frac{\epsilon_p}{|\epsilon|} \simeq \frac{\lambda}{\pi\sqrt{2\pi}} \frac{|q|}{\sigma^{\frac{2}{3}}} k_c \left(\frac{\Omega}{2}\right)^{\frac{7}{3}} n_{k_c} \ , \tag{2.106}$$

with $k_c = \sqrt{(\Omega/2)^2 - m^2}$ and which, as expected, reduces to Eq. (2.105) in the limit $m \to 0$. As the momentum of the produced particles decreases with m, the energy damped into brane particle-modes is smaller for heavier particles.

The analysis of the energy radiated into brane particle-modes is more difficult to perform in the expanding universe case, as more effects have to be taken into account. First, we need to recall the approximate relation between $\tilde{n}_k$ and the physical particle number. Next, we need to notice that the mode functions χ_k are redshifted by a factor of $a(t)^{-\frac{3}{2}}$ with respect to the harmonic oscillator mode functions X_k. Finally, for the purposes of determining the energy density of the produced particles, we may take $\omega_k(t) \simeq k/a(t)$. Then, we have

$$\epsilon_p(t) \simeq \frac{1}{a(t)^5} \int \frac{dk\ k^3}{8\pi^2} \tilde{n}_k \ . \tag{2.107}$$

We see that the energy density of the produced particles is redshifted by the usual power of a^{-3}, but is further reduced due to the redshift of the physical momentum

and energy of the modes. We can use the expressions obtained for the particle number produced by the resonance in Eq. (2.94) to determine $\tilde{n}_k$, as we have concluded that the effects of the non-resonant periods are subdominant. Writing them in terms of the comoving momentum of the modes, we conclude that, for type (iii) modes,

$$\epsilon_p(t) \propto \int dk\ k^3 \exp\left(\frac{q_0^2\Omega_0^2\pi}{8\gamma}\frac{1}{k^2}\right) . \tag{2.108}$$

To determine the limits of this integral, one must recall that, at a given time, only a finite number of modes has entered the resonance band. In particular, one may use the value computed in Eq. (2.98) as the upper limit of this integral, although some of these modes have not yet been completely excited by the resonance. The lower limit of the integral will be the first type (iii) mode, with $k = k_* \equiv k_{c0}\sqrt{1+|q_0|}$. This gives a finite energy density radiated into brane modes at each finite time $t > t_0$. This energy density is redshifted by Hubble expansion, but at the same time modes with increasing energy enter the resonance band. This process will, however, stop at some point, as our approximations will break down when the motion of the probe becomes relativistic and gets too close to the central stack. Even if the resonance mechanism persists in this limit, although certainly in a different form, the probe will eventually modify its trajectory, either by colliding with the central stack or via some other mechanism that stabilizes its motion.

The contribution of type (ii) modes is obviously finite and can be computed by integrating Eq. (2.107) using the corresponding expression for $\tilde{n}_k$ given in Eq. (2.94), with $k_{c0} < k < k_*$. No particular insight is, however, gained by computing these integrals, as the dominant contributions are given by high momentum modes which enter the resonance band at late times, when the effects of expansion may be neglected. We may then effectively use the results obtained in the non-expanding case, with the values of q and Ω at the end of the resonance mechanism.

2.2.4 Radiation into bulk modes

As discussed in [122], the probe's orbital motion may induce not only the production of brane-bound particles but also radiation into bulk modes, namely gravitational, RR form and dilatonic fields. This is due to the accelerated motion of the probe brane and most of the power is radiated into lower-spin fields, in particular scalar fields which couple to the brane's orbital monopole moment.

The probe will thus lose energy through this process, contributing to the decay of its orbit. This will certainly modify the mechanism of resonant production of particle-modes in the brane, namely by varying the orbital frequency, which determines the comoving momentum of the modes that are excited by the parametric resonance. One then expects the effects of radiation into bulk modes to be quite similar to those induced by the universe's expansion, so that we will not analyze this process in detail. Nevertheless, it is important to estimate its contribution to orbital decay.

The power radiated into bulk scalar modes was estimated in [122], where it was shown that the number of orbits the probe can complete before the interbrane distance becomes of order l_s is approximately given by:

$$\mathcal{N} \simeq \frac{2}{3\pi}\left(\frac{r_i}{l_s}\right)^{\frac{3}{2}} \frac{1}{(g_s^3 N)^{\frac{1}{2}}} \ , \tag{2.109}$$

where r_i is the initial value of the physical radius of the orbit, assuming it is circular[8]. This expression shows that, for the probe to complete a large number of orbits before decay, it needs to be at a large distance from the central stack, in units of the string length. Also, one needs $g_s^3 N \ll 1$ to obtain a sufficiently large value of $\mathcal{N}$. This value should be compared to the number of orbits required for an effective resonance, of order $(\pi|q|)^{-1}$ for $H = 0$. Hence, the production of a significant number of particles

[8]This is sufficient for an estimate of the decay time, even though we are interested in low eccentricity orbits.

requires $\mathcal{N} \gg (\pi|q|)^{-1}$, which gives for the initial orbital radius:

$$\frac{r_i}{l_s} \gg \left(\frac{3}{2|q|}\right)^{\frac{2}{3}} N^{\frac{1}{3}} g_s \ . \tag{2.110}$$

For example, if $|q| \simeq 10^{-3}$ and there are 10 branes in the central stack, we need $r_i \gtrsim 300 g_s l_s$ for the resonance to be effective, which is not too large a number taking into account that g_s is parametrically small.

As, in the analysis of the parametric resonance mechanism, we have assumed the interbrane distance to be large compared to the string length, we expect the effects of radiation into bulk modes to be initially negligible. This process should, however, become more important as the orbit decays and the probe brane accelerates. It is even possible that, at late times, it overcomes Hubble expansion as the main energy loss process. Nevertheless, the end of the resonance should still be determined by the break down of the non-relativistic and large distance approximation, as this also controls the amount of energy damped into bulk modes.

2.3 Effects of transverse space compactification

So far we have considered the probe to move at distances from the central stack which are small compared to the size of the transverse space directions. In this section, we will include the leading order effects of the finite transverse space and show that they may lead to the creation of orbital angular momentum and low eccentricity orbits, which constitute key ingredients for the development of the parametric resonance.

We will consider the simplest case of compactifying the three transverse directions on an isotropic 3-torus of size $R_\perp$, defined by the identifications $y^i \leftrightarrow y^i + R_\perp$. As mentioned earlier, the harmonic function $h(r)$ needs to be modified in this case by including the appropriate 'brane images', according to Eq. (2.5). These are placed in points with coordinates $y^i = n_i R_\perp$, with integer n_i, defining a hypercubic lattice

corresponding to the covering space of the 3-torus, $(\mathbb{R}/\mathbb{Z})^3$. Although toroidal compactifications are too simple to give acceptable phenomenology, this will be sufficient to illustrate the main effects of compactification on the probe brane's trajectory.

The interbrane potential associated with the generalized harmonic function Eq. (2.5) is obtained by computing the propagator for a massless field on a torus:

$$\nabla^2 G(\mathbf{y}, \mathbf{y}') = \delta(\mathbf{y} - \mathbf{y}') - \frac{1}{V_\perp} \,, \tag{2.111}$$

where $V_\perp \equiv R_\perp^3$ is the volume of the transverse 3-torus. The term $-\frac{1}{V_\perp}$ is included for consistency, so that the integral of both sides of Eq. (2.111) over the compact manifold vanishes. This term arises naturally from the curvature of the non-compact 4-dimensional spacetime and gives a negative contribution to the interbrane potential which, for an approximately homogeneous internal manifold, can be assumed to be smeared over the whole transverse volume [93]. If one expands the Green's function $G(\mathbf{y}, \mathbf{y}')$ in terms of eigenfunctions of the Laplacian operator ∇^2, one concludes that the $-\frac{1}{V_\perp}$ term removes the unphysical zero-mode which makes the Green's function diverge. It has been shown that one can write the massless propagator on the 3-torus in terms of an integral involving the Jacobi-theta function θ_3 [125]:

$$G(\mathbf{y}) \equiv G(\mathbf{y}, \mathbf{0}) = \frac{1}{R_\perp} \int_0^\infty \mathrm{d}s \, \left[1 - \prod_{i=1}^{3} \theta_3 \left(\frac{\pi \, y^i}{R_\perp}, e^{-4\pi^2 s} \right) \right] \,. \tag{2.112}$$

Although this expression gives the full compact space propagator, it is rather difficult to work with and we are mainly interested in the leading order modifications introduced by compactification when the probe is moving closer to the central stack than to any of its images. Notice, however, that orbits around any of the brane images are nevertheless equivalent due to the symmetries of the hypercubic lattice. In [164], an expansion of this propagator about the origin was computed using Ewald's method for calculating potentials in hypercubic lattices in the context of solid state physics.

The leading corrections to the central $1/r$ potential are then given by:

$$G(\mathbf{y}) = -\frac{1}{4\pi r} - \frac{r^2}{6V_\perp} - \frac{C_S}{V_\perp^{\frac{1}{3}}} - A_4 h_4(\mathbf{y}) - A_6 h_6(\mathbf{y}) - \dots \tag{2.113}$$

The values for the coefficients of the various terms were found numerically to be $C_S = -0.21$, $A_4 = 0.44$ and $A_6 = 0.0072$. The functions $h_4(\mathbf{y})$ and $h_6(\mathbf{y})$ are harmonic functions of order $(r/R_\perp)^4$ and $(r/R_\perp)^6$, respectively, and the series continues with harmonic terms of higher (even) orders. The leading harmonic correction to the propagator is given by:

$$h_4(\mathbf{y}) = \frac{1}{R_\perp^5}\left[\sum_{i=1}^{3}(y^i)^4 - 3\sum_{i\neq j=1}^{3}(y^i)^2(y^j)^2\right] . \tag{2.114}$$

Recalling that the function $h(\mathbf{y})$ contributes to the interbrane potential through the graviton-dilaton and RR-form interactions, we may write this potential for $Q_6 \ll r \ll R_\perp$ to order $(r/R_\perp)^4$ as

$$V(\mathbf{y}) = -2Q_6\left[\frac{1}{r} + \frac{2\pi}{3R_\perp}\left(\frac{r}{R_\perp}\right)^2 + \frac{4\pi A_4}{R_\perp}\left(\frac{r}{R_\perp}\right)^4 f\left(\frac{y^i}{r}\right) + \dots\right] , \tag{2.115}$$

where we defined the function

$$f\left(\frac{y^i}{r}\right) \equiv \left[\sum_{i=1}^{3}\left(\frac{y^i}{r}\right)^4 - 3\sum_{i\neq j=1}^{3}\left(\frac{y^i}{r}\right)^2\left(\frac{y^j}{r}\right)^2\right] . \tag{2.116}$$

Thus, to leading order, the potential is modified by two repulsive contributions arising from the overall attraction of the image branes, their coefficients being suppressed by a factor $1/R_\perp$, so that their effects are negligible for large transverse volume. The 'jellium' term, of order $(r/R_\perp)^2$ and whose name arises in the context of solid state physics, gives an isotropic contribution while the 'asymmetry' term, of order $(r/R_\perp)^4$, gives an anisotropic contribution to the potential.

We will be more interested in the effects of the asymmetry term, as its breaks the rotational symmetry of the transverse space and gives a potential source of orbital angular momentum. The effects of the jellium term will, however, be more significant close to the central stack. It is easy to show that, for large transverse volume, this term will, to leading order, make the probe brane's orbits precess. This is due to its repulsive nature and, for small eccentricity orbits, the deficit angle is approximately given by $\Delta\theta \simeq 32\pi^2(l^2/R_\perp Q_6(T_6V_3)^2)^3$. This effect will, however, be suppressed at late times as the probe's angular momentum is redshifted away by Hubble expansion.

The inclusion of the asymmetry term makes the analysis quite difficult, as the potential depends on both angular coordinates in the transverse space. This may lead, in particular, to non-planar orbits of the probe brane. However, if we set $y^3 = \dot{y}^3 = 0$ initially, the probe will feel no force along this direction and its trajectory will be confined to the (y^1, y^2) plane as before. We will focus on this particular case, bearing in mind that non-planar trajectories may generically arise.

Within these assumptions, the problem reduces, as before, to the evolution of the canonically normalized complex scalar field ϕ, defined in Eq. (2.10), in an expanding universe. Its potential can be written as

$$V(\phi) = -\frac{\sigma}{|\phi|} - \sigma_J|\phi|^2 - \sigma_A(\phi_R^4 + \phi_I^4 - 6\phi_R^2\phi_I^2) \ , \tag{2.117}$$

where $\phi = \phi_R + i\phi_I$, σ was defined in Eq. (2.20) and

$$\sigma_J \equiv \frac{8\pi}{3}\frac{Q_6}{R_\perp^3} \ , \qquad \sigma_A = \frac{32\pi A_4}{T_6V_3}\frac{Q_6}{R_\perp^5} \tag{2.118}$$

give the strength of the jellium and asymmetry terms. This potential is no longer invariant under the global $U(1)$ symmetry of the non-compact case, signaling that the probe's angular momentum is no longer conserved. This is quite similar to the $U(1)$-violating potential governing the evolution of the scalar field in the Affleck-Dine

mechanism [46], where non-conservation of angular momentum plays a crucial role in generating the baryon asymmetry in our universe. The potential remains, however, invariant under the hypercubic group symmetries $\phi_{R,I} \to -\phi_{R,I}$ and $\phi_R \leftrightarrow \phi_I$, i.e. under $\pi/2$ rotations as well as reflections about the $\theta = \pi/4$ axis, as one can easily conclude by writing Eq. (2.116) for $y^3 = 0$ as

$$f(\theta) = 1 - 2\sin^2(2\theta) \ . \tag{2.119}$$

Hence, we only need to consider initial conditions such that $\phi_R \geq \phi_I \geq 0$ or equivalently $0 \leq \theta \leq \pi/4$. The $U(1)$ symmetry violation precludes a complete analytical description of the orbits. However, it is not difficult to obtain a qualitative insight into the main features of the probe's trajectories. If the probe is placed significantly far from the central stack, but still closer to it than to any of the image branes, the asymmetry term will not be negligible and some angular momentum will be created or destroyed. If the probe has no angular momentum initially, then it will necessarily acquire some and be placed in an orbit around the central stack, instead of just falling towards it along the radial direction. As both the jellium and the asymmetry interactions are repulsive, it is possible that the probe does not remain bound to the central stack, becoming connected to one or more branes in the hypercubic lattice[9].

Hubble expansion will, however, redshift the probe's energy and angular momentum, so that one expects the probe to become bound to only one brane stack image at late times. As the orbital radius decreases, the $U(1)$-violating term becomes less significant and the particle number associated with ϕ becomes asymptotically constant, i.e. the angular momentum varies only due to the universe's expansion.

Due to the hypercubic symmetries, in the $\theta = 0, \pi/4$ axes the force acting on the probe will be along the radial direction, as $f'(\pi/4) = f'(0) = 0$, and no angular

[9]If more than one image brane is relevant, the expansion of the potential in Eq. (2.115) is no longer valid and the form of the full potential must be analyzed.

momentum will be created in these particular directions. For $0 < \theta < \pi/4$, angular momentum creation should, however, be a generic feature.

To have a better understanding of how the initial conditions affect the amount of angular momentum created or destroyed, we have computed the force acting on the probe brane and the associated torque, given by:

$$\mathbf{F} = -\nabla V = -\frac{\partial V}{\partial \phi_R}\mathbf{e_R} - \frac{\partial V}{\partial \phi_I}\mathbf{e_I} \ , \qquad \tau = |\phi \times \mathbf{F}| = -\phi_R \frac{\partial V}{\partial \phi_I} + \phi_I \frac{\partial V}{\partial \phi_R} \ , \quad (2.120)$$

where ϕ defines a vector in the (ϕ_R, ϕ_I) plane. Recall that the torque gives the variation of the angular momentum, which in terms of the particle number density n defined in Eq. (2.13) can be written as:

$$\frac{dn}{dt} + 3Hn = \tau \ . \quad (2.121)$$

We have plotted the isotorque contours for some particular parameter values in Figure 2.7. We have restricted the position of the probe to the region $y^1, y^2 < 0.5R_\perp$, where the expansion of the potential about $r = 0$ is sufficiently accurate and the probe's motion is bound to the central stack[10].

Observing this figure we see that the torque is maximized close to the boundary of the region mentioned above (darker areas for $0 \leq \theta \leq \pi/4$). Also, the longer the probe's trajectory remains close to this boundary the more angular momentum it is likely to gain. Thus, maximum angular momentum creation should occur if the probe is placed just below the centre of the hypercubic cell.

The initial value of the Hubble rate will also affect the amount of angular momentum created. If it is of the same order of magnitude as the orbital frequency, one expects the probe to be driven into lower torque regions within a few periods. Lower

[10]This may not be true near the limits of this region, as the actual region where the force points towards the central stack has a more complicated shape.

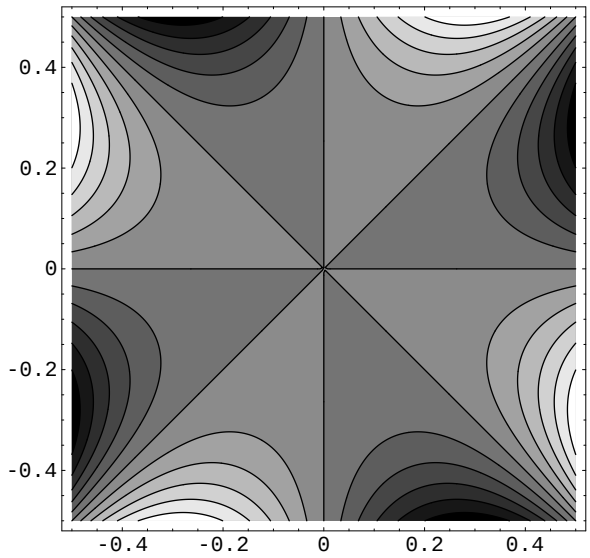

Figure 2.7: Torque acting on the probe brane in the (y^1, y^2) plane. Coordinates are normalized to the size of the transverse torus, $R_\perp = 2 \times 10^4$, with $Q_6 = 100$ and $T_6 V_3 = 1$. Note that the torque changes sign at $\theta = n\pi/4$, $n \in \mathbb{Z}$, being negative for $0 < \theta < \pi/4$, and its magnitude increases away from the origin.

values of H should allow the angular momentum to oscillate significantly as the probe moves through alternate regions of positive and negative torque, but no net angular momentum will be gained after the first few orbits and the asymptotic value of the comoving particle number $N = na^3$ is determined by the initial path.

We have simulated the evolution of the probe brane numerically to illustrate this discussion, setting the initial conditions as follows:

$$\phi_{R,I}(t_0) = \sqrt{\frac{T_6 V_3}{2}} \delta_{R,I} R_\perp \ , \qquad \dot{\phi}_{R,I} = 0 \ , \tag{2.122}$$

with $\delta_R > \delta_I$, giving $0 < \theta < \pi/4$, and $\delta_{R,I} < 0.5$, which ensures that the probe is placed initially within the region where it is bound to the central stack. We have also computed the eccentricity of the orbit, as defined in Eq. (2.22), with the probe's energy density including both the jellium and asymmetry terms. This quantity should only become meaningful at late times, when the latter terms become negligible, but its evolution tracks the creation of angular momentum along the probe's trajectory.

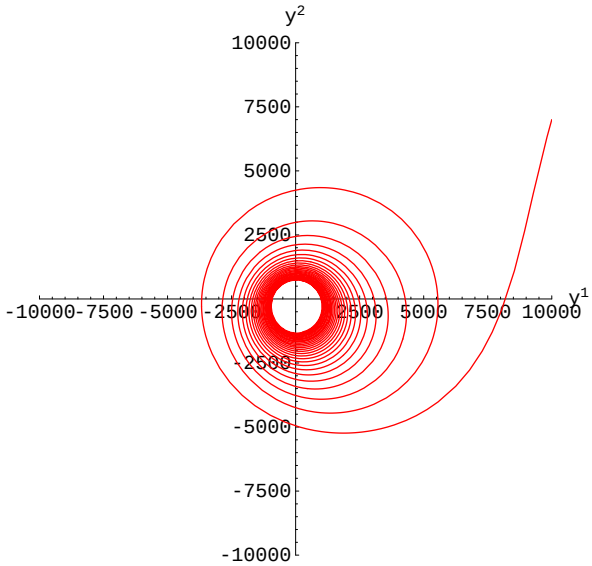

Figure 2.8: Results obtained numerically for the probe brane's trajectory for $Q_6 = 100$, $R_\perp = 2 \times 10^4$ and $T_6 = V_3^{-1}$. The probe is placed initially at the point $(\delta_R, \delta_I) = (0.50, 0.35)$ for $t_0 = 2 \times 10^6$ and we consider a matter-dominated universe.

Figure 2.8 shows an example of the results obtained for the probe's orbit, with the probe placed initially below the centre of the hypercubic cell so that a significant angular momentum is produced during its motion. One observes, as expected, a small orbital precession and the decay of the orbit into regions of lower torque, driving the eccentricity towards a constant value, $e = 0.28$. Initial conditions were chosen so that the inverse Hubble parameter is comparable to the orbital period and, hence, the orbit is quickly stabilized. Notice the similarities with the example in Figure 2.1, although no initial angular momentum exists in this case.

In Figure 2.9 we plot the asymptotic values of the eccentricity obtained numerically for different initial positions in the plane (ϕ_R, ϕ_I) and two distinct values of the initial Hubble parameter in a matter-dominated universe.

In both cases, smaller eccentricity orbits are obtained near the larger torque regions below the centre of the hypercubic cell, as expected. Some angular momentum is in general produced, although most initial conditions lead to highly eccentric orbits, with $e > 0.9$.

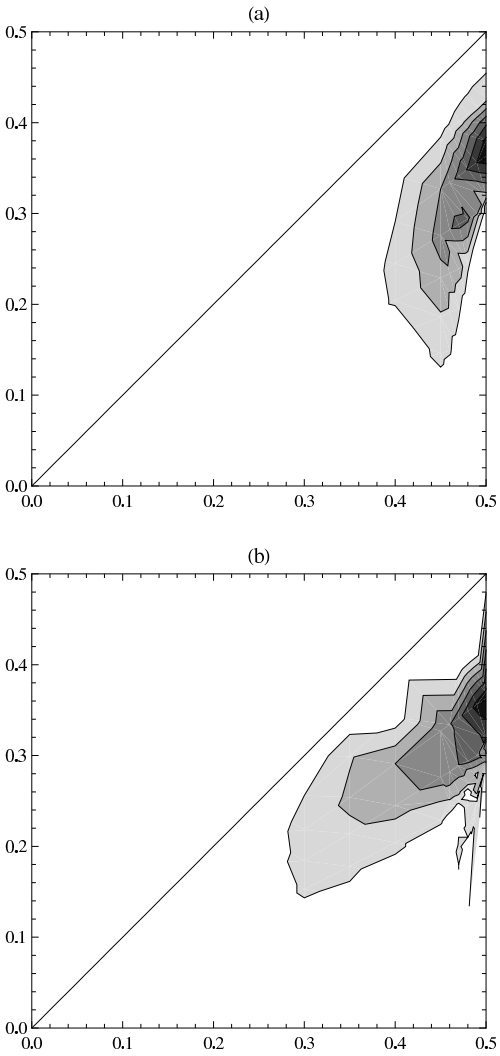

Figure 2.9: Asymptotic values of the orbital eccentricity in the plane (δ_R, δ_I), with $\delta_R \geq \delta_I$, assuming $Q_6 = 100$, $R_\perp = 2 \times 10^4$ and $T_6 = V_3^{-1}$, in a matter-dominated universe. The motion of the probe starts at (a) $t_0 = 1 \times 10^6$ and (b) $t_0 = 5 \times 10^6$. Contours were plotted for $e = n/10$, with $n = 3, \ldots, 9$, and darker regions correspond to lower eccentricities.

Orbits are generically less eccentric if the motion starts at later times, with smaller Hubble damping of the asymmetry term. Furthermore, the combination of the asymmetry term and Hubble expansion makes the final eccentricity vary in a non-trivial way with the initial position of the probe, namely near $\delta_R \simeq 0.5$, where the orbits may in some cases become unbound. The asymptotic eccentricity also depends significantly on the values of Q_6 and $R_\perp$.

2.4 Stabilization and cosmological implications

Cosmological applications of the branonium parametric resonance are largely determined by the system's final configuration. As discussed above, the $D6-\overline{D6}$ system is unstable, as the probe loses energy and angular momentum due to Hubble expansion. At some stage, the distance between the probe and the central stack of branes will consequently become of the order of the string length (although our approximations break down long before this happens). When this occurs, the scalar mode associated with open strings stretching between the probe and the source branes becomes tachyonic, signaling an instability of the system [165]. Condensation of this tachyonic mode then leads to the annihilation of the probe anti-brane with one of the branes in the central stack. The non-supersymmetric nature of the $D6-\overline{D6}$ configuration is behind this instability, making the system evolve into a 1/2 BPS stack of $(N-1)$ $D6$ branes, with the same total charge as the original configuration but a lower energy.

After annihilation, the energy of the particles produced in the probe brane by the parametric resonance, as well as the probe's residual energy, will necessarily be transfered to the surviving d.o.f., both in the central stack and in the bulk. If a significant fraction is radiated into the source branes, the resonance will be responsible for a late reheating of the central stack and play a significant role in the subsequent evolution of our universe. A more detailed analysis of this process would, however,

require an extension of our results beyond the limits of their applicability.

More interesting scenarios may arise if some additional mechanism stabilizes the probe brane before annihilation takes place, in which case the produced particles may survive after the resonance mechanism ends. Stabilization of branonium systems necessarily implies the introduction of new interactions in the system or a modification of the existing ones. An attractive possibility for stabilizing multiple brane systems was suggested in [166]. When supersymmetry breaking occurs, it is often the case that one or more fields within the supermultiplets of the theory acquire masses, their value being set by the energy scale at which SUSY is broken. In [166], it was suggested that one or more gauge fields in the supergravity theory may become massive after SUSY breaking, while the graviton-dilaton modes remain massless. These gauge potentials will then induce short-range interactions which, if repulsive, may balance the graviton-dilaton atraction between different branes. Notice that the probe anti-brane itself breaks supersymmetry but does not induce bulk gauge field masses, so that other sources of SUSY breaking need to be considered in this case.

Suppose, for example, that the C_1 RR-form and consequently its magnetic dual form C_7 become massive after SUSY breaking. The RR-interaction can then be modelled by a Yukawa potential whose strength may be different from the graviton-dilaton part. At distances large compared to Q_6 but small compared to the size of the transverse dimensions, the relevant terms in the interbrane potential are:

$$V(r) = T_6 V_3 Q_6 \left(\lambda \frac{e^{-M_{RR} r}}{r} - \frac{1}{r} \right) , \tag{2.123}$$

where M_{RR} is the mass of the RR C_7-potential and λ the associated Yukawa coupling. If, as we have assumed so far, the probe is a $\overline{D6}$-brane, the RR-interaction, although short-ranged, is attractive and cannot balance the $\frac{1}{r}$ gravitational part. If, however, the probe is a $D6$-brane, we have $\lambda > 0$ and stabilization of the system may be possible

at short distances. In this case, for $r \gg M_{RR}^{-1}$, the RR-interaction is exponentially suppressed and the probe's motion is governed by the graviton-dilaton term. The evolution of the probe brane will, in this case, be very similar to that of a probe anti-brane in a massless RR-form background, the potential having half the strength of the potential in the latter case. This difference does not modify the qualitative features of the probe's trajectory and all the results derived in the previous sections remain valid if we make the substitution $Q_6 \to Q_6/2$.

The fate of a probe $D6$-brane will, however, be quite different than that of a probe $\overline{D6}$. As the probe's orbit decays due to the universe's expansion, the interbrane distance will eventually become of order M_{RR}^{-1}, at which point the repulsive RR-interaction becomes relevant and stabilization may be possible. For $M_{RR}^{-1} \gg Q_6$, the potential given in Eq. (2.123) has a local minimum formally given by:

$$r_0 = -M_{RR}^{-1}\left[1 + W\left(-\frac{1}{\lambda e}\right)\right] , \tag{2.124}$$

where $W(z)$ is the Lambert W-function, defined as the inverse of $f(W) = We^W$. One expects the probe to settle at this local minimum after its angular momentum redshifts away. This may not be the absolute minimum of the full potential, which includes supergravity and string theory corrections for $r \sim Q_6$ and $r \sim l_s$, respectively. Hence, absolute stabilization of the probe cannot be guaranteed, but it is reasonable to expect at least a very long-lived metastable state if $r_0 \sim M_{RR}^{-1} \gg Q_6 \gg l_s$.

From the properties of the Lambert W-function, one concludes that $r_0 = 0$ for $\lambda = 1$, being positive for $\lambda > 1$, and that r_0 strictly grows with λ. Hence, stabilization at large distances from the central stack is only possible if the RR-repulsion is stronger than the gravitational attraction, as expected. As the Yukawa parameter λ will not, in general, be much larger than 1, one expects the probe to stabilize at distances

$r_0 \sim M_{RR}^{-1}$. For instance, if $\lambda - e/2 \ll 1$, where e is the natural logarithm base,

$$r_0 \approx M_{RR}^{-1}\sqrt{\frac{8\lambda}{e} - 3}\ . \tag{2.125}$$

The scale of supersymmetry breaking will then determine the cosmological implications of the particle production mechanism analyzed in this work. If SUSY is broken at very high energies, inducing a large mass for the RR-potential, the probe will stabilize very close to the central stack and no tachyonic modes are present to induce annihilation. The stable probe and the central stack will then be characterized by a general broken gauge symmetry group $U(N) \times U(M)$, where $M \ll N$ is the number of branes in the probe, with an exponentially large number of particles charged under the $U(M)$ gauge group if the resonance develops before stabilization occurs. This may be relevant, for example, to the generation of the baryon asymmetry in our universe.

On the other hand, a soft SUSY breaking mass stabilizes the probe at large distances. The parametric resonance may then be relevant for dark matter production, as particles in the probe's world-volume interact weakly with the visible sector, the latter being embedded in the central stack. Furthermore, these particles may be supermassive, although parametrically smaller than the string scale, so that this could provide an effective mechanism for a non-thermal production of WIMPZILLAS [13].

One also expects the parametric resonance to amplify other bosonic modes living in the probe's world-volume, such as Yang-Mills fields if the probe has more than one brane. If these mediate baryon number-violating forces, their interactions with central stack fields could then provide a mechanism for GUT-baryogenesis [167], in which case the probe would need to be stabilized before nucleosynthesis.

It is also possible for fermionic particles living in the probe's world-volume to be produced in resonance, although Pauli blocking makes this process significantly different from the bosonic case, according to the discussion given in [168]. Thus, if

the probe can be stabilized, a resonant production of fermionic dark matter particles may also be achieved through this process.

One also expects the interbrane distance field to oscillate about the local minimum of the potential, possibly generating a second stage of resonant amplification. This may be induced from coupling to other fields, as in the standard preheating mechanism, or gravitationally, as in the case described in this chapter. Although this second stage may contribute significantly to the final particle number density in the probe brane's world-volume, we will not discuss it in further detail but rather refer the reader to the discussions given in this chapter and in the literature [36, 37, 158].

Another attractive cosmological implication of considering a probe $D6$-brane is related to its evolution during inflation. It is possible in both cases for the field ϕ to be overdamped during inflation, if its potential is sufficiently flat (for example, from large transverse volume suppression). However, in the case of a probe brane, the potential will be exactly flat during inflation if SUSY breaking only occurs at a later stage. The probe will then remain in the same position during inflation rather then being quickly driven towards the central stack. Initial conditions favourable to angular momentum generation may then be achieved after inflation in this case.

We emphasize that these scenarios depend on the embedding of the SM in this setup and on the SUSY breaking mechanism, which lie outside the scope of this thesis.

In our analysis, the parametric resonance arises only for $D6-\overline{D6}$ systems, where the $1/r$ potential leads to closed elliptical orbits in a non-expanding universe. This oscillatory behaviour of the interbrane distance field is crucial for the development of the resonance, although closed orbits are not required as e.g. in an expanding universe. Thus, other $Dp-\overline{Dp}$ branonium systems with $p<6$, where the probe trajectories are unbounded from below, cannot exhibit such resonant particle production. Additional stabilization potentials may, however, provide the required oscillations, allowing for a resonant particle production in other branonium systems.

Chapter 3

Light string resonances from Randall-Sundrum throats

As discussed in chapter 1, string excitations may provide one of the best probes of string theory compactifications, there being a possibility of observing them in the near future if the string scale lies close to the TeV scale, such as in large volume or warped compactifications. The latter seem to be generic features of the string landscape in the context of flux compactifications, with the warping providing an exponential rescaling of all mass scales along the throat. It is then natural to consider the spectrum of string Regge excitations in these geometries which, as discussed in chapter 1, are well described by the effective 5-dimensional RS construction. This scenario incorporates all the main generic characteristics of string theory throats, thus providing a simple framework within which we may analyze the spectrum of massive string resonances, although deviations from a pure AdS slice with rigid boundaries may introduce additional effects.

In particular, as mentioned in the introduction of this thesis, string realizations of the RS model suggest that string states are not necessarily much heavier than KK excitations, namely close to the IR tip of the throat, where the AdS curvature scale

may become comparable to the 5-dimensional mass scale. This leads to the generic expectation that the lightest Regge excitations are those with the largest overlap with the Higgs brane in the RS construction, being consequently associated with the heavier quarks.

Hence, in this chapter, we describe the inclusion of spin-3/2 excitations of bulk SM fermions in the RS construction. We follow a bottom-up approach that takes into account both the 10-dimensional origin of the fields and the phenomenological features of their spin-1/2 counterparts, which will allow us to derive both qualitative and quantitative aspects of their potential signatures in collider experiments, namely the Tevatron and the LHC.

3.1 Spin-3/2 fields in the Randall-Sundrum model

Let us begin by considering a massive 5-dimensional Dirac vector-spinor field Ψ_M, $M = 0, \ldots, 3, 5$, living in the bulk of the RS geometry, Eq. (1.7). This field is then described by the 5D extension of the Rarita-Schwinger action [169][1]:

$$S_5 = \int d^4x \int dy \sqrt{-G} \bar{\Psi}_M \gamma^{MNP} \left(D_N + \frac{1}{3} M_\Psi \gamma_N \right) \Psi_P \ , \tag{3.1}$$

where the covariant derivative is given by

$$D_M \Psi_N = \partial_M \Psi_N - \Gamma^P_{MN} \Psi_P + \frac{1}{2} \omega_M^{AB} \gamma_{AB} \Psi_N \ , \tag{3.2}$$

with Γ^P_{MN} denoting the 5-dimensional Christoffel symbols and ω_M^{AB} the components of the associated spin-connection. In Eq. (3.1), the 5D curved space gamma matrices γ^M, $M = 0, \cdots, 5$, are related to the corresponding flat space representation γ^a via $\gamma_M = e^a_M \gamma_a$, where $e^a_\mu = e^{-ky} \delta^a_\mu$ for $a, \mu = 0, \cdots, 3$, $e^5_5 = 1$ and all other components

[1] Our definition of M_Ψ differs from that in [169], corresponding in our case to the physical pole in the 5D propagator.

of the vielbein vanish. We have also defined the antisymmetric product $\gamma^{MNP} = \gamma^{[M}\gamma^{N}\gamma^{P]}$. We assume the mass term is generated in a gauge invariant way with respect to the spinorial transformation $\Psi_M \to \Psi_M + \partial_M \epsilon$, where ϵ is a spinorial gauge parameter, and parametrize the bulk mass as $M_\Psi = ck$ for some real constant c. We may also use this gauge invariance to set $\Psi_5 = 0$ [169], so that it suffices to denote the field by Ψ_μ, $\mu = 0, \ldots, 3$.

As for the case of bulk spin-1/2 fermions, it is convenient to separate the vector-spinor in its chiral components $\Psi_\mu^{L,R} = \pm\gamma_5 \Psi_\mu^{L,R}$. These admit a KK decomposition of the form:

$$\Psi_\mu^{L,R}(x,y) = \frac{1}{\sqrt{L}} \sum_n \psi_{\mu n}^{L,R}(x) e^{2ky} f_n^{L,R}(y) \ , \tag{3.3}$$

where the KK mode-functions are normalized as:

$$\frac{1}{L}\int_0^L dy e^{ky} f_m^{L,R*} f_n^{L,R} = \delta_{mn} \ . \tag{3.4}$$

Using the equations of motion derived from the Rarita-Schwinger action, one concludes that the rhd and lhd mode functions satisfy the coupled differential equations:

$$(\partial_5 + M_\Psi) f_n^R = m_n e^{ky} f_n^L \ , \qquad (-\partial_5 + M_\Psi) f_n^L = m_n e^{ky} f_n^R \ , \tag{3.5}$$

where m_n is the 4D (Dirac) mass of the $n-$th KK mode. These are in fact the same equations satisfied by the KK mode functions of a bulk spin-1/2 field [80], which is not surprising since the Rarita-Schwinger vector-spinor satisfies the 5-dimensional Dirac equation. It is convenient to define $t = e^{k(y-L)}$, so that $\epsilon \leq t \leq 1$, where $\epsilon = e^{-kL} \sim 10^{-16}$ in order to solve the hierarchy problem. In terms of this variable,

the KK mode equations can be written as:

$$t^2\partial_t^2 f_n^{L,R} + \big(x_n^2 t^2 - c(c \mp 1)\big) f_n^{L,R} = 0 \ , \tag{3.6}$$

where $x_n \equiv (m_n/k\epsilon) \sim (m_n/\text{TeV})$ and the + (–) sign corresponds to the rhd (lhd) modes. These equations have the general solution:

$$\begin{aligned} f_n^R(t) &= \sqrt{t}\big[a_n^R J_{c+\frac{1}{2}}(x_n t) + b_n^R J_{-c-\frac{1}{2}}(x_n t)\big] \ , \\ f_n^L(t) &= \sqrt{t}\big[a_n^L J_{\frac{1}{2}-c}(x_n t) + b_n^L J_{c-\frac{1}{2}}(x_n t)\big] \ , \end{aligned} \tag{3.7}$$

where $J_\alpha(x)$ represents a Bessel function of the first kind. Eq. (3.5) then implies $a_n^R = b_n^L$ and $a_n^L = -b_n^R$.

To determine the KK spectrum, one needs to impose b.c. for the mode functions in the UV ($t = \epsilon$) and IR ($t = 1$) branes. Bulk quarks and leptons, which have analogous KK mode solutions, satisfy the same b.c. in both branes (either Dirichlet or Neumann), with opposite b.c. for lhd and rhd modes, according to Eq. (3.5). If this were also the case for their spin-3/2 excitations, it would necessarily lead to 4D massless chiral vector-spinors. Then, through Yukawa couplings to the Higgs field, these would typically acquire masses of the same order of their SM spin-1/2 counterparts, which is phenomenologically unacceptable. However, one is free to impose distinct b.c. in the two branes. This eliminates all spin-3/2 chiral zero-modes, the lightest resonances corresponding to the first KK modes of the underlying 5-dimensional fields.

We may then have two possible b.c. assignments for lhd modes, which we denote by (a) (–,+) and (b) (+,–), where – refers to Dirichlet and + to Neumann b.c. in the (UV,IR) branes. As $\epsilon \ll 1$, the KK masses are approximately given by the zeros of

the following Bessel functions:

$$(a)\begin{cases} J_{\frac{1}{2}+c}(x_n) \simeq 0, & c \geq \frac{1}{2} \\ J_{-\frac{1}{2}-c}(x_n) \simeq 0, & c < \frac{1}{2} \end{cases} \quad , \quad (b)\begin{cases} J_{-\frac{1}{2}+c}(x_n) \simeq 0, & c \geq -\frac{1}{2} \\ J_{\frac{1}{2}-c}(x_n) \simeq 0, & c < -\frac{1}{2} \end{cases} . \tag{3.8}$$

Note that the two types of b.c. are related by the redefinition $c \to -c$. In Figure 3.1 we plot the values of the first KK mode mass as a function of the bulk mass parameter c. As one may observe, there exist values of c for which this mode can become quite light.

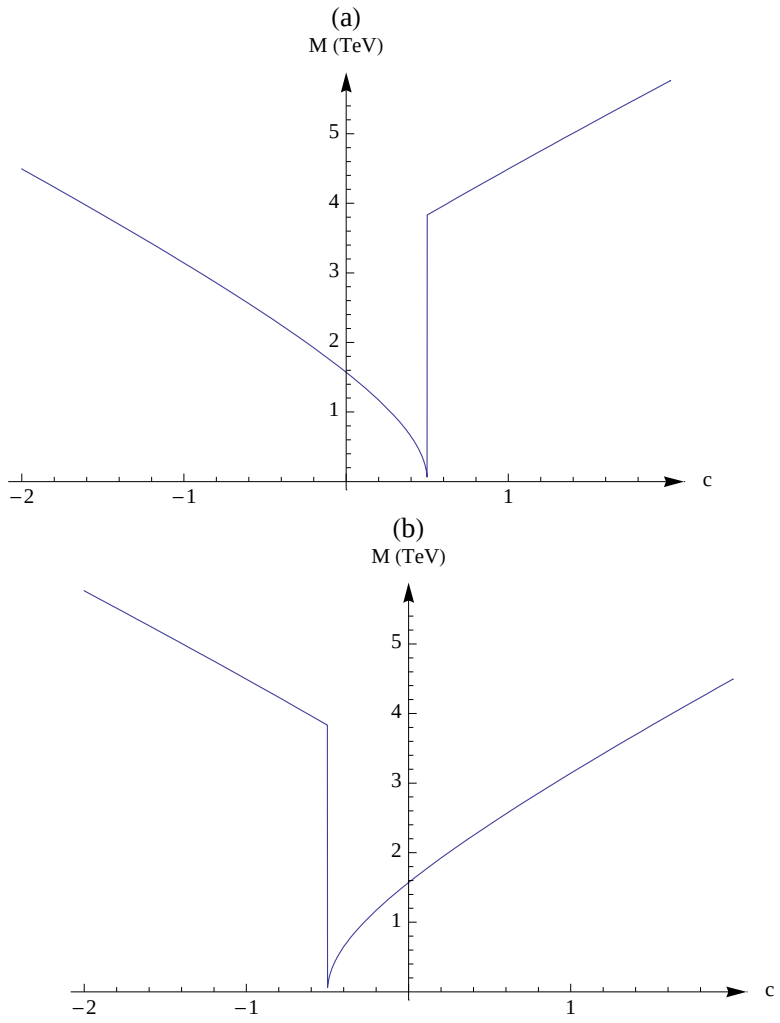

Figure 3.1: Mass of the first KK mode of a spin-3/2 resonance for (a) (–,+) and (b) (+,–) mixed boundary conditions as a function of the bulk mass parameter c.

We have, however, made no assumptions about the values of the bulk mass parameter so far. Quark and lepton bulk masses must be distinct to explain the observed 4D fermion mass hierarchy [80]. In string theory, these states are massless in the decompactification limit and have an associated tower of higher-spin states with a mass gap of the order of the fundamental string scale. Compactification into a 5-dimensional RS throat should, hence, induce bulk masses for the spin-1/2 ground states, subsequently affecting all higher-spin excitations. There is, however, no fundamental reason to assume the mass gap between the resonances is affected by the mechanism that produces bulk fermion masses. Thus, we expect the bulk mass of the spin-3/2 resonances to include the mass of its spin-1/2 counterpart, $c_{0i}k$, and an extra string theory contribution, sk, which we assume to be the same for all spin-3/2 resonances and, as discussed previously, also of the order of the fundamental 5D mass scale, so that $c_i = c_{0i} + s$.

The bulk masses of SM quarks and leptons determine their Yukawa couplings and hence their masses and CKM mixing, and phenomenology requires these masses to be close to the values $-k/2$ and $k/2$ for $SU(2)_W$ doublet and singlet fields, respectively [170]. For a single generation of quarks q, u, d it is then useful to define the bulk mass parameters as $c_{0q} \equiv M_q/k$ and $c_{0u,d} \equiv -M_{u,d}/k$. The corresponding 4-dimensional Yukawa coupling is then related to the respective 5-dimensional coupling by:

$$\lambda_{u,d} = \lambda_5 k \left(\frac{1/2 + c_{0u,d}}{e^{(1+2c_{0u,d})kL} - 1} \right)^{1/2} \left(\frac{1/2 + c_{0q}}{e^{(1+2c_{0q})kL} - 1} \right)^{1/2} e^{(1+c_{0u,d}+c_{0q})kL} \ , \tag{3.9}$$

where one assumes $\lambda_5 k \sim 1$. Note that this result neglects the effects of brane-localized operators in the 5-dimensional equations of motion, which is a good approximation for the fermion mass spectrum [170]. Eq. (3.9) illustrates how UV-localized fermions, with $c_{0q,u,d} \lesssim -1/2$, lead to exponentially small Yukawa couplings, hence describing the masses of first and second generation quarks and also all lepton gen-

erations. The large top Yukawa coupling requires significantly larger bulk mass parameters, in particular for the singlet component. In [80], it was shown that UV localization of light fermions suppresses their couplings to KK gauge bosons, making them universal and hence preventing large FCNC effects. The latter might then be significant only for third generation quarks, but constraints from flavour-changing processes are much weaker in that case.

Experimental data cannot, however, fully determine all SM bulk mass parameters, preventing a precise computation of the spin-3/2 resonance spectrum. One expects, however, all allowed spectra to exhibit a large separation between the mass of singlet top excitations and all remaining spin-3/2 resonances, due to the required difference between their bulk masses. To illustrate this point, we have used the set of quark bulk mass parameters given in [170] (see also [171] and [172]), which is consistent with all experimental constraints concerning quark masses and mixing, to compute the first KK masses of the associated spin-3/2 resonances, Q_i, U_i and D_i, $i = 1, 2, 3$. Our results are shown in Figure 3.2.

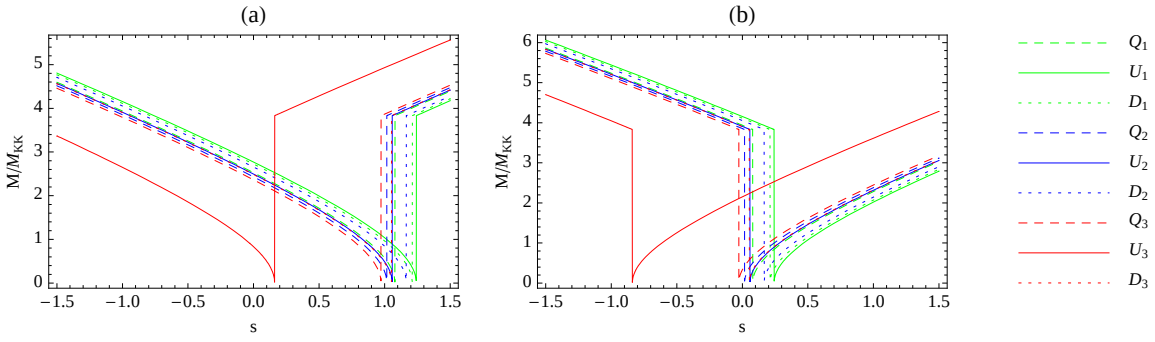

Figure 3.2: Mass of the first KK mode of spin-3/2 quark excitations as a function of the string bulk mass contribution for (a) (–,+) and (b) (+,–) b.c. for lhd components of doublet modes, with singlet modes satisfying opposite boundary conditions. Masses are normalized to the nominal KK scale, $M_{KK} = k\epsilon \sim \mathcal{O}(\text{TeV})$.

Recall that, in Eq. (3.9), we defined the bulk mass parameters for singlet and doublet excitations with opposite signs. Consequently, each plot in Figure 3.2 depicts singlet and doublet fields which satisfy opposite b.c., with plot (a) corresponding to the same IR b.c. satisfied by all spin-1/2 fermions.

Although not shown explicitly, lepton resonances will generically lie close to the first and second generation quark excitations, as they have similar bulk mass parameters. These results clearly show that the singlet top excitation is significantly lighter (heavier) than all others for negative (positive) s. The sign of the string bulk mass parameter is undetermined in the absence of a concrete string compactification, although negative values may naively seem more natural given that $c_0 \lesssim -1/2$ for most fermions. Also, there is a sizeable range of s for which the singlet top excitation is lighter than the KK mass scale (the lightest KK excitations have mass $\simeq 2.45 M_{KK}$ in RS models). As we will discuss in the next sections, it is phenomenologically more interesting and viable to have a light singlet top excitation while all other resonances are much heavier, so that we will focus on this possibility.

One must also take into account that brane-localized Yukawa operators may modify the spectrum of spin-3/2 resonances after electroweak symmetry breaking. Such operators mix doublet and singlet states via the Higgs field and may (i) involve only spin-3/2 fields or (ii) mix spin-1/2 and spin-3/2 fields. However, their effects are naturally suppressed by powers of v/M_{KK}, where v denotes the Higgs vev, and may thus be neglected to lowest order. Furthermore, operators of type (i) vanish to leading order when doublet and singlet states satisfy the same b.c. in the IR. The same happens for operators of type (ii) in the case where spin-3/2 resonances have the same IR b.c. as their spin-1/2 counterparts, which could be interpreted as a natural consequence of the intrinsic UV nature of string theory effects.

3.2 Spin-3/2 rhd top interactions

Motivated by the spectrum of spin-3/2 resonance states outlined in section 3.1 we will focus on the case where the sole light ($M <$ few TeV) spin-3/2 state is the partner of the rhd top, which we denote by t_R^*. Such states are least constrained by current direct searches, but as we will show below can still be copiously produced at the LHC, and have the added advantage of relatively easily evading flavour-changing and rare-decay constraints.

Although the form of the low energy interactions of spin-3/2 resonances should ultimately arise from the underlying theory at high energies, such as string theory or a confining gauge theory leading to composite quark and leptons, we follow a bottom-up effective-field-theory approach and use a generic interaction Lagrangian involving the resonances and respecting the gauge symmetries of the SM. Such an effective field theory must break down at high energy due to the non-renormalizable nature of interacting spin-3/2 theories. Thus our theory is endowed with a cutoff Λ (the maximum value of which we will later estimate), which suppresses higher dimension operators[2].

We start by considering a generic Dirac vector-spinor ψ_μ of mass M in four dimensions, transforming in the fundamental representation of a local gauge group G and representing the first KK mode of an underlying 5-dimensional spin-3/2 field. A minimally coupled vector-spinor is described by the gauge-invariant Rarita-Schwinger Lagrangian [190], defined up to a parameter A which is related to the presence of unphysical spin-1/2 degrees of freedom in the vector-spinor field ψ_μ (see eg [180]). We take the value $A = -1$, so that:

$$\mathcal{L}_4 = i\bar{\psi}_\mu \gamma^{\mu\nu\rho} D_\nu \psi_\rho + M\bar{\psi}_\mu \gamma^{\mu\rho}\psi_\rho \ , \tag{3.10}$$

[2]Theories of interacting spin-3/2 fields have been studied in the literature, mainly in the context of the Δ baryon-resonances [173–180] or gravitinos in supergravity [181], although studies of interacting spin-3/2 resonances of SM quarks and leptons can also be found [182–189].

with the standard gauge covariant derivative $D_\mu = \partial_\mu - igA_\mu$, where g is the gauge coupling and A_μ the gauge field. Following from this ψ_ρ satisfies the Dirac equation. The free Lagrangian also implies the constraint

$$\gamma^\rho \psi_\rho = 0\,, \tag{3.11}$$

which, however, is violated when interactions with A_μ are included. The free Lagrangian yields the propagator [184]:

$$\mathcal{P}^{\mu\nu} = \frac{1}{p^2 - M^2}\left[-(\not{p} + M)\left(\eta^{\mu\nu} - \frac{p^\mu p^\nu}{M^2}\right) - \frac{1}{3}\left(\gamma^\mu + \frac{p^\mu}{M}\right)(\not{p} - M)\left(\gamma^\mu + \frac{p^\nu}{M}\right)\right]\,, \tag{3.12}$$

where the expression in square brackets gives the associated polarization tensor. As excited fermions, the spin-3/2 resonances have the same SM quantum numbers and gauge couplings as their spin-1/2 counterparts which, in the case of t_R^*, correspond to the $(3,1)_{2/3}$ representation of the SM gauge group.

The numerator of the propagator in Eq. (3.12) contain terms involving three powers of the momentum. This leads to cross-sections which go like positive powers of the energy in the UV, an observation which is symptomatic of the field theory of higher-spin particles. As the cross-section rises indefinitely, tree-level unitarity is violated at some point. One can get a rough estimate of the unitarity bound by simply considering the amplitude of elastic scattering in the s-wave only. For gluon-mediated interactions arising from Eq. (3.10), tree-level unitarity is then respected for $\sqrt{s} \lesssim 7M$. Of course it is possible for the effective theory describing the resonance to break down before this scale, but as a working hypothesis we will take $\Lambda = 7M$ unless otherwise specified.

As we will see, Eq. (3.10) already contains the leading order interaction responsible for the dominant production mode of the spin-3/2 resonances at the Tevatron and the LHC, but does not allow for its decay. Therefore we are also interested in interactions

involving both spin-3/2 and spin-1/2 states, which allow the decay of the resonances into SM fermions. These will *a priori* include dimension-4 'kinetic' and 'mass mixing' interactions of the form

$$\mathcal{L}_4^{\rm mix} \;=\; i\alpha_1\bar{\psi}_\mu(\eta^{\mu\nu}+w\gamma^\mu\gamma^\nu)D_\nu P_{R,L}\chi + \alpha_2\bar{\psi}_\mu\gamma^\mu P_{R,L}\chi + \text{h.c.}\ , \qquad (3.13)$$

where $P_{R,L}\chi$ denotes a chiral spin-1/2 state with the same quantum numbers as the ψ_μ excitation. As for KK excitations of SM fermions or generically any model of new vector-like quark and lepton families, one may always choose a basis where kinetic and mass terms are diagonal, so that terms such as Eq. (3.13) are unphysical. However, we must also consider the Yukawa operators mentioned in the previous section, which are of the form

$$\mathcal{L}_{Higgs} = \lambda\ \bar{\chi}\ i\sigma_2 H^*\ \gamma_\mu\psi^\mu + \text{h.c.}\ , \qquad (3.14)$$

where χ represents a lhd quark $SU(2)_W$ doublet in the case where ψ_μ represents the t_R^* resonance. These operators are not necessarily diagonal in the above mentioned basis, so that generically there will be dimension-4 mixing between spin-1/2 and spin-3/2 mass eigenstates in weak interactions.

Although the interactions with the physical Higgs boson vanish for on-shell spin-3/2 states due to the constraint Eq. (3.11), for spin-3/2 resonances appearing in internal lines the new Higgs-mediated interactions may in general lead to flavour-violating rare processes. However, these FCNC do not severely constrain the couplings λ or the masses of the t_R^* state, because their FCNC effects are suppressed by the same mechanism that suppresses the couplings of KK fermions to SM fermions and Higgs in RS models of flavour physics [170,172,191]. Also, as discussed in the previous section, the effects of these operators are small for $v \ll M_{KK}$ and may be further suppressed depending on the choice of b.c. in the IR. Hence, we expect all dimension-4 weak operators mixing spin-1/2 and spin-3/2 states to be suppressed.

This mixing will be absent in strong interactions involving spin-1/2 and spin-3/2 states, which may only occur via dimension-5 operators of the form:

$$\mathcal{L}_5 \;=\; i\frac{a}{\Lambda}\bar{\psi}_\mu(\eta^{\mu\alpha}+z\gamma^\mu\gamma^\alpha)F_{\alpha\beta}\gamma^\beta P_{R,L}\chi + \text{h.c.}\;, \tag{3.15}$$

where for $SU(2)_W$ singlet excitations terms involving lhd SM fermions are further suppressed by v/Λ. Here we assume that the mass scale Λ sets the strength of the dimension-5 operators, and a is an $\mathcal{O}(1)$ coefficient that one may expect to scale with the associated coupling constant $a \sim g$. The parameter z is the so-called *off-shell parameter*, as the constraint $\gamma^\mu\psi_\mu = 0$ eliminates the contribution of this interaction for physical spin-3/2 states. Several discussions on the value of this parameter can be found in the literature (see eg [175]). A popular choice is the value $z = -\frac{1}{4}$, first obtained in [173]. Other authors have found from field-theoretical arguments the value $z = -\frac{1}{2}$ [174], while some phenomenological approaches use $z = 0$ [183]. All of these various specifications of z rely on effective field theories with several formal problems, and, given the observed discrepancy, we do not believe a solid value of z can be established using this type of approach and leave it as a free parameter of the interaction Lagrangian. Also, due to the physical constraint $\gamma^\mu\psi_\mu = 0$, the value of z affects neither the decay width of the resonance at leading order, nor the dominant (pair) production mechanism.

For singlet excitations, the interaction Eq. (3.15) contains, in addition to the gluonic field strength, couplings to the photon and the Z-boson, which, if $a_i \sim g_i$, are sub-dominant. The strong interactions in Eq. (3.15) are not necessarily flavour-diagonal, but it is easy to show that, assuming that in the 5D AdS theory the suppression of higher dimension operators is by powers of the 5D Planck mass M_5, couplings of the light quarks to the resonances will be more strongly suppressed than those of the top. Another way to express this is to say that the light-quarks are UV-localized,

and thus exposed to higher mass-scales than the IR-localized top quark. Thus, the coupling of t_R^* to the top-quark will be dominant compared to other possible flavour-violating couplings. As we will see later, the gluonic operator in Eq. (3.15) gives the dominant contribution for single-production of the t_R^* resonance at the LHC.

We conclude this section by noting that one can attempt to constrain the masses and couplings of the spin-3/2 resonances via low-energy observables and precision tests. These will be directly analogous to the constraints applicable to the KK modes of the SM fermions in usual RS model-building [170]. However the spin-3/2 sector fields (with the exception of t_R^*) are generically heavier than the fermion KK modes, and their mixings with the SM fermions can be naturally suppressed, so that it is easy to accommodate the constraints for large regions of parameter space. Specifically, the vector-like $SU(2)_W$ singlet t_R^* is loosely constrained by low-energy observables and precision tests such as the oblique electroweak observables S, T and U, four-fermion operators, FCNC observables like ϵ'/ϵ [192] and rare decays like $b \to s\gamma$ [193], even if its mass is below the TeV-scale. Although such observables might help constraining the mass of this state, a detailed analysis cannot be done in a model-independent way, lying beyond the scope of this chapter. Better constraints can, however, be obtained by direct searches, a topic we discuss in the next section.

3.3 Experimental Signatures

We expect the dominant decay modes of t_R^* to be into a rhd top and a gluon, via the interaction Eq. (3.15) (in accord with the results of string theory calculations in flat space [194]), in addition to $t_R^* \to \gamma t$ via analogous dimension-5 interaction terms, and $t_R^* \to Ht$, $t_R^* \to Zt$ and $t_R^* \to W^+ d_i$ via the suppressed dimension-4 mixings Eqs.(3.13) and (3.14) (see [195] and references therein for the related case of a spin-1/2 singlet excitation). Despite the dimension-5 nature of the top+gluon channel, it corresponds

to a strong interaction, while the last three decay channels occur via dimension-4 interactions suppressed by small mixing angles for $v \ll M_{KK}$, and possibly further suppressed for specific choices of IR b.c., as discussed earlier. Resonances with smaller KK masses should be more sensitive to IR effects, so one expects a larger fraction of weak decays in this case, although in general the strong and weak channels may have comparable branching ratios. Note that the weak decay channels will get other contributions from transition-magnetic-moment-like interactions of the type given in Eq. (3.15).

The various decay channels may lead to distinctive final states useful for separating t_R^* production from the SM background, but unfortunately their branching ratios depend on the unknown coefficients a_i for $SU(3)$ and $U(1)_Y$ and on the Yukawa couplings. As the $t_R^* \to tg$ partial width is $\Gamma_{tg} \simeq a^2 M^3/(48\pi\Lambda^2)$, where M is the mass of the resonance, and given that we expect $M < \Lambda$, it is clear that $\Gamma_{tg} \ll M$. This should also hold for the weak decay channels, as for spin-1/2 vector-like excitations [196]. Hence, this allows us to use the narrow-width approximation (NWA), thus considering the production and decay of the resonance as a two-step process.

Armed with the justification of the NWA, we may safely proceed to the calculation of the production cross-sections of the resonance in proton-proton (and proton-antiproton) collisions. As we will see, the dominant production mechanism is typically pair-production via the interaction of Eq. (3.10). The contributing diagrams coming from this operator are shown in Figure 3.3.

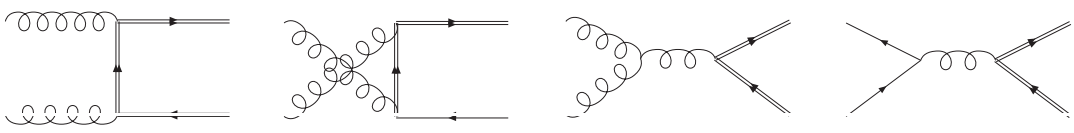

Figure 3.3: Feynman diagrams contributing to pair-production of singlet top spin-3/2 resonances (double lines) via gluon-fusion and $q\bar{q}$ annihilation (except $t\bar{t}$).

There are, in principle, diagrams in which the dimension-5 operator of Eq. (3.15) contributes, but these are strongly suppressed for the values of Λ used below. We note that pair-production of spin-3/2 states has been considered by [184, 185]. We find, consistently with the results of these authors, that cross-sections for pair-production at the LHC are quite large. For example, the production cross-section for a resonance mass of 300 GeV is $\sim 10^3$ pb, while a minimally coupled spin-1/2 particle of the same mass would be pair-produced with cross-sections ~ 10 pb. This difference is due to the fact that partonic cross-sections for a spin-3/2 particle go like s^3 in the UV, whereas those of a spin-1/2 particle decrease as s^{-1}. Therefore, upon convolution with the parton distribution functions (PDF) to obtain the hadronic cross-sections, the integral picks up more contributions from the large x region, where x is the momentum fraction carried by the partons. This violent UV behaviour also means that pair-production violates unitarity at some scale, which we estimate to be $\sqrt{s} \approx 7M$, as discussed above. A simple way to parametrize the inevitable slop in this scale is to impose a hard centre-of-mass energy cut-off $\sqrt{s_0}$ on the partonic cross-sections.

For single-production, the dominant diagrams come from the strong interaction in the operator of Eq. (3.15), and two types of diagrams need to be computed. The first type describes gluon-fusion into a rhd top and a t_R^* resonance. There are six of these diagrams, as shown in Figure 3.4. The second type is annihilation of quark-antiquark pairs, with the same final states, also shown in Figure 3.4.

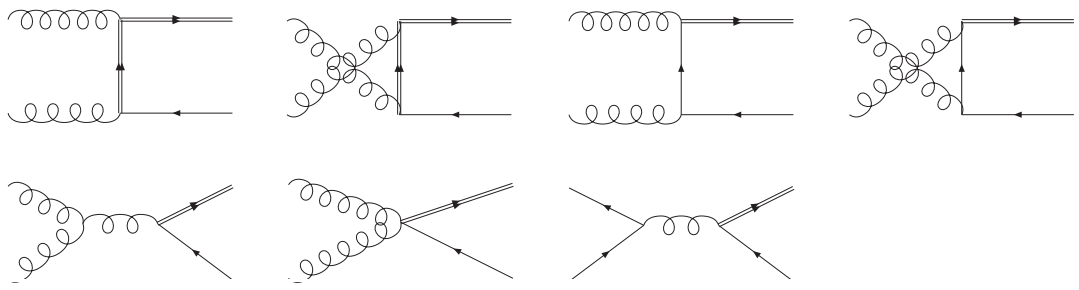

Figure 3.4: Feynman diagrams contributing to single-production of t_R^* spin-3/2 resonances (double lines) via gluon-fusion and $q\bar{q}$ annihilation.

There are also diagrams involving top quarks in the initial state, but the top content of the proton is miniscule so that these diagrams give a negligible contribution. The dominant process is gluon-fusion, as one would naively expect.

We employed the package CalcHEP version 2.5.j [197] to calculate the cross-sections. We have computed analytically the decay width and the last two diagrams in Figure 3.4 and checked their agreement with the results obtained using this package. The PDF used were the CTEQ6L set [198], while $m_t = 171.2$ GeV [2].

In Figure 3.5, we show the behaviour of the hadronic cross-sections against the mass of the resonance.

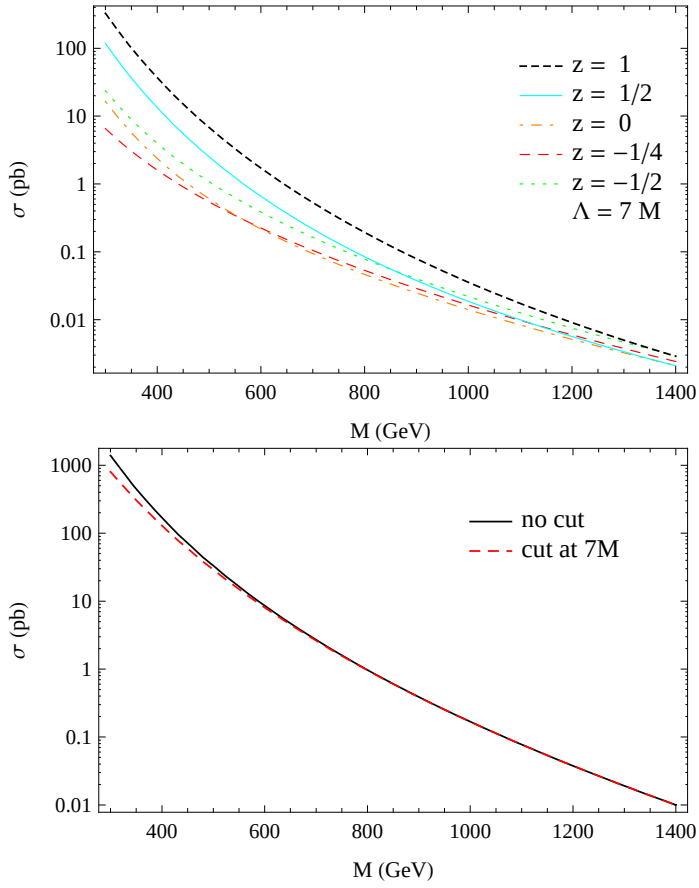

Figure 3.5: Plots of the leading-order (LO) cross-section for production of t_R^* against its mass, in pp collisions at 14 TeV, with K-factor of 1. The upper figure shows single-production for various values of z, while the bottom plot displays the total cross-section for pair-production, with and without a unitarity cut.

The upper plot shows the single-production cross-section for various values of the parameter z. Guided by our estimate of the unitarity-violation scale, we use a value of $\Lambda = 7M$, with smaller values of Λ leading to a higher single-t_R^* production rate as the latter goes like $1/\Lambda^2$. Recall that Λ is a vestige of the 5-dimensional theory, and will thus depend on the profiles of the fields in the extra-dimension, and hence on the mass of the resonance. Note that the only diagrams which have a z-dependence are those with intermediate spin-3/2 propagation.

The bottom plot in Figure 3.5 shows pair-production with and without a unitarity cut s_0. It is clear that pair-production dominates over single-production for most values of z, unless the unitarity cut is very low. Moreover, pair-production depends very weakly on the off-shell parameter z and Λ (for $\Lambda > 2$ TeV) and is therefore more model-independent from a theoretical perspective, with a smaller SM background, which suggests that this channel might be more promising for detection purposes. Although single-production might have interesting experimental signatures, we will focus on pair-production in what follows. Note that the effect of the cut-off at $s_0 = 7M$ is very mild, reducing the production cross-section by 15% for $M = 300$ GeV but only by 3% for $M = 400$ GeV, and is negligible for larger masses. This is related to the fortuitous cut-off enforced by the steeply falling PDF at scales below the unitarity bound for almost all resonance masses considered.

To our knowledge, no direct searches for spin-3/2 quark excitations have been done so far. Heavy up-like $SU(2)_W$ singlet spin-1/2 vector quark excitations have, however, been searched for in $p\bar{p}$ collisions by the CDF collaboration [199–201] at centre-of-mass energies of 1.96 TeV. These searches assume that the dominant decay channel of the spin-1/2 resonance is due to mass mixing with the SM top, decaying mainly into Wd_i, where d_i is a down-type SM quark, and a lower-bound for the mass of such a quark excitation is quoted as 311 GeV. Calculating the cross-section for production of the t_R^* spin-3/2 resonance at Tevatron energies, plotted in Figure 3.6,

and using the SM background quoted in [199, 200], we find a lower bound on its mass $M > 340$ GeV for a 2σ margin of exclusion. Note that this is pessimistically large, as it assumes 100% decay into Wd_i, which we expect to compete with the other decay modes, as explained above.

Interestingly, the existence of a mild excess of observed events at the Tevatron as reported by the CDF [199] and DØ [202] collaborations can possibly be explained by a t_R^* resonance with a mass of about 400 GeV. Because of the somewhat enhanced production cross-section of the t_R^* at the Tevatron the excess is possibly better accommodated than with a standard top-prime, avoiding the need for the assistance of an extra s-channel colour-octet exotic [200]. Note that at the Tevatron the dominant production is via $q\bar{q}$ parton events, so the enhancement of the cross-section at the Tevatron is less than that at the LHC where gg parton events occur with a $t-$ or u-channel t_R^* propagator.

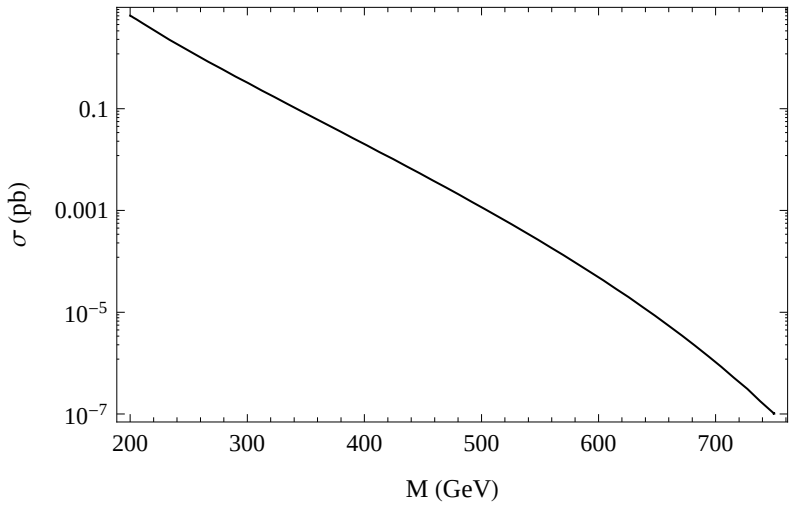

Figure 3.6: Plot of the LO cross-section for pair-production of t_R^* against the their mass, in $p\bar{p}$ collisions at 1.96 TeV with K-factor of unity.

Finally, we now touch on the potential observability of these resonances at the LHC. We will content ourselves here with a rather simplistic measure of discovery, namely a simple signal vs background criterion $S/\sqrt{B} \geq 5$, with no regard to angular

distributions, or the details of decay cascades. Although these constitute crucial facets of the production and detection of any unstable higher-spin resonance, they require a more thorough analysis, which is out of the scope of this thesis.

The $t_R^* \to W^+ b$ decay mode is particularly interesting for direct searches, and we can in fact use it to estimate an upper-bound for the mass of spin-3/2 singlet resonances observable at the LHC. We utilize the background quoted in [203], where pair-production of spin-1/2 up-like singlets decaying into $W^+ b$ is considered. In [203], it is found that spin-1/2 singlets with mass up to 1.1 TeV should be detectable at the LHC. Assuming all decays occur in the $W^+ b$ channel and that the same K-factor as for spin-1/2 quark excitations applies, we find that spin-3/2 singlets with mass $\lesssim 1.35$ TeV should be accessible at the LHC, reflecting the enhancement of the production rate for higher-spin particles.

A combined search using the full set of decay channels including $t_R^* \to tg, tZ, tH$, and $t\gamma$ should raise this upper bound, so we view $M < 1.35$ TeV as a conservative estimate for discovery of the t_R^* at the LHC.

Chapter 4

Black hole superradiance

4.1 The Kerr superradiant instability

The issue of black hole stability plays a central role in General Relativity and is crucial for our understanding of the rich high-energy phenomenology associated with compact astrophysical systems. The issue of stability of the Schwarzschild geometry was first addressed in the seminal paper by Regge and Wheeler [204] and later by Vishveshwara [205] and Wald [206], showing that small perturbations of this spherically symmetric space were exponentially damped in time. It has been known for a few decades that this is not, however, the case for rotating Kerr black holes [207], which suffer from the well-known superradiant instability [208–216].

This instability is a direct consequence of the presence of an 'ergoregion' surrounding the outer horizon of the black hole, where ordinary causal matter experiences inertial frame-dragging and cannot remain at rest with respect to an asymptotic observer. In this region, the Killing vector corresponding to time translations becomes space-like, so that the associated conserved energy may become negative for some observers. Classically, this leads to the so-called Penrose process [217, 218], by which one may extract energy and angular momentum from the spinning black hole. One

can consider a projectile directed towards the black hole along a time-like trajectory but aimed in such a way that it misses the outer horizon. One could then conceive a timer mechanism that sets off a fragmentation process that breaks the projectile into two parts while it is inside the ergoregion. One of the fragments may then carry a negative energy and fall into the black hole, while the remaining fragment escapes to infinity carrying an energy larger than that of the original fragment. One can also show that the same reasoning holds for the angular momentum of both fragments.

Superradiance is a well-known phenomenon in several quantum [219,220] and also classical systems [221] and was first described for the case of spinning black holes by Zeldovich [208]. If one considers the scattering of wave modes of the form $e^{-i\omega t+im\phi}$, where ϕ denotes the Boyer-Lindquist azimuthal angle in the Kerr geometry [222], one can show that for co-rotating ($m > 0$) incident waves satisfying the condition $\omega < m\Omega$ the scattered wave is amplified, where $\Omega = \frac{a}{r_+^2+a^2}$ is the angular velocity of a Kerr black hole of mass M and spin $J = aM$ at the outer horizon, r_+. The total energy and angular momentum radiated to infinity are hence larger than that of the incident wave, in a similar fashion to what happens in the Penrose process described above. Press and Teukolsky proposed that, by surrounding the black hole with a mirror, one could use multiple wave-scattering to extract an enormous amount of energy from the black hole, a mechanism they suggestively named the *black hole bomb* [223] and that was further analyzed in [213].

Practical implementations of such a mechanism seem difficult to conceive, although it has been proposed in [224, 225] that the inner boundary of the accretion disks which are expected to surround astrophysical black holes may effectively act as a mirror and produce enough energy via superradiant scattering of magnetosonic plasma waves to feed the mysterious and highly-energetic gamma-ray bursts. A natural mirror is, however, provided for fields with a non-zero mass [209, 210]. It is well-known that stable orbits around a black hole are an exclusive feature of particles

with a non-vanishing mass, so that massive fields exhibit a set of bound states in the Kerr background corresponding to wave-packets moving along such orbits. These wave-packets will always have a non-vanishing tail inside the black hole's ergoregion, leading to a continuous amplification of bound states satisfying the superradiant condition. Such states have a complex frequency with a small positive imaginary part, so that their occupation number grows exponentially in time. Pauli blocking prevents this amplification for fermionic states [226], so that superradiant bound states are an exclusive feature of bosonic fields (see [227] for a recent analysis of fermions in the Kerr background).

Several attempts have been made in the literature to analytically determine the growth rate of superradiant bound states for massive scalar fields. The difficulty in solving the massive Klein-Gordon equation in the Kerr background has limited the analysis to the regimes $M\mu \gg 1$ [210] and $M\mu \ll 1$ [211, 212], where μ denotes the mass of the scalar field[1]. In both cases the obtained growth rates were shown to be quite small, with the imaginary part of the frequency $\omega_I M$ scaling as $e^{-1.84\mu M}$ and $(\mu M)^9$ in the large and small mass limits, respectively. These studies suggest as well that the growth rate is maximal for extremal holes with $a = M$ and for P-waves with $l = m = 1$, on which we will focus in this chapter. The spectrum of massive scalar bound states has also been studied numerically in [215] and later in [216], using a continued-fraction method which confirmed these expectations. The latter analysis revealed a maximum growth rate in the $l = m = 1$ case given by $\omega_I M \simeq 1.5 \times 10^{-7}$, for $\mu M \simeq 0.42$ and $a = 0.999M$, in agreement with the former, where a similar value was observed for $a = 0.994$ and $\mu M = 0.45$.

Hence, numerical results suggest that the superradiant instability is more pronounced in the regime $\mu M \sim 1$, where the particle's Compton wavelength is comparable to the horizon radius, inducing a larger overlap of the field with the ergoregion.

[1] We consider geometrized units such that $\hbar = c = G = 1$.

This regime has proven hard to analyze with analytical methods and motivated a recent study of this phenomenon in [228]. By separating the exterior of the black hole into two overlapping regions where the field equations are exactly solvable and matching the obtained solutions within their common domain of validity, the authors obtained a defining equation for the superradiant bound state spectrum valid for $\mu M \sim 1$. The novelty of their method resides in the use of the black hole's angular momentum rather than the particle's mass to define the two regions, thus eliminating the need for large and small mass approximations in order to solve the relevant equations. The results in [228] exhibit, however, a huge discrepancy with respect to the numerical analysis in [215, 216], with a maximum growth rate of $\omega_I M \simeq 1.7 \times 10^{-3}$, four orders of magnitude larger than the one mentioned above.

Understanding this discrepancy is crucial for the study of the phenomenological aspects of scalar superradiant bound states in the Kerr background, in particular as this process may lead to the significant spin down of rapidly-rotating black holes. Astrophysical black hole candidates have been primarily found in X-ray binaries and Active Galactic Nuclei (AGN), with masses in the range $3M_\odot - 30M_\odot$ for stellar mass black holes and $10^6 M_\odot - 10^9 M_\odot$ for supermassive black holes, where $M_\odot$ denotes the solar mass [229]. The lightest known scalar is the neutral pion, with $\mu = 134.98$ MeV and a mean lifetime $\tau_\pi \simeq 8.4 \times 10^{-17}$ s [2], so that it may only significantly affect small black holes of about 10^{12} kg, given the condition $\mu M \sim 1$. Hence, pionic bound states cannot produce observable effects on astrophysical systems, although they may influence the dynamics of small primordial black holes postulated to be produced during inflation [210]. However, this depends crucially on whether the instability can develop significantly before the pions decay. While a large amplification of pionic bound states can be attained using the analytical results of [228], where the time scale for the instability is $\tau \sim 1.3 \times 10^{-21}$ s, the numerical results of [215, 216] yield $\tau \sim 1.5 \times 10^{-17}$ s, in which case pion emission would be very ineffective.

The effects of black hole superradiance have gained a new phenomenological interest within the context of the string axiverse proposal described in the introduction of this thesis [150]. Within the plethora of ultra-light axions that may arise in string theory compactifications, one expects several scalar particles with masses in the correct range to significantly spin down astrophysical black holes. In particular, the condition $\mu M \sim 1$ requires $\mu \lesssim 10^{-10}$ eV for a significant number of particles to be produced around stellar mass or supermassive black holes, so that string axions constitute the leading candidates for this process to occur in astrophysical environments.

This 'axionic cloud' may then possibly lead to several interesting observational effects e.g. via axion-photon conversion in the surrounding stellar and galactic magnetic fields and through the emission of gravitational waves, via quantum mechanical transitions between superradiant and non-superradiant states, as well as axion annihilations. Furthermore, black holes with mass $M \sim \mu^{-1}$ for a given axion should exhibit a very low angular momentum, so that looking for gaps in the mass-spin Regge plot for astrophysical black holes may provide an effective method to search for these ultra-light states. Other exciting possibilities may also arise in the context of the so-called 'bosenova' effect, first observed in ultra-cold atom systems, where the axion Bose-Einstein condensate produced by superradiance may collapse due to self-interactions, leading to the ejection of some of these particles into the surrounding medium. A detailed study of these and other potential phenomenological aspects is, however, out of the scope of this thesis, and may be found in [152].

Rotating black holes may thus provide the ideal 'laboratory' to explore the sub-eV frontier of string theory compactifications, a task that requires a good understanding of the spectrum of scalar bound states in Kerr backgrounds and of the corresponding superradiant growth rates. This is fundamental e.g. to have an accurate description of the shape of the above mentioned gaps or of the trajectories followed by black holes in the Regge plane as they lose mass and spin due to axion emission. Moreover,

black holes may also gain angular momentum from the surrounding accretion disks, a process that may compete with the superradiant spin down if the instability does not develop sufficiently fast.

The rich phenomenology associated with the superradiant instability thus requires a more detailed study of its properties and an analysis of the above mentioned discrepancy. With this goal in mind, we describe in this chapter two possible techniques to compute the spectrum of scalar bound states, comparing them with previously employed numerical and analytical procedures.

4.2 Massive scalar fields in the Kerr background

We start by considering the background spacetime created by a spinning black hole, described by the Kerr metric, which in Boyer-Lindquist coordinates [222] takes the form[2]

$$\begin{aligned} ds^2 &= \left(1-\frac{2Mr}{\rho^2}\right)dt^2 + \frac{4aMr\sin^2\theta}{\rho^2}dtd\phi - \frac{\rho^2}{\Delta}dr^2 - \rho^2 d\theta^2 - \\ &- \left[(r^2+a^2)\sin^2\theta + \frac{2Mr}{\rho^2}a^2\sin^4\theta\right]d\phi^2 \ , \end{aligned} \tag{4.1}$$

where $\Delta = r^2 + a^2 - 2Mr$ and $\rho^2 = r^2 + a^2\cos^2\theta$, with the zeros of the former at $r_\pm = M \pm \sqrt{M^2 - a^2}$ giving the outer and inner horizons of the black hole.

In curved space, the massive Klein-Gordon equation is given by:

$$(\nabla^\mu \nabla_\mu - \mu^2)\Phi = 0 \ . \tag{4.2}$$

In the Kerr background, the scalar field Φ then admits a mode expansion of the form:

$$\Phi_{lm}(t, r, \theta, \phi) = e^{-i\omega t} R_{lm}(r) S_{lm}(\theta) e^{im\phi} \ , \tag{4.3}$$

[2]Note that, in this chapter, we will use the $(+,-,-,-)$ metric signature, following the literature's *de facto* convention for this topic.

where $\omega = \omega_R + i\omega_I$ is the complex frequency of the mode characterized by the indices $l = 0, 1, \ldots$ and $-l \leq m \leq l$. The latter correspond to the usual angular momentum and azimuthal projection indices for spherical harmonics in the Schwarzschild limit $a \to 0$. In the general case, they label the solutions of the spheroidal harmonic equation [230] corresponding to the angular part of Eq. (4.2):

$$\left[\frac{1}{\sin\theta}\frac{d}{d\theta}\left(\sin\theta\frac{d}{d\theta}\right) - a^2q^2\cos^2\theta - \frac{m^2}{\sin^2\theta}\right]S_{lm} = A_{lm}S_{lm} \ , \tag{4.4}$$

where $q = \sqrt{\mu^2 - \omega^2}$ and A_{lm} is the angular eigenvalue, corresponding to the separation constant relating the radial and angular parts of the Klein-Gordon equation. The regularity of the solution of Eq. (4.4) at the poles $\theta = 0, \pi$ determines a discrete set of angular eigenvalues, which for $a^2q^2 \ll 1$ are given by an expansion of the form:

$$A_{lm} = l(l+1) + \sum_{k=1}^{\infty} c_{klm}a^{2k}q^{2k} \ . \tag{4.5}$$

We are interested in studying bound states for which ω is only slightly smaller than μ, i.e. $aq \ll 1$, so that it will be sufficient to consider the first few terms in this expansion, which can be found in [230]. The radial Teukolsky equation is given by [231]:

$$\frac{d}{dr}\left(\Delta\frac{dR_{lm}}{dr}\right) + \left[\frac{K^2}{\Delta} - a^2\omega^2 + 2ma\omega - \mu^2r^2 - A_{lm}\right]R_{lm} = 0 \ , \tag{4.6}$$

where $K = (r^2 + a^2)\omega - am$. For extremal Kerr black holes, with $a = r_+ = r_- = M$, it is useful to introduce the rescaled distance to the horizon:

$$x \equiv \frac{r - r_+}{r_+} = \frac{r}{M} - 1 \ , \tag{4.7}$$

and the function $\Psi_{lm}(x) = xR_{lm}(x)$, which satisfies the Schrödinger-like equation:

$$\frac{d^2\Psi_{lm}}{dx^2} + \left[\omega^2 - V(\omega, x)\right]\Psi_{lm} = 0 \ , \tag{4.8}$$

where

$$V(\omega, x) = -\frac{4\varpi^2}{x^4} - \frac{8\omega\varpi}{x^3} + \frac{\beta(\beta-1)}{x^2} - \frac{2q\nu}{x} + \mu^2 \tag{4.9}$$

and we have defined:

$$\nu \equiv \frac{2\omega^2 - \mu^2}{q} \ , \qquad \varpi \equiv \omega - m\Omega \ , \qquad \beta(\beta-1) \equiv A - 7\omega^2 + \mu^2 \ , \tag{4.10}$$

where all quantities are measured in units of M, $\Omega = 1/2$ in the extremal case and we have omitted the indices l, m for simplicity. Without loss of generality, we use the following solution for the coefficient β:

$$\beta = \frac{1}{2}\left(1 + \sqrt{1 + 4A - 28\omega^2 + 4\mu^2}\right) \simeq l + 1 \ , \tag{4.11}$$

where we have taken the limit $\omega \sim \mu \ll 1$ in the last expression, explicitly showing that β labels the angular momentum of the solution. It is a particular feature of the extremal case that one can readily write the radial equation in this form without using the tortoise coordinate, defined by [210]:

$$\frac{dy}{dx} = \frac{r^2 + a^2}{\Delta} \qquad \Rightarrow \qquad y = x + 2\log x - \frac{2}{x} \ . \tag{4.12}$$

Despite its simple form, the potential determining the dynamics of the radial function depends on the mode frequency, making this problem hard to solve exactly. To better understand the form of this potential, we use the solution for the real part of the mode frequency that we will obtain later on in Eq. (4.19). This is illustrated in Figure 4.1 for $l = m = 1$ and $\mu M = 0.4$.

The potential can be divided into (i) a sharp potential close to the horizon, (ii) a finite centrifugal barrier and (iii) a potential well. In terms of the tortoise coordinate,

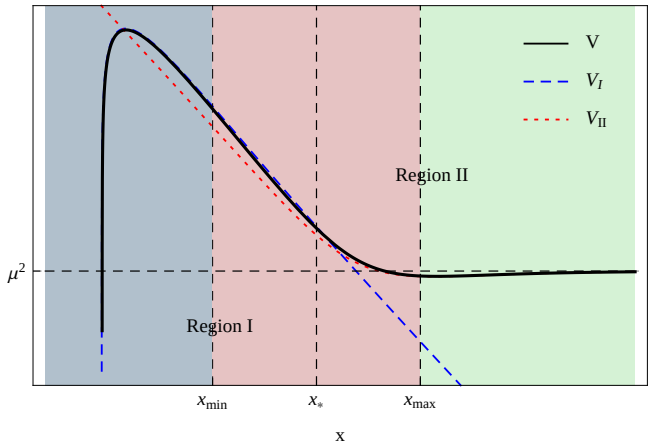

Figure 4.1: Potential for $l = m = 1$ and $\mu M = 0.4$ (solid line). Regions I and II correspond, respectively, to $x < x_{max} = (2q)^{-1}$ and $x > x_{min} = -4\varpi$. The point $x_* = \sqrt{-2\varpi/q}$ corresponds to the trial match point discussed in section 4.4.

the sharp potential tends to a constant value $2m\Omega\omega - m^2\Omega^2$ close to the horizon, which is negative for superradiant modes [150]. The definitions of regions I and II, as well as the particular values of x shown in Figure 4.1, will become clear in the next sections, but they roughly separate the interior and the exterior of the ergoregion.

The physical picture behind the superradiant amplification of the modes has a simple interpretation in terms of this potential. The Hydrogen-like bound states of the potential well may "anti-tunnel" [150] into the ergoregion and, while a fraction may penetrate the black hole's horizon, the remaining part will be reflected with a larger amplitude for $\omega < m\Omega$. This energy remains localized in the potential well rather than being radiated to infinity, as the wave packets are bound to the black hole, effectively inducing multiple scatterings as if a mirror was placed around the horizon. This results in a small positive imaginary part of the frequency, making the occupation number of the bound states grow exponentially according to Eq. (4.3). This effect should be smaller for higher multipoles, for which the barrier height increases and the "tunneling amplitude" is suppressed.

In order to determine the spectrum of bound states, one needs to impose boundary conditions. These correspond to an "ingoing wave" at the horizon and an exponen-

tially decaying mode at infinity [210, 212], which in terms of the tortoise coordinate defined in Eq. (4.12) can be written as:

$$\Psi_{lm}(y) \to \begin{cases} \frac{1}{y} e^{-i\varpi y}, & y \to -\infty \\ e^{-qy}, & y \to +\infty \end{cases} . \tag{4.13}$$

Recall that $y \sim -\frac{2}{x}$ and $y \sim x$ close to the horizon and at infinity, respectively. One can rewrite the radial equation in a more convenient form by considering the function $F_{lm}(x) = x^{-\beta}\Psi_{lm}(x)$, which satisfies

$$\left[x^2 \frac{d^2}{dx^2} + 2\beta x \frac{d}{dx} + \frac{4\varpi^2}{x^2} + \frac{8\omega\varpi}{x} + 2q\nu x - q^2 x^2\right] F = 0 \ . \tag{4.14}$$

This cannot be solved exactly but admits approximate solutions in two different regions. These may be matched in a common domain of validity to yield the spectrum of bound states with the boundary conditions in Eq. (4.13), which will be the topic of the remainder of this chapter.

4.3 Functional matching

As mentioned in the previous section, Eq. (4.14) can be simplified in two distinct regions by noting that the first two terms in the potential may be neglected for $-4\varpi/x \ll 1$, where $\varpi < 0$ for superradiant modes, while the last two terms may be neglected for $2qx \ll 1$. This defines the regions I and II depicted in Figure 4.1 such that $x < x_{max} = (2q)^{-1}$ and $x > x_{min} = -4\varpi$, respectively. In Figure 4.1 we have also plotted the approximate forms of the potential obtained by neglecting the relevant terms in each region, denoted by $V_I(x)$ and $V_{II}(x)$.

If one is able to determine solutions of the radial equation in these regions, one may determine the spectrum by matching the obtained functions in the overlap region,

$x_{min} \ll x \ll x_{max}$. The existence of such a region requires $-8\varpi q < 1$, a condition that we cannot *a priori* ensure to be satisfied without computing the spectrum. We will nevertheless assume that this is the case and use it later as a consistency check.

The radial equation can be reduced in both regions to the confluent hypergeometric equation, although in region I this requires a change of variable to $y = -2/x$. Note that this variable corresponds to the near-horizon form of the tortoise coordinate, so that we use the same notation for both to emphasize this fact. Also, as $y \simeq x$ for large x, the radial equation becomes, in each region, the confluent hypergeometric equation in the corresponding limit of the tortoise coordinate. This reduction requires writing $F(y) = e^{\alpha y} G(x)$ with an appropriate choice of the complex parameter α in each case. After imposing the boundary conditions Eq. (4.13), we obtain the following solutions:

$$\begin{aligned} F_I(x) &= A_I e^{\frac{2i\varpi}{x}} U(1-\beta-2i\omega, 2-2\beta, -4i\varpi/x) \ , \\ F_{II}(x) &= A_{II} e^{-qx} U(\beta-\nu, 2\beta, 2qx) \ , \end{aligned} \tag{4.15}$$

where $A_{I,II}$ are normalization constants and $U(a,b,z)$ is the confluent hypergeometric function which is regular as $|z| \to \infty$. In the overlap region, we may take the $|z| \to 0$ limit of the latter, given by [230]:

$$U(a,b,z) \sim \frac{\pi}{\sin(\pi b)} \left[\frac{1}{\Gamma[1+a-b]\Gamma[b]} - \frac{z^{1-b}}{\Gamma[a]\Gamma[2-b]} \right] . \tag{4.16}$$

This yields for the corresponding Ψ functions:

$$\begin{aligned} \Psi_I(x) &= -A_I \frac{\pi}{\sin(2\pi\beta)} \left[\frac{x^\beta}{\Gamma[\beta-2i\omega]\Gamma[2-2\beta]} - \frac{(-4i\varpi)^{2\beta-1} x^{1-\beta}}{\Gamma[1-\beta-2i\omega]\Gamma[2\beta]} \right] , \\ \Psi_{II}(x) &= A_{II} \frac{\pi}{\sin(2\pi\beta)} \left[\frac{x^\beta}{\Gamma[1-\beta-\nu]\Gamma[2\beta]} - \frac{(2q)^{1-2\beta} x^{1-\beta}}{\Gamma[\beta-\nu]\Gamma[2-2\beta]} \right] . \end{aligned} \tag{4.17}$$

Hence, both functions have a common functional form in the overlap region, and one

may match the coefficients of the x^{β} and $x^{1-\beta}$ terms to obtain the following condition:

$$\frac{\Gamma[1-\beta-\nu]}{\Gamma[\beta-\nu]} = (-8i\varpi q)^{2\beta-1}\frac{\Gamma[\beta-2i\omega]}{\Gamma[1-\beta-2i\omega]}\left(\frac{\Gamma[2-2\beta]}{\Gamma[2\beta]}\right)^2 . \tag{4.18}$$

For the matching to be possible, $-8\varpi q < 1$ and, as in the small mass limit $2\beta - 1 \simeq 2l + 1 > 0$, we conclude that the rhs of this condition is suppressed, so that the lhs should vanish to leading order, which implies:

$$\beta - \nu = -n \;\Rightarrow \qquad \omega \approx \mu\left(1 - \frac{(\mu M)^2}{2(l+1+n)^2}\right) , \tag{4.19}$$

where n is a non-negative integer. This reproduces the Hydrogen-like spectrum obtained in previous works for $\mu M \ll 1$ [212, 216], although significant deviations are observed for $\mu M \sim 1$, where corrections to the real part of the frequency arise both from the polynomial equation $\beta - \nu = -n$ and from the finiteness of the rhs of Eq. (4.18). This expression confirms nevertheless our physical intuition about the Hydrogen-like nature of the massive bound states in the black hole's potential well.

We need to go beyond this leading approximation to obtain the imaginary part of the spectrum and with this purpose we have used *Mathematica* to numerically obtain the roots of Eq. (4.18). The *FindRoot* command can be used for this purpose, requiring an initial value for which we considered the relevant root of $\beta - \nu = -n$ in each case. In Figure 4.2, we plot the results for $l = m = 1$ and $n = 0$, for which we expect the maximum growth rate.

In Figure 4.2(a), one observes a smooth increase of the growth rate with μ, with a sharp decrease close to the endpoint of the spectrum, where the superradiant condition is no longer satisfied and which for $\mu M \ll 1$ lies close to $m/2$. Although this is in agreement with the numerical results of [215, 216], one also observes two peak-like structures separated by a sharp decrease in $\omega_I M$. One of these "peaks" was also observed in [228] and is behind the four orders of magnitude discrepancy between the

two types of analysis. Figure 4.2(b) depicts a detail of this feature and should be compared with Figure 1 in [228].

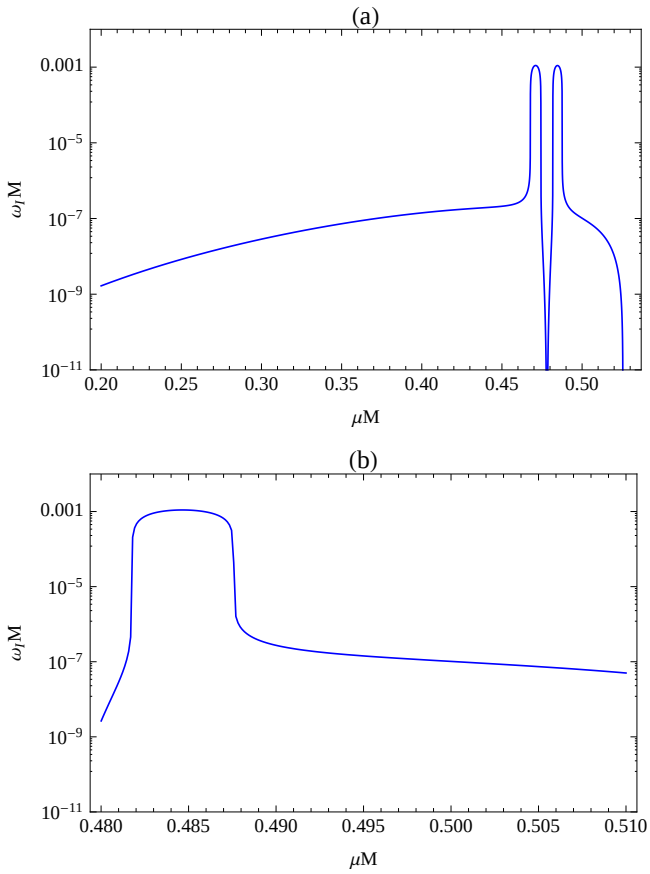

Figure 4.2: Results obtained for the imaginary part of the frequency obtained using the functional matching approach for $l = m = 1$ and $n = 0$, illustrating (a) the smooth part and the two peaks and (b) a detail of the second peak.

One should note, however, that the matching condition Eq. (4.18) involves several gamma functions, some of which may develop poles for some values of μ. In particular, $\Gamma[2 - 2\beta]$ has poles for $\beta = 1 + p/2$, where p is a non-negative integer. Using the lowest order result in Eq. (4.19) for ω_R, one obtains poles in this function for:

$$\mu^2 = \frac{(2l+1)^2 - (p+1)^2}{24} \ , \tag{4.20}$$

which gives $\mu \simeq 0.46$ for $l = p = 1$, in the region where the peak-like features are observed. The shape of this pole is illustrated in Figure 4.3, showing that it occurs

exactly at the value of μM where the sharp decrease in the growth rate is observed. This suggests that the peak-like structures are most likely unphysical and simply a consequence of the approximations involved in deriving Eq. (4.18).

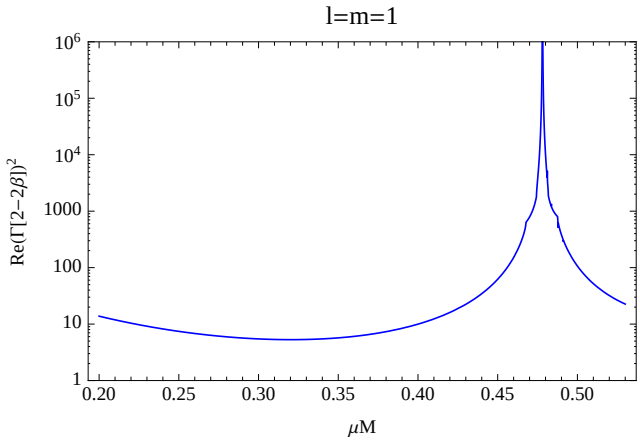

Figure 4.3: Real part of the function $(\Gamma[2-2\beta])^2$ appearing in the matching condition Eq. (4.18), illustrating the pole at the value of μM where the sharp decrease in the growth rate of the instability is obtained using the functional matching method.

In fact, the limit taken in Eq. (4.16) is not valid close to these poles. To see this, we may rewrite the solution in region I as:

$$F_I(x) = A_I e^{\frac{2i\varpi}{x}}(-4i\varpi/x)^{2\beta-1}U(\beta - 2i\omega, 2\beta, -4i\varpi/x) \ , \tag{4.21}$$

where we used that [230]:

$$U(a, b, z) = z^{1-b}U(1 + a - b, 2 - b, z) \ . \tag{4.22}$$

In this form, we have $b = p + 2$ for both solutions, $p \in \mathbb{Z}_0^+$, so that the correct $|z| \to 0$ limit of the confluent hypergeometric function is given by [230]:

$$U(a, b, z) \sim \frac{(-1)^b\big[\log z + \psi(a) + \gamma - \psi(b)\big]}{\Gamma[b]\Gamma[a - b + 1]} + \frac{\Gamma[b-1]}{\Gamma[a]}z^{1-b} \ , \tag{4.23}$$

where $\psi(x)$ denotes the Digamma function and γ the Euler-Mascheroni constant.

Using this expression, the solutions in the two regions become:

$$\begin{aligned}
\psi_I(x) &= A_I\Bigg[-\frac{(4i\varpi)^{2\beta-1}\big[\log(-4i\varpi/x)+\psi(\beta-2i\omega)+\gamma-\psi(2\beta)\big]}{\Gamma[2\beta]\Gamma[1-\beta-2i\omega]}x^{1-\beta}+ \\
&\quad +\frac{\Gamma[2\beta-1]}{\Gamma[\beta-2i\omega]}x^{\beta}\Bigg], \\
\psi_{II}(x) &= A_{II}\Bigg[\frac{(-1)^{2\beta}\big[\log(2qx)+\psi(\beta-\nu)+\gamma-\psi(2\beta)\big]}{\Gamma[2\beta]\Gamma[1-\beta-\nu]}x^{\beta}+ \\
&\quad +\frac{(2q)^{1-2\beta}\Gamma[2\beta-1]}{\Gamma[\beta-\nu]}x^{1-\beta}\Bigg].
\end{aligned} \tag{4.24}$$

Hence, the functions cannot be matched in this case, as the $\log x$ corrections are associated with distinct powers of x in each solution. Such terms are generically significant in the vicinity of points for which $\beta = 1 + p/2$, so that the functional matching procedure can only be used away from the above mentioned poles.

In particular, one cannot *a priori* neglect the effects of the logarithmic corrections near the peaks illustrated in Figure 4.2, even though all gamma functions are finite in this case, due to their obvious proximity to the pole. Furthermore, the discrepancy with respect to the numerical results of [215, 216] suggests that these corrections are indeed significant. The number of poles increases as we consider higher multipoles, making it hard to trust this technique in general. This is disappointing, as it precludes the use of the functional matching method in some regions of parameter space.

4.4 Point matching

The functional matching method is not the only technique one can use to obtain the spectrum, and a simple alternative consists in matching the functions and their first derivatives at a point. This technique is widely used in problems in which the potential has two clearly separated regions where the solutions take distinct forms. In this case, however, we have two overlapping regions where one can find approximate solutions to the radial equation. Nevertheless, choosing a match point in the overlap

of regions I and II, we may ensure that both functions are sufficiently close to the exact solution and thus obtain a good approximation to the spectrum. One cannot, however, hope to obtain an accurate prediction for the superradiant growth rate, as this would require an exact prescription for the choice of the match point, which we do not have *a priori*.

Matching the functions in Eq. (4.15) at a generic point x, one obtains:

$$1+2(1-\beta-2i\omega)\tfrac{U(2-\beta-2i\omega,3-2\beta,-4i\varpi/x)}{U(1-\beta-2i\omega,2-2\beta,-4i\varpi/x)}=\frac{qx^2}{2i\varpi}\left[1+2(\beta-\nu)\tfrac{U(\beta-\nu+1,2\beta+1,2qx)}{U(\beta-\nu,2\beta,2qx)}\right] \quad (4.25)$$

where we have used that $U'(a,b,z)=-aU(a+1,b+1,z)$ [230]. A good trial match point is $x_*=\sqrt{-2\varpi/q}$, as this corresponds to the value of x for which the absolute values of the arguments of the confluent hypergeometric functions in both regions are the same, simultaneously giving the geometric mean of the values of x_{min} and x_{max} defined in section 4.2, which give the 'boundaries' of the two regions. This ensures that the matching condition $x_{min}<x<x_{max}$ is satisfied if such an overlap region can be found. We then obtain for this particular choice:

$$1+2(1-\beta-2i\omega)\tfrac{U(2-\beta-2i\omega,3-2\beta,iz_*)}{U(1-\beta-2i\omega,2-2\beta,iz_*)}=i\left(1+2(\beta-\nu)\tfrac{U(\beta-\nu+1,2\beta+1,z_*)}{U(\beta-\nu,2\beta,z_*)}\right), \quad (4.26)$$

with $z_*=\sqrt{-8\varpi q}<1$ for an overlap region to exist. We have determined the roots of this condition numerically for $l=m=1,\ 2$ and 3, which give the largest growth rates, via the same procedure used for the functional matching method in the previous section. These results are plotted in Figure 4.4, along with the corresponding solutions obtained using functional matching and the numerical continued-fraction method in [216] for the case $a=0.999M$, which corresponds to the largest black hole spin analyzed in the latter work. We also plot in this figure the results obtained by choosing different points within the overlap region, $x_{min}<x<x_{max}$, giving an effective uncertainty for the match point method.

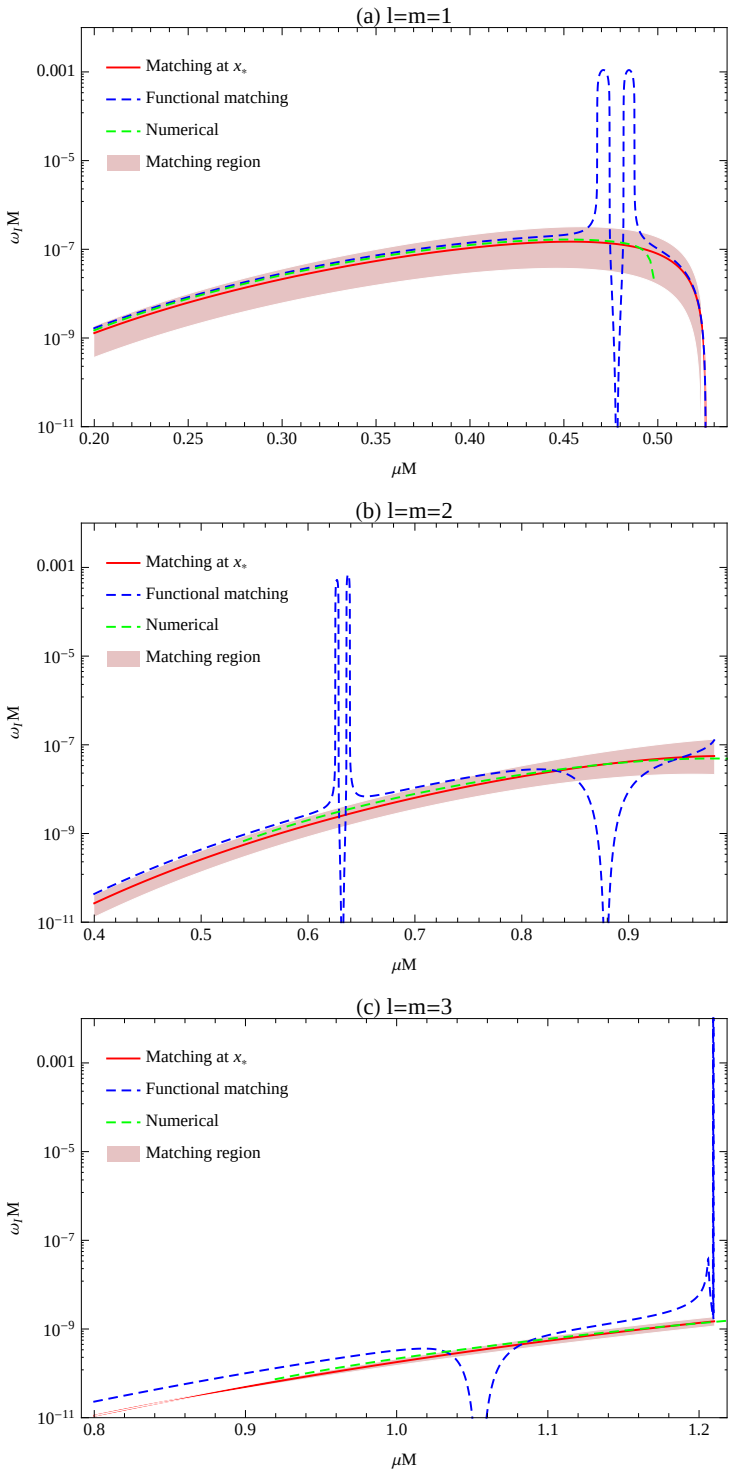

Figure 4.4: Results obtained for the imaginary part of the mode frequency using the point matching method for $l = m = 1,\ 2,\ 3$, with $n = 0$, along with the uncertainty associated with the choice of match point. Also shown are the results obtained with functional matching and the numerical solutions of [216] for $a = 0.999M$.

As one may observe in the three plots in Figure 4.4, the point matching procedure gives a smooth evolution of $\omega_I M$ as a function of μM and does not exhibit any peak-like features as those obtained using the functional matching. For the first three multipoles, these results are in good agreement with the numerically obtained values for $a = 0.999M$, although they differ significantly close to the endpoint of the superradiant spectrum. In fact, the endpoint corresponds to $\varpi = 0$, which is extremely sensitive to the black hole's spin, extending the superradiant spectrum to larger μ as one approaches extremality.

For $l = m = 1$, both the numerical and functional matching results (away from the pole) lie within the shaded region and are in good agreement with the values obtained from point matching at x_*, showing that in this case the latter is extremely close to the optimal match point. The upper (lower) limit of the shaded region corresponds to matching at x_{min} (x_{max}), mainly due to the fact that the Hydrogen-like function $\psi_{II}(x)$ has a larger overlap with the ergoregion if the matching is implemented closer to the horizon. The maximum growth rate for matching at x_* occurs for $\mu M \simeq 0.454$, for which $\omega_I M \simeq 1.49 \times 10^{-7}$, in good agreement with the numerical results of [215, 216], despite the difference in the black hole's angular momentum and the uncertainty in the choice of the match point. These results clearly show that the four orders of magnitude discrepancy between the results of [228] and [215, 216] are unphysical.

For $l = m = 2$ and 3, Figure 4.4 shows only a small range of μM, mainly as for large masses the number of poles in the matching condition becomes quite large, which precludes any decent comparison with the point matching technique. For the mass values shown in Figures 4.4(b) and (c), one observes a significantly larger discrepancy between the two analytical techniques away from the poles as compared to the $l = m = 1$ case, with the point matching results lying much closer to the corresponding numerical curves. This suggests that the approximations involved in deriving the functional matching condition fail for these multipoles even for μM away from the

expected poles, so that this method does not give reliable results in this case.

To get a better comparison between the point matching and the numerical methods, we plot in Figure 4.5 the results for the first three multipoles with $l = m$ and $n = 0$, including values for matching at x_*, the associated uncertainty and also the numerical curves for $a = 0.99M$ and $a = 0.999M$ obtained in [216].

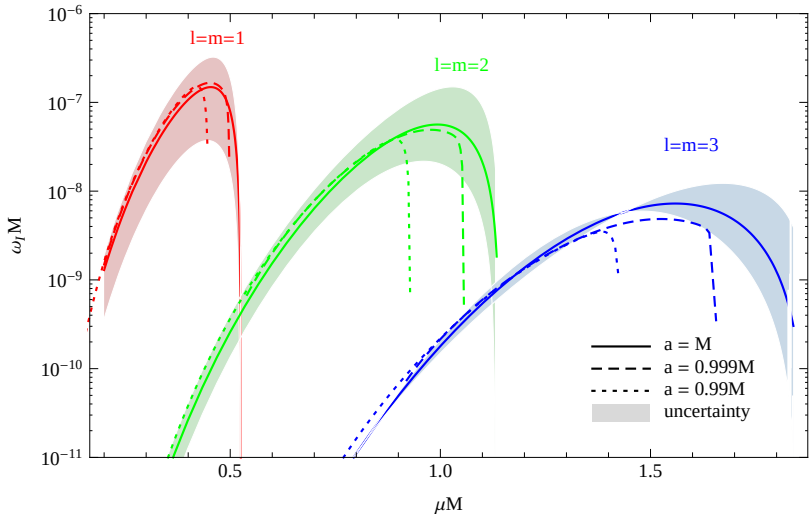

Figure 4.5: Results for the imaginary part of the mode frequency obtained using the point matching technique for the first three multipoles with $l = m$ and $n = 0$, including the numerical solutions of [216] for $a = 0.99M$ and $a = 0.999M$.

As expected, the maximum growth rate decreases for larger values of $l = m$, as in these cases the overlap of the radial function with the ergoregion becomes smaller. The agreement between the point-matching and the numerical curves is extremely good, apart from the vicinity of the endpoint where one observes a large discrepancy. In fact, these deviations are larger for the higher multipoles, which is expected as the sensitivity of the condition $\varpi = 0$ to the value of a is much greater for larger m. This can be readily seen by comparing the two numerical curves for $a = 0.99M$ and $a = 0.999M$ for each multipole.

The spread in the values of $\omega_I M$ due to the size of the matching region is larger in the neighbourhood of the maximum growth rate for the first two multipoles. As discussed earlier, this can be seen as an effective uncertainty associated with the point

matching technique, although one should take into account that both $V_I(x)$ and $V_{II}(x)$ are not good approximations to the radial potential close to the limits of the matching region. On the other hand, a larger spread in the values of $\omega_I M$ indicates a wider overlap region, which ensures that both $\psi_I(x_*)$ and $\psi_{II}(x_*)$ are good approximations to the exact radial function at x_* and is confirmed by the good agreement with the results for $a = 0.999M$ up to the value of μM giving the maximum growth rate.

The results for $l = m = 3$ exhibit, however, a more significant deviation from the numerical ones for small μM. This is somewhat puzzling, as the uncertainty due to the choice of the match point is negligible in this region. To better investigate these results, we have used the spectrum computed at the match point x_* to determine the 'boundaries' of regions I and II for this multipole. The separation of the two regions for this particular case is illustrated in Figure 4.6.

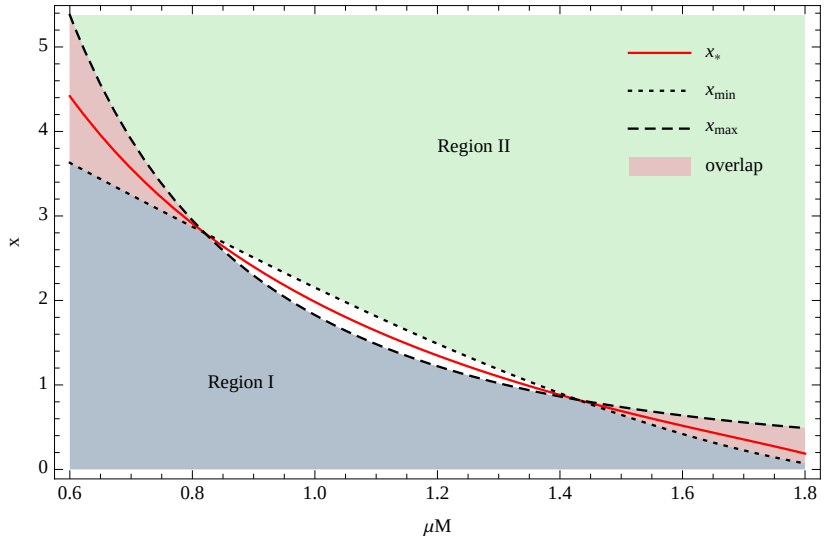

Figure 4.6: Matching region for $l = m = 3$ and $n = 0$ as a function of the scalar mass. The unshaded region denotes the values of μM for which no overlap region exists.

As one can easily conclude from this figure, there is no overlap region for $0.8 \lesssim \mu M \lesssim 1.4$, which explains the more significant discrepancy for $l = m = 3$ with respect to the numerical results in this part of parameter space. For these values, x_{min} is only slightly larger than x_{max}, so that the spread in the corresponding values of $\omega_I M$ is

quite small. One has to take into account, however, that part of this deviation is due to the non-extremality of the numerical results, a fact that precludes a more accurate determination of the effects of the absence of a matching region. Nevertheless, we may safely conclude that, despite this difference, the point matching at x_* gives a good approximation to the numerically obtained values of $\omega_I M$.

4.5 Discussion

Despite the absence of a precise prescription to determine the match point, the method described in the previous section eliminates the deficiencies of the traditional functional matching method by circumventing the use of approximate expressions for the hypergeometric function $U(a, b, z)$ that preclude the use of this method in the vicinity of anomalous poles. Consequently, this method provides the best agreement with the numerical computations in [215] and [216], being considerably simpler than a full numerical solution and giving a good theoretical insight on the form of the bound state radial functions. This is crucial for several phenomenological purposes, in particular for determining the backreaction of the axionic clouds formed via superradiant emission around astrophysical black holes. This may, for example, affect the gravity wave signal produced by inspiralling companions, which may lie within the reach of future observatories such as LISA and Advanced LIGO [150, 152].

It is worth mentioning that the results we have obtained seem to be in conflict with those of [214], as pointed out in [232]. In this numerical analysis of the scalar superradiant instability, the authors estimated a growth rate $\omega_I M = 2 \times 10^{-5}$ for $\mu M = 0.25$, which is two orders of magnitude larger than the maximum value obtained in the present analysis. The numerical method used in [214] is, however, fundamentally different from the continued-fraction method employed in [215, 216]. In particular, it computes the time evolution of a particular scalar mode in the Kerr background

rather than determining the spectrum of superradiant bound states. Moreover, the selected mode has a frequency $\omega = \mu$ which, as discussed in the present and in earlier analyses, does not correspond to a scalar bound state. Although our results show that the frequency of bound states is very close to the scalar mass μ when the latter is small, as explicitly obtained in Eq. (4.19), they also suggest that small deviations in the real part of the spectrum may produce large (unphysical) effects in the growth rate of the instability. Also, the above mentioned value is derived under the assumption that the mode is growing exponentially, while the estimated e-folding time is in fact much larger than the numerically sampled interval. Thus, the claim in [232] for the existence of a regime where the superradiant growth rate is much larger than the results obtained in this chapter is, in our opinion, unjustified and involves a non-trivial extrapolation of the results obtained in [214].

Recently [232], the authors of [228] explicitly showed that all gamma functions involved in their matching condition are finite for values of μM in the region corresponding to one of the peaks obtained for $l = m = 1$, claiming that this validates the functional matching method used in their analysis. This does not, however, contradict the results described earlier, as the existence of a pole between the two peaks requires the use of Eq. (4.23) in place of Eq. (4.16) for the $|z| \to 0$ limit of the hypergeometric function $U(a, b, z)$. The true deficiency of the functional matching method resides in this subtle observation, which introduces non-negligible logarithmic corrections in the approximate solutions, producing the large unphysical peaks that are absent in the point matching and numerical results. Moreover, the peak-like structures observed for $l = m = 1$ do not coincide exactly with those obtained in [228], occurring in this case for smaller values of the scalar mass. Given that distinct analyses exhibit similar features at different points in parameter space, this further suggests that both peaks are simply the product of unsuitable approximations and should not be interpreted as physical enhancements of the superradiant growth rate.

The existence of an overlap region for all the values of μM considered for $l = m = 1$ ensures the applicability of the point matching procedure in this case, although failing for the phenomenologically less relevant higher multipoles. On the other hand, the analysis of [228] is restricted to the regime $\omega \sim m\Omega \sim \mu$, precluding the use of the matching procedure for small scalar masses. This difference arises from the distinct definitions of the regions I and II used in this chapter and in [228], with the extremality condition playing an important role in this case.

An extension of the point matching technique for $a < M$, although outside the scope of this thesis, would be useful for a better comparison with the numerical growth rates obtained in [216] close to the endpoint of the superradiant spectrum, as the continued-fraction method used in the latter work is designed for non-extremal black holes. Also, realistic black holes can only be spun up up to $a \simeq 0.998M$, as estimated by Thorne in [233] taking into account the effects of radiation from the surrounding accretion disks. The extremal black hole bomb is nevertheless a very good approximation to the latter case, only differing significantly close to the endpoint of the spectrum, where the growth rate becomes very small.

The results obtained with this method reveal a maximum growth rate $\omega_I M \simeq 1.5 \times 10^{-7}$ which, for pions, corresponds to a time scale for the development of the instability of $\tau = 1.43 \times 10^{-17}$ s in a Kerr black hole with $M = 8.65 \times 10^{11}$ kg. This is only about 17% of the pion's mean lifetime, which suggests that, even for small primordial black holes, pions cannot extract sufficient energy and angular momentum from the black hole via the superradiant instability. Thus, the proposed string axion-black hole bomb [150] remains the only viable possibility for astrophysical black hole superradiance, being worth to investigate the many interesting phenomena associated with it.

Chapter 5

Conclusion

In this thesis, we have analyzed some of the novel features introduced by string theory compactifications in low-energy phenomenology by considering effective field theory descriptions of string theory scenarios. These effects arise from different levels of compactification, leading to distinct BSM applications in the context of cosmology, collider physics and astrophysical systems.

In chapter 2, we have studied brane-world scenarios in the context of D6-$\overline{\text{D6}}$ branonium bound states, showing that the elliptical orbits of the probe anti-brane induce a (narrow) parametric resonance in its world-volume, for particle masses parametrically smaller than the string scale.

Hubble expansion makes the orbits decay, shifting the resonance towards higher momentum particle modes, so that each mode can only be excited during a finite period. A large number of particles may nevertheless be produced at late times with no significant backreaction on the orbital motion, for suitable initial conditions such that other sources of instability such as bulk radiation have negligible effects.

We have also shown that elliptical orbits are a natural consequence of the broken rotational invariance of the compact transverse space, due to the presence of the central brane stack. While annihilation seems inevitable for a probe $\overline{D6}$-brane, more

interesting cosmological applications of this mechanism, such as dark and baryonic matter generation, may arise for a probe $D6$-brane if SUSY breaking renders the associated RR-field massive, leading to a (meta)stable branonium configuration.

In chapter 3, we considered the spectrum of spin-3/2 Regge excitations of quarks and leptons in warped string compactifications, modeled by an effective 5-dimensional Randall-Sundrum throat. By postulating a universal string contribution to their bulk masses, in addition to that of their spin-1/2 SM counterparts, as well as opposite IR/UV boundary conditions to eliminate chiral zero modes, we have shown that the rhd top excitation, t_R^*, is the lightest of such states in a significant region of parameter space, possibly lying below the TeV scale.

While such a resonance can be easily accommodated within present experimental constraints, it may be copiously (pair-)produced at the LHC, decaying mainly via $t_R^* \to tg$ or $t_R^* \to Wb$, with model dependent branching ratios. If the latter channel is dominant, a preliminary signal-to-background estimate suggests that discovery may be possible up to masses of 1.35 TeV. Also, the recent mild excess of $WWjj$ events reported by CDF could be more easily explained by a rdh top spin-3/2 excitation of ~ 400 GeV than with a more standard fourth generation quark.

Finally, in chapter 4, we have analyzed the superradiant instability of Kerr black holes, motivated by the string axiverse proposal, which suggests that ultra-light axions with masses $\mu \lesssim 10^{-10}$ eV may significantly spin down astrophysical black holes.

Focusing on extremal geometries, where the instability is maximal, we have computed the bound state spectrum by matching the near- and far-region solutions of the massive Klein-Gordon equation in their common domain of validity. While matching their functional form leads to unphysical enhancements of the instability growth rate, due to the approximations involved, we have shown that matching at a single point gives a good agreement with previous numerical analyses, providing the first (semi-)analytical computation in the phenomenologically interesting regime, $\mu M \sim 1$.

String theory brings together a huge number of *a priori* unrelated physical systems, from super-heavy dark matter particles to TeV-scale states or sub-eV axions, of which the analysis performed in this thesis provides only a small sample. Whether string theory provides the long-sought 'theory of everything' will, however, ultimately be decided by experiment. This thesis illustrates how potential signatures of string theory compactifications may be found in different types of experiment, from underground proton collisions to astronomical observations, but whereas each individual search may only probe a small 'island' within the vast string landscape, only the *ensemble* of possible effects may give us a fuller picture.

Appendix A

Particle number in an expanding universe

The particle number produced by the branonium parametric resonance for type (ii) and (iii) modes can be estimated by computing the integral in Eq. (2.93). This will give the physical particle number apart from constant factors and small contributions from the time the mode spends outside the resonance band. Also, the physical particle number density will also be redshifted by an $a(t)^{-3}$ factor due to Hubble expansion. Focusing on the particle number produced by the resonance, we have:

$$\log n_k(z) = \begin{cases} 0, & z < z_i \ , \\ 2\int_{z_i}^{z} \mu_k(z')dz', & z_i \leq z \leq z_2 \ , \\ 2\int_{z_i}^{z_2} \mu_k(z')dz', & z > z_2 \ . \end{cases} \tag{A.1}$$

In order to compute this function, let us write the exponent $\mu_k(z)$ in the form:

$$\mu_k(z) = \frac{1}{2}\sqrt{az^2 + bz + c} \ , \tag{A.2}$$

where

$$a = q_0^2\xi^2 - A_{k0}^2\gamma^2 \ , \qquad b = 2(q_0^2\xi + A_{k0}(A_{k0}-1)\gamma) \ , \qquad c = q_0^2 - (A_{k0}-1)^2 \ . \tag{A.3}$$

For all modes of interest, $a < 0$, while we have $c \geq 0$ for type (ii) modes and $c < 0$ for type (iii) modes. The sign of the constant b will not affect our results. It is also useful to define $d^2 \equiv b^2 - 4ac$, which is explicitly given by

$$d^2 = 4q_0^2\big(2A_{k0}(A_{k0}-1)\xi\gamma + (A_{k0}-1)^2\xi^2 + A_{k0}^2\gamma^2\big) \ , \tag{A.4}$$

and is positive for all type (ii) and type (iii) modes. With these considerations, we find, for $z_i \leq z \leq z_2$,

$$\log n_k(z) = \frac{1}{2a}\left[(2az'+b)\mu_k(z') + \frac{d^2}{\sqrt{-a}}\arcsin\left(\frac{2az'+b}{d}\right)\right]_{z_i}^{z} \ . \tag{A.5}$$

Taking into account that $\mu_k(0) = \sqrt{c}/2$, $\mu_k(z_1) = \mu_k(z_2) = 0$ and also that $(2az_1 + b)/d = -(2az_2 + b)/d = 1$, we can write the total particle number produced by the resonance for each type (ii) mode as:

$$\log n_k^{(ii)}(z_2) = -\frac{1}{4a}\left[b\sqrt{c} + \frac{d^2}{2\sqrt{-a}}\left(\frac{\pi}{2} + \arcsin\left(\frac{b}{d}\right)\right)\right] \ . \tag{A.6}$$

Similarly, for type (iii) modes, we obtain

$$\log n_k^{(iii)}(z_2) = \frac{\pi}{8}\frac{d^2}{(-a)^{\frac{3}{2}}} \ . \tag{A.7}$$

It is easy to check that Eqs. (A.6) and (A.7) give the same result for the mode in the transition between types (ii) and (iii), corresponding to $A_{k0} = 1 + |q_0|$ or $\beta = 1$, as expected. Recalling that $|q_0| \ll 1$, these expressions can be approximated by those given in Eq. (2.94).

Bibliography

[1] J. L. Hewett, *The Standard model and why we believe it*, in Boulder 1997, Supersymmetry, supergravity and supercolliders 3-83 [arXiv:hep-ph/9810316].

[2] C. Amsler *et al.* [Particle Data Group], *Review of particle physics*, Phys. Lett. B **667**, 1 (2008).

[3] L. Camilleri, E. Lisi and J. F. Wilkerson, *Neutrino masses and mixings: status and prospects*, Ann. Rev. Nucl. Part. Sci. **58**, 343 (2008).

[4] S. Ray, *Renormalization group evolution of neutrino masses and mixing in seesaw models: a review* (2010) [arXiv:1005.1938 [hep-ph]].

[5] G. G. Ross, *Grand Unified Theories*, Frontiers in Physics Lecture Note Series **60** (Benjamin/Cummings, Reading, MA, 1984).

[6] S. Raby, *SUSY GUT model building*, Eur. Phys. J. C **59**, 223 (2009) [arXiv:0807.4921 [hep-ph]].

[7] I. Aitchinson, *Supersymmetry in particle physics* (Cambridge University Press, Cambridge, UK, 2007).

[8] F. Zwicky, *Spectral displacement of extra galactic nebulae*, Helv. Phys. Acta **6**, 110 (1933).

[9] G. Bertone, D. Hooper and J. Silk, *Particle dark matter: evidence, candidates and constraints*, Phys. Rept. **405**, 279 (2005) [arXiv:hep-ph/0404175].

[10] M. Milgrom, *A modification of the newtonian dynamics as a possible alternative to the hidden mass hypothesis*, Astrophys. J. **270**, 365 (1983); *A modification of the newtonian dynamics: implications for galaxies*, Astrophys. J. **270**, 371 (1983); *A modification of the newtonian dynamics: implications for galaxy systems*, Astrophys. J. **270**, 384 (1983); J. Bekenstein and M. Milgrom, *Does the missing mass problem signal the breakdown of newtonian gravity?*, Astrophys. J. **286**, 7 (1984).

[11] D. Clowe *et al.*, *A direct empirical proof of the existence of dark matter*, Astrophys. J. **648**, L109 (2006) [arXiv:astro-ph/0608407].

[12] D. Larson *et al.*, *Seven-year Wilkinson Microwave Anisotropy Probe (WMAP) observations: power spectra and WMAP-derived parameters* (2010) [arXiv:1001.4635 [astro-ph.CO]].

[13] E. W. Kolb, D. J. H. Chung and A. Riotto, *WIMPzillas!*, in Buenos Aires 1998, Trends in theoretical physics **2**, 91-105 [arXiv:hep-ph/9810361].

[14] R. Bernabei *et al.*, *New results from DAMA/LIBRA*, Eur. Phys. J. C **67**, 39 (2010) [arXiv:1002.1028 [astro-ph.GA]]; C. E. Aalseth *et al.* [CoGeNT collaboration], *Results from a search for light-mass dark matter with a p-type point contact Germanium detector* (2010) [arXiv:1002.4703 [astro-ph.CO]]; Z. Ahmed *et al.* [The CDMS-II Collaboration], *Results from the final exposure of the CDMS II experiment* (2010) [arXiv:0912.3592 [astro-ph.CO]].

[15] J. E. Kim, *Light pseudoscalars, particle physics and cosmology*, Phys. Rept. **150**, 1 (1987).

[16] C. A. Baker *et al.*, *An improved experimental limit on the electric dipole moment of the neutron*, Phys. Rev. Lett. **97**, 131801 (2006) [arXiv:hep-ex/0602020].

[17] W. C. Griffith *et al.*, *Improved limit on the permanent electric dipole moment of Hg-199*, Phys. Rev. Lett. **102**, 101601 (2009).

[18] R. N. Mohapatra and G. Senjanovic, *Natural suppression of strong P And T noninvariance*, Phys. Lett. B **79**, 283 (1978).

[19] A. E. Nelson, *Naturally weak CP violation*, Phys. Lett. B **136**, 387 (1984).

[20] S. M. Barr, *Solving the strong CP problem without the Peccei-Quinn symmetry*, Phys. Rev. Lett. **53**, 329 (1984).

[21] R. D. Peccei and H. R. Quinn, *CP conservation in the presence of Instantons*, Phys. Rev. Lett. **38**, 1440 (1977).

[22] S. Weinberg, *A new light boson?*, Phys. Rev. Lett. **40**, 223 (1978).

[23] F. Wilczek, *Problem of strong P and T invariance in the presence of instantons*, Phys. Rev. Lett. **40**, 279 (1978).

[24] P. Svrcek and E. Witten, *Axions in string theory*, JHEP **0606**, 051 (2006) [arXiv:hep-th/0605206].

[25] R. D. Peccei, *A short review of axions*, in Tokyo H. E. Phys. 1978, 0385 (1978).

[26] E. W. Kolb and M. S. Turner, *The early universe* (Westview Press, Chicago, USA, 1994).

[27] S. Perlmutter *et al.* [Supernova Cosmology Project Collaboration], *Measurements of omega and lambda from 42 high-redshift supernovae*, Astrophys. J. **517**, 565 (1999) [arXiv:astro-ph/9812133].

[28] A. G. Riess *et al.* [Supernova Search Team Collaboration], *Observational evidence from supernovae for an accelerating universe and a cosmological constant*, Astron. J. **116**, 1009 (1998) [arXiv:astro-ph/9805201].

[29] A. D. Linde, *The inflationary universe*, Rept. Prog. Phys. **47**, 925 (1984).

[30] S. Weinberg, *The cosmological constant problem*, Rev. Mod. Phys. **61**, 1 (1989).

[31] T. Padmanabhan, *Cosmological constant: the weight of the vacuum*, Phys. Rept. **380**, 235 (2003) [arXiv:hep-th/0212290].

[32] E. J. Copeland, M. Sami and S. Tsujikawa, *Dynamics of dark energy*, Int. J. Mod. Phys. D **15**, 1753 (2006) [arXiv:hep-th/0603057].

[33] A. H. Guth, *'The inflationary universe: a possible solution to the horizon and flatness problems*, Phys. Rev. D **23**, 347 (1981).

[34] A. D. Linde, *A new inflationary universe scenario: a possible solution of the horizon, flatness, homogeneity, isotropy and primordial monopole problems*, Phys. Lett. B **108**, 389 (1982); *Coleman-Weinberg theory and a new inflationary universe scenario*, Phys. Lett. B **114**, 431 (1982). *Temperature dependence of coupling constants and the phase transition in the Coleman-Weinberg theory*, Phys. Lett. B **116**, 340 (1982); *Scalar field fluctuations in expanding universe and the new inflationary universe scenario*, Phys. Lett. B **116**, 335 (1982).

[35] A. Albrecht and P. J. Steinhardt, *Cosmology for Grand Unified Theories with radiatively induced symmetry breaking*, Phys. Rev. Lett. **48**, 1220 (1982).

[36] J. H. Traschen and R. H. Brandenberger, *Particle production during out-of-equilibrium phase transitions*, Phys. Rev. D **42**, 2491 (1990); L. Kofman, A. D. Linde and A. A. Starobinsky, *Reheating after inflation*, Phys. Rev. Lett. **73**, 3195 (1994) [arXiv:hep-th/9405187]; Y. Shtanov, J. H. Traschen and R. H. Brandenberger, *Universe reheating after inflation*, Phys. Rev. D **51**, 5438 (1995) [arXiv:hep-ph/9407247]; D. Boyanovsky *et al.*, *Dissipation via particle production in scalar field theories*, Phys. Rev. D **51**, 4419 (1995) [arXiv:hep-ph/9408214];

M. Yoshimura, *Catastrophic particle production under periodic perturbation*, Prog. Theor. Phys. **94**, 873 (1995) [arXiv:hep-th/9506176]; D. I. Kaiser, *Post inflation reheating in an expanding universe*, Phys. Rev. D **53**, 1776 (1996) [arXiv:astro-ph/9507108]; S. Y. Khlebnikov and I. I. Tkachev, *Classical decay of inflaton*, Phys. Rev. Lett. **77**, 219 (1996) [arXiv:hep-ph/9603378].

[37] L. Kofman, A. D. Linde and A. A. Starobinsky, *Towards the theory of reheating after inflation*, Phys. Rev. D **56**, 3258 (1997) [arXiv:hep-ph/9704452]; P. B. Greene *et al.*, *Structure of resonance in preheating after inflation*, Phys. Rev. D **56**, 6175 (1997) [arXiv:hep-ph/9705347]; G. N. Felder, L. Kofman and A. D. Linde, *Instant preheating*, Phys. Rev. D **59**, 123523 (1999) [arXiv:hep-ph/9812289].

[38] A. D. Linde, *Inflationary cosmology*, Lect. Notes Phys. **738**, 1 (2008) [arXiv:0705.0164 [hep-th]].

[39] J. M. Cline, *Baryogenesis* (2006) [arXiv:hep-ph/0609145].

[40] A. G. Cohen, A. De Rujula and S. L. Glashow, *A matter-antimatter universe?*, Astrophys. J. **495**, 539 (1998) [arXiv:astro-ph/9707087].

[41] A. D. Sakharov, *Violation of CP invariance, C asymmetry, and baryon asymmetry of the universe*, Pisma Zh. Eksp. Teor. Fiz. **5**, 32 (1967) [JETP Lett. **5**, 24 (1967 SOPUA,34,392-393.1991 UFNAA,161,61-64.1991)].

[42] F. R. Klinkhamer and N. S. Manton, *A saddle point solution in the Weinberg-Salam theory*, Phys. Rev. D **30**, 2212 (1984).

[43] M. Yoshimura, *Unified gauge theories and the baryon number of the universe*, Phys. Rev. Lett. **41**, 281 (1978) [Erratum-ibid. **42**, 746 (1979)].

[44] A. G. Cohen, D. B. Kaplan and A. E. Nelson, *Baryogenesis at the weak phase transition*, Nucl. Phys. B **349**, 727 (1991).

[45] M. Fukugita and T. Yanagida, *Baryogenesis without Grand Unification*, Phys. Lett. B **174**, 45 (1986).

[46] I. Affleck and M. Dine, *A new mechanism for baryogenesis*, Nucl. Phys. B **249**, 361 (1985); M. Dine, L. Randall and S. D. Thomas, *Baryogenesis from flat directions of the supersymmetric Standard Model*, Nucl. Phys. B **458**, 291 (1996) [arXiv:hep-ph/9507453].

[47] K. Eppley and E. Hannah, *The necessity of quantizing the gravitational field*, Found. Phys. **7**, 5 (1977).

[48] S. D. Mathur, *The information paradox: a pedagogical introduction*, Class. Quant. Grav. **26**, 224001 (2009) [arXiv:0909.1038 [hep-th]].

[49] J. B. Hartle and S. W. Hawking, *Wave function of the universe*, Phys. Rev. D **28**, 2960 (1983).

[50] B. S. DeWitt, *Quantization of fields with infinite-dimensional invariance groups III: generalized Schwinger-Feynman theory*, J. Math. Phys. **3**, 1073 (1962); *Quantum Theory of Gravity I: the canonical theory*, Phys. Rev. **160**, 1113 (1967); *Quantum theory of gravity II: the manifestly covariant theory*, Phys. Rev. **162**, 1195 (1967); *Quantum theory of gravity III: applications of the covariant theory*, Phys. Rev. **162**, 1239 (1967); *The quantum and gravity: the Wheeler-DeWitt equation*, in 8th Marcel Grossmann meeting, Jerusalem, Israel, 22-27 June 1997. For a historical overview see, e.g., B. DeWitt, *Quantum Gravity yesterday and today*, Gen. Rel. Grav. **41**, 413 (2009) [Erratum-ibid. **41**, 671 (2009)] [arXiv:0805.2935 [physics.hist-ph]].

[51] G. 't Hooft and M. J. G. Veltman, *One loop divergencies in the theory of gravitation*, Annales Poincare Phys. Theor. A **20**, 69 (1974).

[52] M. H. Goroff and A. Sagnotti, *The ultraviolet behavior of Einstein gravity*, Nucl. Phys. B **266**, 709 (1986).

[53] R. P. Woodard, *How far are we from the quantum theory of gravity?*, Rept. Prog. Phys. **72**, 126002 (2009) [arXiv:0907.4238 [gr-qc]].

[54] S. Carlip, *Quantum gravity: a progress report*, Rept. Prog. Phys. **64**, 885 (2001) [arXiv:gr-qc/0108040].

[55] C. Rovelli, *Loop quantum gravity*, Living Rev. Rel. **11**, 5 (2008).

[56] S. R. Coleman and J. Mandula, *All possible symmetries of the S matrix*, Phys. Rev. **159**, 1251 (1967).

[57] S. Dimopoulos and H. Georgi, *Softly broken supersymmetry and SU(5)*, Nucl. Phys. B **193**, 150 (1981).

[58] S. P. Martin, *A supersymmetry primer*, in Kane, G.L. (ed.): Perspectives on supersymmetry 1-98 (1997) [arXiv:hep-ph/9709356].

[59] D. G. Cerdeno and C. Munoz, *An introduction to supergravity*, prepared for the 6th Hellenic School and Workshop on Elementary Particle Physics, Corfu, Greece, 6-26 September 1998.

[60] B. de Wit, *Supergravity*, in Les Houches 2001, Gravity, gauge theories and strings 1-135 [arXiv:hep-th/0212245].

[61] E. Witten, *Search for a realistic Kaluza-Klein theory*, Nucl. Phys. B **186**, 412 (1981).

[62] Z. Bern *et al.*, *The ultraviolet behavior of $\mathcal{N} = 8$ supergravity at four loops*, Phys. Rev. Lett. **103**, 081301 (2009) [arXiv:0905.2326 [hep-th]].

[63] E. Witten, *Dynamical breaking of supersymmetry*, Nucl. Phys. B **188**, 513 (1981).

[64] K. A. Intriligator and N. Seiberg, *Lectures on supersymmetry breaking*, Class. Quant. Grav. **24**, S741 (2007) [arXiv:hep-ph/0702069].

[65] M. A. Luty, *2004 TASI lectures on supersymmetry breaking*, in Boulder 2004, Physics in $D \geq 4$ 495-582 [arXiv:hep-th/0509029].

[66] T. Kaluza, *Zum unitätsproblem der physik*, Sitzungsber. Preuss. Akad. Wiss. Berlin (Math. Phys.) **1921**, 966 (1921); O. Klein, *Quantum theory and five dimensional theory of relativity*, Z. Phys. **37**, 895 (1926) [Surveys High Energ. Phys. **5**, 241 (1986)].

[67] K. R. Dienes, *New directions for new dimensions: an introduction to Kaluza-Klein theory, large extra dimensions, and the brane world*, in Boulder 2002, Particle physics and cosmology, 447-545.

[68] C. Csaki, *TASI lectures on extra dimensions and branes*, in Boulder 2002, Particle physics and cosmology, 605-698 [arXiv:hep-ph/0404096].

[69] I. Oda, *Localization of various bulk fields on a brane* (2000) [arXiv:hep-th/0009074].

[70] M. Mintchev and L. Pilo, *Localization of quantum fields on branes*, Nucl. Phys. B **592**, 219 (2001) [arXiv:hep-th/0007002].

[71] N. Arkani-Hamed, S. Dimopoulos and G. R. Dvali, *Phenomenology, astrophysics and cosmology of theories with sub-millimeter dimensions and TeV scale quantum gravity*, Phys. Rev. D **59**, 086004 (1999) [arXiv:hep-ph/9807344].

[72] N. Kaloper *et al.*, Compact hyperbolic extra dimensions: branes, Kaluza-Klein modes and cosmology, Phys. Rev. Lett. **85**, 928 (2000) [arXiv:hep-ph/0002001].

[73] E. W. Kolb and R. Slansky, *Dimensional reduction in the early universe: where have the massive particles gone?*, Phys. Lett. B **135**, 378 (1984).

[74] H. C. Cheng, K. T. Matchev and M. Schmaltz, *Radiative corrections to Kaluza-Klein masses*, Phys. Rev. D **66**, 036005 (2002) [arXiv:hep-ph/0204342].

[75] T. Appelquist, H. C. Cheng and B. A. Dobrescu, *Bounds on universal extra dimensions*, Phys. Rev. D **64**, 035002 (2001) [arXiv:hep-ph/0012100].

[76] G. Burdman and Y. Nomura, *Unification of Higgs and gauge fields in five dimensions*, Nucl. Phys. B **656**, 3 (2003) [arXiv:hep-ph/0210257].

[77] L. Randall and R. Sundrum, *A large mass hierarchy from a small extra dimension*, Phys. Rev. Lett. **83**, 3370 (1999) [arXiv:hep-ph/9905221]; *An alternative to compactification*, Phys. Rev. Lett. **83**, 4690 (1999) [arXiv:hep-th/9906064].

[78] W. D. Goldberger and M. B. Wise, *Modulus stabilization with bulk fields*, Phys. Rev. Lett. **83**, 4922 (1999) [arXiv:hep-ph/9907447].

[79] W. D. Goldberger and M. B. Wise, *Bulk fields in the Randall-Sundrum compactification scenario*, Phys. Rev. D **60**, 107505 (1999) [arXiv:hep-ph/9907218].

[80] T. Gherghetta and A. Pomarol, *Bulk fields and supersymmetry in a slice of AdS*, Nucl. Phys. B **586**, 141 (2000) [arXiv:hep-ph/0003129].

[81] A. Athenodorou, B. Bringoltz and M. Teper, *The closed string spectrum of SU(N) gauge theories in 2+1 dimensions*, Phys. Lett. B **656**, 132 (2007) [arXiv:0709.0693 [hep-lat]].

[82] K. Becker, M. Becker and J. H. Schwarz *String theory and M-theory: a modern introduction* (Cambridge University Press, Cambridge, UK, 2007).

[83] J. Polchinski, *String theory* (Cambridge University Press, Cambridge, UK, 1998).

[84] J. Scherk and J. H. Schwarz, *Dual models and the geometry of space-time*, Phys. Lett. B **52**, 347 (1974).

[85] P. Ramond, *Dual theory for free fermions*, Phys. Rev. D **3**, 2415 (1971).

[86] A. Neveu and J. H. Schwarz, *Factorizable dual model of pions*, Nucl. Phys. B **31**, 86 (1971).

[87] M. B. Green and J. H. Schwarz, *Supersymmetrical dual string theory*, Nucl. Phys. B **181**, 502 (1981); *Supersymmetrical dual string theory. 2. Vertices and trees*, Nucl. Phys. B **198**, 252 (1982); *Supersymmetrical dual string theory. 3. Loops and renormalization*, Nucl. Phys. B **198**, 441 (1982); *Supersymmetrical string theories*, Phys. Lett. B **109**, 444 (1982); *Covariant description of superstrings*, Phys. Lett. B **136**, 367 (1984).

[88] F. Gliozzi, J. Scherk and D. I. Olive, *Supersymmetry, supergravity theories and the dual spinor model*, Nucl. Phys. B **122**, 253 (1977); *Supergravity and the spinor dual model*, Phys. Lett. B **65**, 282 (1976).

[89] D. J. Gross and V. Periwal, *String perturbation theory diverges*, Phys. Rev. Lett. **60**, 2105 (1988).

[90] J. Scherk and J. H. Schwarz, *Dual field theory of quarks and gluons*, Phys. Lett. B **57**, 463 (1975).

[91] P. Candelas *et al.*, *Vacuum configurations for superstrings*, Nucl. Phys. B **258**, 46 (1985).

[92] S. B. Giddings, S. Kachru and J. Polchinski, *Hierarchies from fluxes in string compactifications*, Phys. Rev. D **66**, 106006 (2002) [arXiv:hep-th/0105097].

[93] S. Kachru *et al.*, *De Sitter vacua in string theory*, Phys. Rev. D **68**, 046005 (2003) [arXiv:hep-th/0301240].

[94] V. Balasubramanian *et al.*, *Systematics of moduli stabilisation in Calabi-Yau flux compactifications*, JHEP **0503**, 007 (2005) [arXiv:hep-th/0502058].

[95] O. DeWolfe et al., *Type IIA moduli stabilization*, JHEP **0507**, 066 (2005) [arXiv:hep-th/0505160].

[96] S. Dimopoulos *et al.*, *Small numbers from tunneling between brane throats*, Phys. Rev. D **64**, 121702 (2001) [arXiv:hep-th/0104239].

[97] S. Dimopoulos *et al.*, *Generating small numbers by tunneling in multi-throat compactifications*, Int. J. Mod. Phys. A **19**, 2657 (2004) [arXiv:hep-th/0106128].

[98] J. F. G. Cascales, F. Saad and A. M. Uranga, *Holographic dual of the standard model on the throat*, JHEP **0511**, 047 (2005) [arXiv:hep-th/0503079].

[99] S. B. Giddings and A. Maharana, *Dynamics of warped compactifications and the shape of the warped landscape*, Phys. Rev. D **73**, 126003 (2006) [arXiv:hep-th/0507158].

[100] A. Hebecker and J. March-Russell, *The ubiquitous throat*, Nucl. Phys. B **781**, 99 (2007) [arXiv:hep-th/0607120].

[101] I. R. Klebanov and A. A. Tseytlin, *Gravity duals of supersymmetric $SU(N) \times SU(N+M)$ gauge theories*, Nucl. Phys. B **578**, 123 (2000) [arXiv:hep-th/0002159].

[102] I. R. Klebanov and M. J. Strassler, *Supergravity and a confining gauge theory: Duality cascades and chi SB-resolution of naked singularities*, JHEP **0008**, 052 (2000) [arXiv:hep-th/0007191].

[103] F. Brummer, A. Hebecker and E. Trincherini, *The throat as a Randall-Sundrum model with Goldberger-Wise stabilization*, Nucl. Phys. B **738**, 283 (2006) [arXiv:hep-th/0510113].

[104] B. Hassanain, J. March-Russell and M. Schvellinger, *Warped deformed throats have faster (electroweak) phase transitions*, JHEP **0710**, 089 (2007) [arXiv:0708.2060 [hep-th]].

[105] M. R. Douglas and S. Kachru, *Flux compactification*, Rev. Mod. Phys. **79**, 733 (2007) [arXiv:hep-th/0610102].

[106] R. Bousso and J. Polchinski, *Quantization of four-form fluxes and dynamical neutralization of the cosmological constant*, JHEP **0006**, 006 (2000) [arXiv:hep-th/0004134].

[107] K. S. Stelle, *BPS branes in supergravity*, in Trieste 1997, High energy physics and cosmology [arXiv:hep-th/9803116].

[108] J. Dai, R. G. Leigh and J. Polchinski, *New connections between string theories*, Mod. Phys. Lett. A **4**, 2073 (1989); J. Polchinski, *Dirichlet-branes and Ramond-Ramond charges*, Phys. Rev. Lett. **75**, 4724 (1995) [arXiv:hep-th/9510017].

[109] M. Berkooz, M. R. Douglas and R. G. Leigh, *Branes intersecting at angles*, Nucl. Phys. B **480**, 265 (1996) [arXiv:hep-th/9606139].

[110] G. Aldazabal *et al.*, *D = 4 chiral string compactifications from intersecting branes*, J. Math. Phys. **42**, 3103 (2001) [arXiv:hep-th/0011073]; L. E. Ibanez, F. Marchesano and R. Rabadan, *Getting just the Standard Model at intersecting branes*, JHEP **0111**, 002 (2001) [arXiv:hep-th/0105155]; D. Bailin, G. V. Kraniotis and A. Love, *Standard-like models from intersecting D4-branes*, Phys. Lett. B **530**, 202 (2002) [arXiv:hep-th/0108131]; D. Cremades, L. E. Ibanez and

F. Marchesano, *Intersecting brane models of particle physics and the Higgs mechanism*, JHEP **0207**, 022 (2002) [arXiv:hep-th/0203160]; A. M. Uranga, *Chiral four-dimensional string compactifications with intersecting D-branes*, Class. Quant. Grav. **20**, S373 (2003) [arXiv:hep-th/0301032]; C. Kokorelis, *New Standard Model vacua from intersecting branes*, JHEP **0209**, 029 (2002) [arXiv:hep-th/0205147]; C. Kokorelis, *Exact Standard Model compactifications from intersecting branes*, JHEP **0208**, 036 (2002) [arXiv:hep-th/0206108]; N. Ohta and P. K. Townsend, *Supersymmetry of M-branes at angles*, Phys. Lett. B **418**, 77 (1998) [arXiv:hep-th/9710129].

For recent reviews see, e.g., R. Blumenhagen *et al.*, *Toward realistic intersecting D-brane models*, Ann. Rev. Nucl. Part. Sci. **55**, 71 (2005) [arXiv:hep-th/0502005]; R. Blumenhagen *et al.*, *Four-dimensional string compactifications with D-Branes, orientifolds and fluxes*, Phys. Rept. **445**, 1 (2007) [arXiv:hep-th/0610327].

[111] M. R. Douglas, *Branes within branes*, in Cargese 1997, Strings, branes and dualities [arXiv:hep-th/9512077]; A. A. Tseytlin, *Harmonic superpositions of M-branes*, Nucl. Phys. B **475**, 149 (1996) [arXiv:hep-th/9604035]; *Composite BPS configurations of p-branes in 10 and 11 dimensions*, Class. Quant. Grav. **14**, 2085 (1997) [arXiv:hep-th/9702163]; M. S. Costa, *Composite M-branes*, Nucl. Phys. B **490**, 202 (1997) [arXiv:hep-th/9609181]; Z. Guralnik and S. Ramgoolam, *Torons and D-brane bound states*, Nucl. Phys. B **499**, 241 (1997) [arXiv:hep-th/9702099].

[112] G. Aldazabal *et al.*, *D-branes at singularities: a bottom-up approach to the string embedding of the Standard Model*, JHEP **0008**, 002 (2000) [arXiv:hep-th/0005067]; A. Hanany and A. Iqbal, *Quiver theories from D6-branes via mirror symmetry*, JHEP **0204**, 009 (2002) [arXiv:hep-th/0108137].

[113] J. M. Maldacena, *The large N limit of superconformal field theories and supergravity*, Adv. Theor. Math. Phys. **2**, 231 (1998) [Int. J. Theor. Phys. **38**, 1113

(1999)] [arXiv:hep-th/9711200].

[114] O. Aharony *et al.*, *Large N field theories, string theory and gravity*, Phys. Rept. **323**, 183 (2000) [arXiv:hep-th/9905111].

[115] J. Erlich, *Recent Results in AdS/QCD*, in PoS CONFINEMENT8, 032 (2008) [arXiv:0812.4976 [hep-ph]].

[116] H. P. Nilles *et al*, *From strings to the MSSM*, Eur. Phys. J. C **59**, 249 (2009) [arXiv:0806.3905 [hep-th]].

[117] C. Vafa, *Evidence for F-Theory*, Nucl. Phys. B **469**, 403 (1996) [arXiv:hep-th/9602022].

[118] T. Gherghetta and J. Giedt, *Bulk fields in AdS(5) from probe D7 branes*, Phys. Rev. D **74**, 066007 (2006) [arXiv:hep-th/0605212].

[119] B. S. Acharya, F. Benini and R. Valandro, *Warped models in string theory* (2006) [arXiv:hep-th/0612192].

[120] G. R. Dvali and S. H. H. Tye, *Brane inflation*, Phys. Lett. B **450**, 72 (1999) [arXiv:hep-ph/9812483]; N. Arkani-Hamed, *et al.*, *Rapid asymmetric inflation and early cosmology in theories with sub-millimeter dimensions*, Nucl. Phys. B **567**, 189 (2000) [arXiv:hep-ph/9903224]; P. Binetruy, C. Deffayet and D. Langlois, *Non-conventional cosmology from a brane-universe*, Nucl. Phys. B **565**, 269 (2000) [arXiv:hep-th/9905012]; J. M. Cline, C. Grojean and G. Servant, *Cosmological expansion in the presence of extra dimensions*, Phys. Rev. Lett. **83**, 4245 (1999) [arXiv:hep-ph/9906523]; C. Csaki, *et al.*, *Cosmology of one extra dimension with localized gravity*, Phys. Lett. B **462**, 34 (1999) [arXiv:hep-ph/9906513]; S. S. Gubser, *AdS/CFT and gravity*, Phys. Rev. D **63**, 084017 (2001) [arXiv:hep-th/9912001]; A. Hebecker and J. March-Russell, *Randall-Sundrum II cosmology,*

AdS/CFT, and the bulk black hole, Nucl. Phys. B **608**, 375 (2001) [arXiv:hep-ph/0103214]; H. A. Bridgman, K. A. Malik and D. Wands, *Cosmological perturbations in the bulk and on the brane*, Phys. Rev. D **65**, 043502 (2002) [arXiv:astro-ph/0107245]; A. Kehagias and E. Kiritsis, *Mirage cosmology*, JHEP **9911**, 022 (1999) [arXiv:hep-th/9910174]; P. Kraus, *Dynamics of anti-de Sitter domain walls*, JHEP **9912**, 011 (1999) [arXiv:hep-th/9910149].

For reviews of brane cosmology in field theory see, e.g., D. Langlois, *Brane cosmology: an introduction*, Prog. Theor. Phys. Suppl. **148**, 181 (2003) [arXiv:hep-th/0209261]; R. Maartens, *Brane-world gravity*, Living Rev. Rel. **7**, 7 (2004) [arXiv:gr-qc/0312059].

[121] G. Shiu and S. H. H. Tye, *Some aspects of brane inflation*, Phys. Lett. B **516**, 421 (2001) [arXiv:hep-th/0106274]; N. T. Jones, H. Stoica and S. H. H. Tye, *Brane interaction as the origin of inflation*, JHEP **0207**, 051 (2002) [arXiv:hep-th/0203163]; J. H. Brodie and D. A. Easson, *Brane inflation and reheating*, JCAP **0312**, 004 (2003) [arXiv:hep-th/0301138]; H. Firouzjahi and S. H. H. Tye, *Closer towards inflation in string theory*, Phys. Lett. B **584**, 147 (2004) [arXiv:hep-th/0312020].

For reviews of brane inflation in string theory see, e.g., E. Kiritsis, *D-branes in Standard Model building, gravity and cosmology*, Fortsch. Phys. **52**, 200 (2004) [Phys. Rept. **421**, 105 (2005 ERRAT,429,121-122.2006)] [arXiv:hep-th/0310001]; S. H. Henry Tye, *Brane inflation: string theory viewed from the cosmos* (2006) [arXiv:hep-th/0610221].

[122] C. P. Burgess et al., *Branonium*, JHEP **0306**, 037 (2003) [arXiv:hep-th/0303170].

[123] K. Takahashi and K. Ichikawa, *Cosmology and two-body problem of D-branes*, Phys. Rev. D **69**, 103506 (2004) [arXiv:hep-th/0310142].

[124] C. P. Burgess *et al.*, *The inflationary brane-antibrane universe*, JHEP **0107**, 047 (2001) [arXiv:hep-th/0105204].

[125] C. P. Burgess *et al.*, *Brane-antibrane inflation in orbifold and orientifold models*, JHEP **0203**, 052 (2002) [arXiv:hep-th/0111025].

[126] S. Kachru *et al.*, *Towards inflation in string theory*, JCAP **0310**, 013 (2003) [arXiv:hep-th/0308055].

[127] D. Baumann and L. McAllister, *Advances in inflation in string theory*, Ann. Rev. Nucl. Part. Sci. **59**, 67 (2009) [arXiv:0901.0265 [hep-th]].

[128] D. Lust, S. Stieberger and T. R. Taylor, *The LHC string hunter's companion*, Nucl. Phys. B **808**, 1 (2009) [arXiv:0807.3333 [hep-th]].

[129] C. T. Hill and E. H. Simmons, *Strong dynamics and electroweak symmetry breaking*, Phys. Rept. **381**, 235 (2003) [Erratum-ibid. **390**, 553 (2004)] [arXiv:hep-ph/0203079].

[130] F. Sannino, *Dynamical stabilization of the Fermi scale: Phase Diagram of strongly coupled theories for (Minimal) Walking Technicolor and unparticles* (2008) [arXiv:0804.0182 [hep-ph]].

[131] S. Cullen, M. Perelstein and M. E. Peskin, *TeV strings and collider probes of large extra dimensions*, Phys. Rev. D **62**, 055012 (2000) [arXiv:hep-ph/0001166].

[132] L. A. Anchordoqui *et al.*, *Jet signals for low mass strings at the LHC*, Phys. Rev. Lett. **100**, 171603 (2008) [arXiv:0712.0386 [hep-ph]]; *Direct photons as probes of low mass strings at the LHC*, Phys. Rev. D **78**, 016005 (2008) [arXiv:0804.2013 [hep-ph]].

[133] L. A. Anchordoqui *et al.*, *Dijet signals for low mass strings at the LHC*, Phys. Rev. Lett. **101**, 241803 (2008) [arXiv:0808.0497 [hep-ph]].

[134] L. A. Anchordoqui *et al.*, *LHC phenomenology for string hunters*, Nucl. Phys. B **821**, 181 (2009) [arXiv:0904.3547 [hep-ph]].

[135] P. Creminelli, A. Nicolis and R. Rattazzi, *Holography and the electroweak phase transition*, JHEP **0203**, 051 (2002) [arXiv:hep-th/0107141].

[136] G. Shiu *et al.*, *Probing the geometry of warped string compactifications at the LHC*, Phys. Rev. Lett. **100**, 031601 (2008) [arXiv:0705.4097 [hep-ph]].

[137] P. McGuirk, G. Shiu and K. M. Zurek, *Phenomenology of infrared smooth warped extra dimensions*, JHEP **0803**, 012 (2008) [arXiv:0712.2264 [hep-ph]].

[138] F. Marchesano, P. McGuirk and G. Shiu, *Open string wavefunctions in warped compactifications*, JHEP **0904**, 095 (2009) [arXiv:0812.2247 [hep-th]].

[139] M. Reece and L. T. Wang, *Randall-Sundrum and strings* (2010) [arXiv:1003.5669 [hep-ph]].

[140] A. D. Linde, *Inflation and axion cosmology*, Phys. Lett. B **201**, 437 (1988).

[141] G. R. Dvali, *Removing the cosmological bound on the axion scale* (1995) [arXiv:hep-ph/9505253].

[142] M. Kawasaki, T. Moroi and T. Yanagida, *Can decaying particles raise the upperbound on the Peccei-Quinn scale?*, Phys. Lett. B **383**, 313 (1996) [arXiv:hep-ph/9510461].

[143] T. Banks and M. Dine, *The cosmology of string theoretic axions*, Nucl. Phys. B **505**, 445 (1997) [arXiv:hep-th/9608197].

[144] T. Banks, M. Dine and M. Graesser, *Supersymmetry, axions and cosmology*, Phys. Rev. D **68**, 075011 (2003) [arXiv:hep-ph/0210256].

[145] T. Flacke *et al.*, *Warped axions*, JHEP **0701**, 061 (2007) [arXiv:hep-ph/0611278].

[146] R. Kallosh *et al.*, *Gravity and global symmetries*, Phys. Rev. D **52**, 912 (1995) [arXiv:hep-th/9502069].

[147] M. Dine *et al.*, *Nonperturbative effects on the string world sheet*, Nucl. Phys. B **278**, 769 (1986).

[148] K. Becker, M. Becker and A. Strominger, *Five-branes, membranes and nonperturbative string theory*, Nucl. Phys. B **456**, 130 (1995) [arXiv:hep-th/9507158].

[149] L. McAllister, E. Silverstein and A. Westphal, *Gravity waves and linear inflation from axion monodromy* (2008) [arXiv:0808.0706 [hep-th]].

[150] A. Arvanitaki *et al.*, *String Axiverse* (2009) [arXiv:0905.4720 [hep-th]].

[151] B. S. Acharya, K. Bobkov and P. Kumar, *An M theory solution to the strong CP problem and constraints on the axiverse* (2010) [arXiv:1004.5138 [hep-th]].

[152] A. Arvanitaki and S. Dubovsky, *Exploring the string axiverse with precision black hole physics* (2010) [arXiv:1004.3558 [hep-th]].

[153] J. G. Rosa and J. March-Russell, *Resonant particle production in branonium*, Phys. Rev. D **77**, 126004 (2008) [arXiv:0711.0658 [hep-th]].

[154] B. Hassanain, J. March-Russell and J. G. Rosa, *On the possibility of light string resonances at the LHC and Tevatron from Randall-Sundrum throats*, JHEP **0907**, 077 (2009) [arXiv:0904.4108 [hep-ph]].

[155] J. G. Rosa, *The extremal black hole bomb*, JHEP **1006**, 015 (2010) [arXiv:0912.1780 [hep-th]].

[156] D. Binosi and L. Theussl, *JaxoDraw: A graphical user interface for drawing Feynman diagrams*, Comput. Phys. Commun. **161**, 76 (2004) [arXiv:hep-ph/0309015].

[157] J. Ellison and A. Lukas, *The stability of branonium*, Phys. Rev. D **70**, 083518 (2004) [arXiv:hep-th/0312110].

[158] H. Collins, R. Holman and M. R. Martin, *Radion induced brane preheating*, Phys. Rev. Lett. **90**, 231301 (2003) [arXiv:hep-ph/0205240]; S. Tsujikawa, K. I. Maeda and S. Mizuno, *Brane preheating*, Phys. Rev. D **63**, 123511 (2001) [arXiv:hep-ph/0012141].

[159] C. Germani, N. E. Grandi and A. Kehagias, *A stringy alternative to inflation: the cosmological slingshot scenario*, Class. Quant. Grav. **25**, 135004 (2008) [arXiv:hep-th/0611246]; *The cosmological slingshot scenario: myths and facts* (2007) [arXiv:0706.0023 [hep-th]].

[160] D. A. Easson *et al.*, *Cycling in the throat*, JHEP **0704**, 026 (2007) [arXiv:hep-th/0701252]; D. A. Easson *et al.*, *Spinflation*, JCAP **0802**, 010 (2008) [arXiv:0709.2666 [hep-th]].

[161] N. D. Birrell and P. C. W. Davies, *Quantum Fields in Curved Space* (Cambridge University Press, Cambridge, UK, 1984).

[162] N. W. McLachlan, *Theory and Application of Mathieu Functions* (Oxford University Press, Oxford, UK, 1947).

[163] L. D. Landau and E. M. Lifshitz, *Mechanics* (Pergamon Press, New York, USA, 1976).

[164] S. Shandera ıet al., *Inter-brane interactions in compact spaces and brane inflation*, JCAP **0402**, 013 (2004) [arXiv:hep-th/0311207].

[165] A. Sen, *Tachyon condensation on the brane antibrane system*, JHEP **9808**, 012 (1998) [arXiv:hep-th/9805170]; *Non-BPS states and branes in string theory*, in Cargese 1999, Progress in string theory and M-theory [arXiv:hep-th/9904207].

[166] G. R. Dvali, *Infrared hierarchy, thermal brane inflation and superstrings as superheavy dark matter*, Phys. Lett. B **459**, 489 (1999) [arXiv:hep-ph/9905204].

[167] E. W. Kolb, A. Linde and A. Riotto, *GUT baryogenesis after preheating*, Phys. Rev. Lett. **77**, 4290 (1996) [arXiv:hep-ph/9606260].

[168] P. B. Greene and L. Kofman, *On the theory of fermionic preheating*, Phys. Rev. D **62**, 123516 (2000) [arXiv:hep-ph/0003018].

[169] I. I. Kogan *et al.*, *Multi-localization in multi-brane worlds*, Nucl. Phys. B **615**, 191 (2001) [arXiv:hep-ph/0107307].

[170] S. Casagrande *et al.*, *Flavor physics in the Randall-Sundrum Model: I. Theoretical setup and electroweak precision tests*, JHEP **0810** (2008) 094 [arXiv:0807.4937 [hep-ph]].

[171] S. J. Huber, *Flavor violation and warped geometry*, Nucl. Phys. B **666**, 269 (2003) [arXiv:hep-ph/0303183].

[172] K. Agashe, G. Perez and A. Soni, *Flavor structure of warped extra dimension models*, Phys. Rev. D **71**, 016002 (2005) [arXiv:hep-ph/0408134].

[173] R. D. Peccei, *Chiral lagrangian calculation of pion-nucleon scattering lengths*, Phys. Rev. **176**, 1812 (1968); **181**, 1902 (1969).

[174] L. M. Nath and B. K. Bhattacharyya, *Photoproduction of pions at low-energy*, Z. Phys. C **5**, 9 (1980).

[175] M. Benmerrouche, R. M. Davidson and N. C. Mukhopadhyay, *Problems of describing spin 3/2 baryon resonances in the effective Lagrangian theory*, Phys. Rev. C **39**, 2339 (1989).

[176] M. A. Luty and J. March-Russell, *Baryons from quarks in the 1/N expansion*, Nucl. Phys. B **426**, 71 (1994) [arXiv:hep-ph/9310369]: M. A. Luty, J. March-Russell and M. J. White, *Baryon magnetic moments in a simultaneous expansion in 1/N and m(s)*, Phys. Rev. D **51**, 2332 (1995) [arXiv:hep-ph/9405272].

[177] J. Kambor, *Heavy baryon chiral perturbation theory and the spin-3/2 delta resonances*, in Baryons 95, 0157-166 (QCD161:I399:1995) [arXiv:hep-ph/9606455].

[178] V. Pascalutsa, *Quantization of an interacting spin-3/2 field and the Delta isobar*, Phys. Rev. D **58**, 096002 (1998) [arXiv:hep-ph/9802288].

[179] V. Pascalutsa and R. Timmermans, *Field theory of nucleon to higher-spin baryon transitions*, Phys. Rev. C **60**, 042201 (1999) [arXiv:nucl-th/9905065].

[180] M. Napsuciale, M. Kirchbach and S. Rodriguez, *Spin 3/2 beyond the Rarita-Schwinger framework*, Eur. Phys. J. A **29**, 289 (2006) [arXiv:hep-ph/0606308].

[181] S. Ferrara and P. van Nieuwenhuizen, *Consistent supergravity with complex spin 3/2 gauge fields*, Phys. Rev. Lett. **37**, 1669 (1976).

[182] R. Walsh and A. J. Ramalho, *Bounds on the electromagnetic interactions of excited spin-3/2 leptons*, Phys. Rev. D **60**, 077302 (1999) [arXiv:hep-ph/9907364].

[183] J. H. Kuhn and P. M. Zerwas, *Excited Quarks And Leptons*, Phys. Lett. B **147**, 189 (1984).

[184] B. Moussallam and V. Soni, *Production of heavy spin 3/2 fermions in colliders*, Phys. Rev. D **39**, 1883 (1989).

[185] D. A. Dicus, S. Gibbons and S. Nandi, *Collider production of spin 3/2 quarks* (1998) [arXiv:hep-ph/9806312].

[186] F. M. L. Almeida *et al.*, *Production and decay of single heavy spin-3/2 leptons in high energy electron-positron collisions*, Phys. Rev. D **53**, 3555 (1996) [arXiv:hep-ph/9509364].

[187] C. J. C. Burges and H. J. Schnitzer, *Virtual effects of excited quarks as probes of a possible new hadronic mass scale*, Nucl. Phys. B **228**, 464 (1983).

[188] N. Arkani-Hamed, J. March-Russell and H. Murayama, *Building models of gauge-mediated supersymmetry breaking without a messenger sector*, Nucl. Phys. B **509**, 3 (1998) [arXiv:hep-ph/9701286].

[189] K. S. Babu *et al.*, *Comments on the high Q^2 HERA anomaly*, Phys. Lett. B **402**, 367 (1997) [arXiv:hep-ph/9703299].

[190] W. Rarita and J. S. Schwinger, *On a theory of particles with half integral spin*, Phys. Rev. **60**, 61 (1941).

[191] M. Blanke *et al.*, *Δ F=2 observables and fine-tuning in a warped extra dimension with custodial protection*, JHEP **0903**, 001 (2009) [arXiv:0809.1073 [hep-ph]].

[192] O. Gedalia, G. Isidori and G. Perez, *Combining direct and indirect kaon CP violation to constrain the warped KK scale*, Phys. Lett. B **682**, 200 (2009) [arXiv:0905.3264 [hep-ph]].

[193] K. Agashe, A. Azatov and L. Zhu, *Flavor violation tests of warped/composite SM in the two-site approach*, Phys. Rev. D **79**, 056006 (2009) [arXiv:0810.1016 [hep-ph]].

[194] L. A. Anchordoqui, H. Goldberg and T. R. Taylor, *Decay widths of lowest massive Regge excitations of open strings*, Phys. Lett. B **668**, 373 (2008) [arXiv:0806.3420 [hep-ph]].

[195] V. D. Barger, M. S. Berger and R. J. N. Phillips, *Quark singlets: implications and constraints*, Phys. Rev. D **52**, 1663 (1995) [arXiv:hep-ph/9503204].

[196] A. Atre *et al.*, *Heavy quarks above the top at the Tevatron*, Phys. Rev. D **79**, 054018 (2009) [arXiv:0806.3966 [hep-ph]].

[197] A. Pukhov, *CalcHEP 3.2: MSSM, structure functions, event generation, batchs, and generation of matrix elements for other packages* (2004) [arXiv:hep-ph/0412191].

[198] J. Pumplin *et al.*, *New generation of parton distributions with uncertainties from global QCD analysis*, JHEP **0207**, 012 (2002) [arXiv:hep-ph/0201195].

[199] A. Lister [CDF Collaboration], *Search for heavy top-like quarks $t' \to Wq$ using lepton plus jets events in 1.96 TeV $p\bar{p}$ collisions*, *Presented at 34th International Conference on High Energy Physics (ICHEP 2008), Philadelphia, Pennsylvania, 30 July - 5 Aug 2008* [arXiv:0810.3349 [hep-ex]].

[200] B. A. Dobrescu, K. Kong and R. Mahbubani, *Prospects for top-prime quark discovery at the Tevatron*, JHEP **0906**, 001 (2009) [arXiv:0902.0792 [hep-ph]].

[201] M. A. Pleier, *Review of top quark properties measurements at the Tevatron*, Int. J. Mod. Phys. A **24**, 2899 (2009) [arXiv:0810.5226 [hep-ex]].

[202] DØ Collaboration, *Search for $t\bar{t}$ resonances in the lepton+jets final state in $p\bar{p}$ collisions at $\sqrt{s} = 1.96\,TeV$*, conference note 5882-CONF, March 2009.

[203] J. A. Aguilar-Saavedra, *Pair production of heavy Q = 2/3 singlets at LHC*, Phys. Lett. B **625**, 234 (2005) [Erratum-ibid. B **633**, 792 (2006)] [arXiv:hep-ph/0506187].

[204] T. Regge and J. A. Wheeler, *Stability of a Schwarzschild singularity*, Phys. Rev. **108**, 1063 (1957).

[205] C. V. Vishveshwara, *Stability of the Schwarzschild metric*, Phys. Rev. D **1**, 2870 (1970).

[206] R. M. Wald, *Note on the stability of the Schwarzschild metric*, J. Math. Phys. **20**, 1056 (1979).

[207] R. P. Kerr, *Gravitational field of a spinning mass as an example of algebraically special metrics*, Phys. Rev. Lett. **11**, 237 (1963).

[208] Y. B. Zeldovich, *The generation of waves by a rotating body*, Pisma Zh. Eksp. Teor. Fiz. **14**, 270 (1971) [JETP Lett. **14**, 180 (1971)]; *Amplification of cylindrical electromagnetic waves from a rotating body*, Zh. Eksp. Teor. Fiz **62**, 2076 (1972) [Sov. Phys. JETP **35**, 1085 (1972)].

[209] T. Damour, N. Deruelle and R. Ruffini, *On quantum resonances in stationary geometries*, Lett. Nuovo Cim. **15**, 257 (1976).

[210] T. J. M. Zouros and D. M. Eardley, *Instabilities of massive scalar perturbations of a rotating black hole*, Annals Phys. **118**, 139 (1979).

[211] S. Detweiler, *Klein-Gordon equation and rotating black holes*, Phys. Rev. D **22**, 2323 (1980).

[212] H. Furuhashi and Y. Nambu, *Instability of massive scalar fields in Kerr-Newman spacetime*, Prog. Theor. Phys. **112**, 983 (2004) [arXiv:gr-qc/0402037].

[213] V. Cardoso *et al.*, *The black hole bomb and superradiant instabilities*, Phys. Rev. D **70**, 044039 (2004) [Erratum-ibid. D **70**, 049903 (2004)] [arXiv:hep-th/0404096].

[214] M. J. Strafuss and G. Khanna, *Massive scalar field instability in Kerr spacetime*, Phys. Rev. D **71**, 024034 (2005) [arXiv:gr-qc/0412023].

[215] V. Cardoso and S. Yoshida, *Superradiant instabilities of rotating black branes and strings*, JHEP **0507**, 009 (2005) [arXiv:hep-th/0502206].

[216] S. R. Dolan, *Instability of the massive Klein-Gordon field on the Kerr spacetime*, Phys. Rev. D **76**, 084001 (2007) [arXiv:0705.2880 [gr-qc]].

[217] R. Penrose, *Gravitational collapse: The role of general relativity*, Riv. Nuovo Cim. **1**, 252 (1969) [Gen. Rel. Grav. **34**, 1141 (2002)].

[218] D. Christodoulou, *Reversible and irreversible transformations in black hole physics*, Phys. Rev. Lett. **25**, 1596 (1970).

[219] C. A. Manogue, *The Klein paradox and superradiance*, Annals of Physics **181**, 261 (1988).

[220] W. Greiner, B. Müller and J. Rafelski, *Quantum electrodynamics of strong fields* (Springer-Verlag, Berlin, Germany, 1985).

[221] Y. B. Zeldovich and A. A. Starobinsky, *Particle production and vacuum polarization in an anisotropic gravitational field*, Sov. Phys. JETP **34**, 1159 (1972) [Zh. Eksp. Teor. Fiz. **61**, 2161 (1971)].

[222] R. H. Boyer and R. W. Lindquist, *Maximal analytic extension of the Kerr metric*, J. Math. Phys. **8**, 265 (1967).

[223] W. H. Press and S. A. Teukolsky, *Floating orbits, superradiant scattering and the black-hole bomb*, Nature **238**, 211 (1972).

[224] M. H. P. M. Putten, *Superradiance in a torus magnetosphere around a black hole*, Science **284**, 115 (1999).

[225] A. N. Aguirre, *On the superradiance of spin-1 waves in an equatorial wedge around a Kerr hole*, Astrophys. J. **529**, L9 (2000) [arXiv:astro-ph/9910403].

[226] W. Unruh, *Separabilty of the neutrino equations in a Kerr background*, Phys. Rev. Lett. **31**, 1265 (1973).

[227] T. Hartman, W. Song and A. Strominger, *The Kerr-Fermi sea* (2009) [arXiv:0912.4265 [hep-th]].

[228] S. Hod and O. Hod, *Analytic treatment of the black-hole bomb*, Phys. Rev. D **81**, 061502 (2010) [arXiv:0910.0734 [gr-qc]].

[229] J. E. McClintock and R. A. Remillard, *Measuring the spins of stellar-mass black holes* (2009), [arXiv:0902.3488 [astro-ph.HE]].

[230] M. Abramowitz and I. A. Stegun, eds., *Handbook of Mathematical Functions With Formulas, Graphs, and Mathematical Tables*, NBS Applied Mathematics Series **55** (National Bureau of Standards, Washington, DC, USA, 1964).

[231] W. H. Press and S. A. Teukolsky, *Perturbations of a rotating black hole. II. Dynamical stability of the Kerr metric*, Astrophys. J. **185**, 649 (1973).

[232] S. Hod and O. Hod, *Comment on 'The extremal black hole bomb'* (2009) [arXiv:0912.2761 [gr-qc]].

[233] K. S. Thorne, *'Disk accretion onto a black hole. 2. Evolution of the hole*, Astrophys. J. **191**, 507 (1974).